UC San Diego

UC San Diego Electronic Theses and Dissertations

Title

Engineering bio-inspired microenvironments for stem cell proliferation and skeletal differentiation

Permalink

https://escholarship.org/uc/item/6s16d605

Author

Hwang, Yongsung

Publication Date

2011

Peer reviewed|Thesis/dissertation

eScholarship.org Powered by the California Digital Library
University of California

UNIVERSITY OF CALIFORNIA, SAN DIEGO

Engineering bio-inspired microenvironments for stem cell proliferation and skeletal differentiation

A dissertation submitted in partial satisfaction of the

requirements for the degree Doctor of Philosophy

in

Materials Science and Engineering

by

Yongsung Hwang

Committee in Charge:

Professor Shyni Varghese, Chair
Professor Gaurav Arya
Professor Sungho Jin
Professor Yu-Hwa Lo
Professor Vlado A. Lubarda

2011

Copyright

Yongsung Hwang, 2011

All rights reserved

The dissertation of Yongsung Hwang is approved, and it is acceptable in quality and form for publication on microfilm:

Chair

University of California, San Diego

2011

Dedicated to my loving wife Anna and my family

who have always shown unfailing love and support

"But seek first his kingdom and his righteousness,

and all these things will be given to you as well."

- Matthew 6:33

TABLE OF CONTENTS

SIGNATURE PAGE.....iii

DEDICATION.....iv

EPIGRAPH.....v

TABLE OF CONTENTS.....vi

LIST OF FIGURES.....xi

LIST OF TABLES.....xv

ACKNOWLEDGEMENTS.....xvi

VITA.....xix

LIST OF PUBLICATIONS.....xix

ABSTRACT OF THE DISSERTATION.....xxi

CHAPTER 1: Introduction..... 1

1.1 Motivation and Background 1

1.1.1 Extracellular matrix and the cell-matrix interaction..... 1

1.1.2 Hydrogel-based artificial ECMs for skeletal tissue regeneration..... 3

1.1.3 Role of physico-chemical cues on self-renewal of human pluripotent stem cells..... 4

1.1.4 Role of chemical cues on stem cell behaviors..... 6

1.1.5 Role of physcial cues on stem cell behaviors..... 8

1.2 Thesis objective 12

1.3 Overview of the dissertation..... 13

1.4 References..... 14

CHAPTER 2: Development and optimization of creating 3D architectures with controlled internal microstructures 19

2.1 Introduction 19

2.2 Materials and Methods 22

2.2.1Materials 22

2.2.2 Synthesis of PEGDA oligomers 22

2.2.3 Synthesis of A6ACA oligomers 23

2.2.4 Synthesis of PEG cryogels 23

2.2.5 Synthesis of A6ACA cryogels 24

2.2.6 Scanning electron microscopy (SEM) 24

2.2.7 Swelling ratio measurement 25

2.2.8 Mechanical testing 25

2.2.9 Mercury intrusion prosimetry (MIP) 25

2.2.10 Microcomputed tomography (MicroCT) 26

2.2.11 Cryogels as cell scaffolds 26

2.2.12 Cell viability test 27

2.2.13 Statistical analysis 27

2.3 Results and Discussion 28

2.3.1 Influence of polymerization conditions on cryogel structures 28

2.3.2 Swelling properties of cryogels 40

2.3.3 Mechanical properties of cryogels 42

2.3.4 Cytocompatibility of cryogels 43

2.4 Conclusion 45

2.5 Acknowledgments 46

2.6 References 47

CHAPTER 3: Interconnected macroporous poly(ethylene glycol) (PEG) cryogels as a cell scaffold for cartilage tissue engineering 50

3.1 Introduction 50

3.2 Materials and Methods 52

3.2.1 Materials 52

3.2.2 Synthesis of PEGDA oligomers 52

3.2.3 Preparation of PEG cryogels 53

3.2.4 Scanning electron microscopy (SEM) of cryogels 53

3.2.5 Isolation of chondrocytes 54

3.2.6 Chondrocytes seeding and culture on PEG cryogels 54

3.2.7 Cell viability test 55

3.2.8 Biochemical assays 55

3.2.9 Histological and immunohistochemical analysis 56

3.2.10 Statistical analysis 57

3.3 Results and Discussion 58

3.3.1 Synthesis and characterization of PEG cryogels 58

3.3.2 Cell proliferation and extracellular matrix (ECM) synthesis in PEG cryogels 60

3.3.3 SEM analysis on chondrocyte-laden PEG cryogels 64

3.3.4 Histological and immunohistochemical analysis 65

3.4 Conclusion 68

3.5 Acknowledgments 68

3.6 References 69

CHAPTER 4: Engineering cell-material interfaces for long-term expansion of human pluripotent ste cells 73

4.1 Introduction 73

4.2 Materials and Methods 76

4.2.1Materials 76

4.2.2 Hydrogel prepation 77

4.2.3 Surface roughness measurements 79

4.2.4 Elastic modulus measurements 79

4.2.5 Water contact angle measurements 80

4.2.6 OCT4-GFP reporter line 80

4.2.7 HPSCs culture 80

4.2.8 Population doubling time (PDT) 81

4.2.9 Immunocytochemistry 81

4.2.10 RNA isolation and quantitative PCR 82

4.2.11 FACS analysis 83

4.2.12 *In vitro* differentiation of HUES9 cells grown on PAm_6-co-PSS_2 hydrogel 83

4.2.13 Karyotype analysis 84

4.2.14 PCR array analysis for various extracellular matrix and adhesion molecules 85

4.2.15 Protein adsorption assay 85

4.2.16 Enzyme-Linked Immunosorbent Assay (ELISA) 86

4.2.17 Statistical analysis 86

4.3 Results and Discussion 87

4.3.1Design and characterization of hydrogels 87

4.3.2 PSS-based hydrogels support self-renewal and long-term expansion of hPSCs 88

4.3.3 Effect of matrix rigidity on hPSCs 95

4.3.4 Effect of charge density of hydrogel on hPSC response 96

4.3.5 Effect of chemical functional group(s) and matrix hydrophobicity on hPSCs 97

4.3.6 Cell-matrix interface on adhesion and growth of hPSCs 100

4.4 Conclusion 104

4.5 Acknowledgements 105

4.6 Refences 106

CHAPTER 5: Conclusions and Future Directions 111

LIST OF FIGURES

Fig. 1.1 Summary of roles of ECM[1]. 2

Fig. 2.1 Photographs (a, b, g, h) and SEM images (c-f, i-l) of heterogeneous cryogel ($I_{0.1}T_{-20}C_S$) and homogeneous cryogel ($I_{0.05}T_{-20}C_S$): (a, g) equilibrium swollen cryogels; (b, h) dried cryogels; (c, i), (e-f, k-l) side view of cryogels; and (d, j) internal fracture surface of cryogels..... 30

Fig. 2.2 Thermograms of cryogelation at different temperatures with reference to DI water. (a) $I_{0.05}T_{-20}C_S$ (b) $I_{0.05}T_{-20}C_F$ (c) $I_{0.05}T_{-14}C_F$ 32

Fig. 2.3 Photograph (a) and SEM images (b-d) of $I_{0.1}T_{-20}C_{F.}$ 34

Fig. 2.4 SEM images of bottom and side view of $I_{0.05}T_{-20}C_F$. 35

Fig. 2.5 SEM images of $I_{0.05}T_{-20}C_F$ and $I_{0.1}T_{-20}C_F$; (a) internal fracture surface of $I_{0.05}T_{-20}C_F$, (b) internal fracture surface of cryogel-like structure of $I_{0.1}T_{-20}C_F$, and (c) internal fracture surface of hydrogel-like structure of $I_{0.1}T_{-20}C_F$ 35

Fig. 2.6 Photographs (a-b) and SEM images (c-f) of hydrogels and homogeneous cryogels: (a) equilibrium swollen network, synthesized at -14^{o}C using 0.1% w/v TEMED; exhibited a hydrogel like appearance (b) equilibrium swollen homogeneous cryogel ($I_{0.05}T_{-14}C_F$), synthesized at -14^{o}C using 0.05% w/v TEMED (c) internal fracture surface of $I_{0.05}T_{-14}C_F$ exhibiting interconnected pores, and (d) internal fracture surface of $I_{0.05}T_{-14}C_F$ shows a closed pore structure (e-f) side view of $I_{0.05}T_{-14}C_F$.. 37

Fig. 2.7 SEM images (a-h) and microCT image (i-j) of columnar (a-d) and spongy (e-h) A6ACA cryogels: (a, c, e, g) top view of cryogels and (b, d, f, h) internal fracture surface of cryogels, and microCT images describing columnar (i) and spongy (j) internal pore structure. 39

Fig. 2.8 Pore size distributions of sponge A6ACA (blue) and columnar A6ACA (red) cryogels.. 39

Fig. 2.9 Swelling kinetics of conventional hydrogels, and the heterogeneous ($I_{0.1}T_{-20}C_S$) and homogeneous cryogels ($I_{0.05}T_{-20}C_S$ and $I_{0.05}T_{-14}C_F$). (From t=1min to t=1440min, * $p < 0.05$ for all cryogels compared to conventional hydrogels; ** $p < 0.05$ for comparison between $I_{0.05}T_{-20}C_S$ and $I_{0.1}T_{-20}C_S$ for whole period of time). 41

Fig. 2.10 (a) Live/Dead assay of chondrocyte-loaded cryogel ($I_{0.05}T_{-20}C_S$) after 36 hours of cell seeding (b) Results of DNA assay showing the amount of DNA with culture

time using $I_{0.1}T_{-20}C_S$ cryogels as cell scaffolds. (* $p < 0.05$ for 1st, 2nd and 4th week of DNA amount compared to Day0) 44

Fig. 3.1 Photographs of PEG cryogels: (a) equilibrium swollen cryogel (b) cryogel compressed between fingers (c) compressed cryogel showing a sponge-like appearance upon removal of force (d) re-swollen cryogel upon immersion in PBS.. 59

Fig. 3.2 (a) SEM image of internal fracture surface of cryogel (scale bar = 50µm) (b) phase contrast microscope image (scale bar = 50µm) (c) live/dead assay of chondrocyte-laden cryogel after 36 hours of *in vitro* cultivation, section is taken vertically from the center of the construct (scale bar = 100µm)..... 59

Fig. 3.3 Results of DNA assay showing DNA content normalized to the dry weight of the cryogel after 4 weeks of *in vitro* cultivation (represented by line hatched bars) and the converted number of chondrocytes in constructs after 4 weeks of *in vitro* cultivation (presented by a dotted line) (* $p < 0.05$ for all comparisons among cultivation periods) 61

Fig. 3.4 Results of biochemical assays (a) GAG content normalized to the dry weight of the cryogel (b) collagen content normalized to the dry weight of the cryogel (c) amount of GAG normalized to the corresponding DNA values (d) amount of collagen normalized to the corresponding DNA values (* $p < 0.05$ for comparisons among cultivation periods)..... 62

Fig. 3.5 SEM images of chondrocytes seeded on PEG cryogels at different magnifications (a, c) (scale bar = 50µm) and (b, d) (scale bar = 20µm): (a, b) after 1 week of *in vitro* cultivation (c, d) after 4 weeks of *in vitro* cultivation (P represents a polymer network and an arrow indicates ECM). 65

Fig. 3.6 Results of H&E staining (a-b), Safranin-O staining (c-d), collagen type II immunostaining (e-f), and collagen type I immunostaining (g-h) of cell-laden done after 1st week of culture (a, c, e, g) and 4th week of culture (b, d, f, h) (scale bar = 100µm). 67

Fig. 4.1 Synthesis of various hydrogels used in this study. 88

Fig. 4.2 Phase contrast images of undifferentiated HUES9 colonies. (a) HUES9 cells grown on PAm_6-*co*-PSS_2 hydrogel (b) HUES9 cells grown on Matrigel (c) HUES9 cells grown on MEF, and (d) comparison of population doubling time between cells grown on Matrigel (blue) and cells grown on PAm_6-*co*-PSS_2 hydrogel (red) 89

Fig. 4.3 Maintenance of pluripotency of HUES9 cells grown on PAm_6-*co*-PSS_2 hydrogel and Matrigel. (a) immunofluorescence of HUES9 cells grown on PAm_6-*co*-PSS_2 hydrogel for cell nuclei (blue) and pluripotent markers, Nanog (red) and Oct4

(green) (b) results of real-time quantitative RT-PCR for gene expressions of pluripotent markers (Nanog and Oct4) (c) FACS analysis of cells showing the majority of cells were pluripotent 91-92

Fig. 4.4 Maintenance of pluripotency of HUES6 cells (a) and hiPSCs (b) grown on PAm_6-*co*-PSS_2 hydrogel demonstrated by immunofluorescence for cell nuclei (blue) and pluripotent markers, Nanog (red) and Oct4 (green). 93

Fig. 4.5 *In vitro* 3 germ layers differentiationof HUES9 cells grown on PAm_6-*co*-PSS_2 hydrogel (a, d) endoderm differentiation (Sox17) (b, e) mesoderm differentiation (smooth muscle actin, SMA) (c, f) ectoderm differentiation (Nestin) (g) endoderm differentiation (CXCR4, FOXA2, Sox17), mesoderm differentiation (SMA, ACTC1), and ectoderm differentiation (Nestin, Sox1, Sox2)..... 94

Fig. 4.6 Karyotype analysis of HUES9 cells grown on PAm_6-*co*-PSS_2 hydrogel using StemPro® medium..... 95

Fig. 4.7 Phase contrast images (a-c) and green fluorescent images (d-f) of HUES9 cells grown on various PSS-based hydrogels having different bulk rigidity (a, d) PAm_6-*co*-PSS_2-L hydrogel, (b, e) PAm_6-*co*-PSS_2-M hydrogel, and (c, f) PAm_6-*co*-PSS_2 hydrogel 96

Fig. 4.8 Phase contrast images (a-c) and green fluorescent images (d-f) of HUES9 cells grown on various PSS-based hydrogels with varying charge density (a, d) PAm_6-*co*-$PSS_{0.5}$ hydrogel, (b, e) PAm_6-*co*-PSS_1 hydrogel, and (c, f) PAm_6-*co*-PSS_2 hydrogel 97

Fig. 4.9 Phase contrast images (a-c) of various hydrogels terminating with -SO_3H functional group (a) initial HUES9 cell attachment on PAm_6-*co*-PSS_2 hydrogel having water contact angle of 23.0^o (b) initial HUES9 cell attachment on PAm_6-*co*-$PSPA_2$ hydrogel having water contact angle of 32.6^o, and (c) no HUES9 cell attachment on PAm_6-*co*-$PMEDSAH_2$ hydrogel having water contact angle of 66.3^o 98

Fig. 4.10 Phase contrast images (a-d) of various hydrogels terminating with -COOH functional group showing no cell adhesion (a) PAm_6-*co*-$PA2AGA_2$ hydrogel having water contact angle of 20.9^o (b) PAm_6-*co*-$PA4ABA_2$ hydrogel having water contact angle of 36.1^o (c) PAm_6-*co*-$PA6ACA_2$ hydrogel having water contact angle of 53.8^o, and (d) PAm_6-*co*-$PA8ACA_2$ hydrogel having water contact angle of 67.3^o. 100

Fig. 4.11 Quantification of (a) various ECM proteins and (b) the amount of bFGF adsorbed to PAm_6-*co*-$PA2AGA_2$ hydrogel (red) and PAm_6-*co*-PSS_2 hydrogel (blue) 101

Fig. 4.12 Hierarchical cluster analysis of mapping 84 gene expression profiles of HUES9 cells grown on MEF, Matrigel, PAm_6-*co*-PSS_2 hydrogel, and PAm_6-*co*-$PSPA_2$ hydrogel. 103

LIST OF TABLES

Table 2.1 Compositions and nomenclature of the cryogels 29

Table 2.2 Physical properties of sponge A6ACA and columnar A6ACA cryogels obtained by MIP.....40

Table 2.3 Mechanical properties of conventional hydrogels, heterogeneous ($I_{0.1}T_{-20}C_S$) and homogeneous cryogels ($I_{0.05}T_{-20}C_S$ and $I_{0.05}T_{-14}C_F$). (* $p < 0.05$ for $I_{0.05}T_{-20}C_S$ and $I_{0.05}T_{-14}C_F$ compared to conventional hydrogels; † $p > 0.05$ for comparison between $I_{0.1}T_{-20}C_S$ and conventional hydrogels; ** $p < 0.05$ for comparison between $I_{0.05}T_{-20}C_S$ and $I_{0.1}T_{-20}C_S$; †† $p > 0.05$ for comparison between $I_{0.05}T_{-20}C_S$ and $I_{0.1}T_{-20}C_S$) 42

Table 4.1 Lists of monomers.....76

Table 4.2 Compositions and nomenclature of hydrogels were summarized, and their elastic modulus and water contact angle were tabulated 78

Table 4.3 Primer sequences for RT-PCR.....82

Table 4.4 Average root mean square (RMS) surface roughness of hydrogels 99

ACKNOWLEDGEMENTS

During my graduate studies at University of California at San Diego, I have been blessed to meet so many talented people. Firstly, I cannot thank my advisor enough for being my mentor; I would like to express my sincerest gratitude to Professor Shyni Varghese for giving me a wonderful opportunity to be part of the greatest journey that I have experienced thus far. Her heartfelt encouragement, guidance, and passion for science always inspire me to joyfully follow my own trail without any hesitation.

I would like to thank my committee members, Prof. Gaurav Arya, Prof. Sungho Jin, Prof. Yu-Hwa Lo, Prof. Vlado A. Lubarda for helpful discussions and suggestions on my dissertation.

I am indebted to all my former and present members of the Varghese group who are my colleagues as well as good friends of mine. In particular, I am truly grateful to Prof. Nathaniel S. Hwang for being a dependable friend and giving me the indispensable foundation of proper cell culture. Without his help, I would not have been able to succeed. Many thanks to Prof. Chao Zhang and Dr. Nivedita Sangaj for teaching me polymer synthesis and for helpful discussion and encouragement, Prof. Chien-Wen Chang for getting me involved in human embryonic stem cell research, Ameya Phadke for sharing the lab bench at day and night together from very beginning and providing me all the valuable suggestions, Veronica Neiman for joyful collaboration, Aereas Aung and Susan Lin who spent time together from the very beginning and their help on many things, Dr. Ramses Ayala, Samuel Suk, and Philip Kyriakakis for helpful suggestions on various

experimental problems, especially related to molecular biology, and also Thomas Hagan for joyful collaboration.

I am also thankful to my colleagues: Dr. Sungsik Hur for teaching me how to use complicated Matlab codes for image analysis and his help was critical for analyzing many data sets, Dr. Youngil Lee for helpful discussion about cell biology and his encouragement, Dr. David Brafman for his wonderful collaboration on human embryonic stem cell experiments, and Dr. Ji-Eun Kim for valuable discussions and help when I was in the middle of challenging situation regarding the culture of human embryonic stem cells.

I would like to recognize and thank Charlotte Lauve for the administrative paperwork, invaluable advice, and numerous informative notices.

I would truly like to thank my wonderful friends who are like family and made this incredible journey possible: Sangman Kim, Dr. Chulmin Choi, Dr. Soonkook Hong, Dr. Kunbae Noh, Jinseok Lee, Namseok Park, Young Oh, Vincent Ham, Eunhae Ryu, Charles Lee, Yongkyung Han, Seongwon Lee, Seoryeong Jung, Seokwoo Han, Yongjin Sim, Kibum Park, Sangduk Lee, Eunwoo Kim, Changhoon Lee, Bumseok Kim, Manseok Ko, Heesang Lee, Doyoung Lee, Pastor Seungjong Lee, Pastor Peter Song, Pastor Sunae Kim, Pastor Gun Oh, Pastor Jonghwi Lee, Junjae La, and Sarah La for their prayer and friendship.

Lastly, I would like to express my deepest gratitude and love to my wife, Anna Lee, and my family: Gyoosang Hwang, Gyungsun Jo, Hyerin Hwang, Bongak Ko, Youngbok Lee, and Jinok Jung for their unfailing love, support, and prayer. Also, I

would like to thank my relatives Woan Hwang, Sookki Hwang, Jaehyun Hwang's family, and Hyangna Hwang's family, for their love and support.

Chapter 1, in part, is a reprint of the material as it appears in Regenerative Medicine, Volume 6, 2011. Hwang, Yongsung; Phadke, Ameya; Varghese, Shyni. The dissertation author was the primary investigator and author of this paper.

Chapter 2, in full, is a reprint of the material as it appears in Journal of Materials Chemistry, Volume 20, 2010. Hwang, Yongsung; Zhang, Chao; Varghese, Shyni. The dissertation author was the primary investigator and author of this paper.

Chapter 3, in full, is a reprint of the material as it appears in Tissue Engineering Part C, Volume 16, 2010. Hwang, Yongsung; Sangaj, Nivedita; Varghese, Shyni. The dissertation author was the primary investigator and author of this paper.

Chapter 4, in full, is currently being prepared for submission for publication of the material. *Chang, Chien-Wen; *Hwang, Yongsung; Hagan, Thomas; Brafman, David; Varghese, Shyni. The dissertation author was the primary investigator and author of this paper.

Yongsung Hwang

La Jolla, September 2011

VITA

2006	Bachelor of Science in Advanced Materials Science and Engineering, Sungkyunkwan University, Korea
2007	Master of Science in Materials Science and Engineering, University of California, San Diego
2011	Doctor of Philosophy in Materials Science and Engineering, University of California, San Diego

LIST OF PUBLICATIONS

[1] Hwang NS, Zhang C, **Hwang Y**, Varghese S. Mesenchymal stem cell differentiation and roles in regenerative medicine. Wiley Interdisciplinary Reviews-Systems Biology and Medicine. 2009;1:97-106.

[2] **Hwang Y**, Zhang C, Varghese S. Poly(ethylene glycol) cryogels as potential cell scaffolds: effect of polymerization conditions on cryogel microstructure and properties. Journal of Materials Chemistry. 2010;20:345-51.

[3] **Hwang Y**, Sangaj N, Varghese S. Interconnected Macroporous Poly(Ethylene Glycol) Cryogels as a Cell Scaffold for Cartilage Tissue Engineering. Tissue Engineering Part A. 2010;16:3033-41.

[4] Phadke A, Zhang C, **Hwang Y**, Vecchio K, Varghese S. Templated Mineralization of Synthetic Hydrogels for Bone-Like Composite Materials: Role of Matrix Hydrophobicity. Biomacromolecules. 2010;11:2060-8.

[5] Ayala R, Zhang C, Yang D, **Hwang Y**, Aung A, Shroff SS, et al. Engineering the cell-material interface for controlling stem cell adhesion, migration, and differentiation. Biomaterials. 2011;32:3700-11.

[6] **Hwang Y***, Phadke A*, Varghese S. Engineered microenvironments for self-renewal and musculoskeletal differentiation of stem cells. Regenerative Medicine. 2011;6:505-24.

[7] Zhang C, Sangaj N, **Hwang Y**, Phadke A, Chang CW, Varghese S. Oligo(trimethylene carbonate)-poly(ethylene glycol)-oligo(trimethylene carbonate)

triblock-based hydrogels for cartilage tissue engineering. Acta Biomaterialia. 2011;7:3362-9.

[8] **Hwang Y**, Zhang C, Aung A, Varghese S. Synthesis and characterization of thermo-responsive p[*N*-isopropylacrylamide-*co*-poly(ethylene glycol) diacrylate] hydrogels for cell sheet engineering. (*manuscript in preparation*)

[9] **Hwang Y***, Neiman V*, Zhang C, Phadke A, Lin S, Barbee K, Varghese S. Synthetic Bioactuators for High Throughput Cell Massaging. *(manuscript in preparation)*

[10] Phadke A*, **Hwang Y***, Varghese S. Synthesis and characterization of internal microstructures of N-Acryloyl-6-aminocaproic acid (A6ACA) cryogels for bone tissue regeneration and in vivo study. *(manuscript in preparation)*

[11] Chang CW*, **Hwang Y***, Brafman D, Hagan T, Lin S, Varghese S. Synthetic Matrices for Long-term Expansion of Pluripotent Human Embryonic Stem Cells. *(manuscript in preparation)*

[12] Nguyen QT, **Hwang Y**, Chen A, Varghese S, Sah R. Mechanical characterization of poly(ethylene glycol) diacrylate hydrogels: Effect of molecular weight and concentration. *(manuscript in preparation)*

ABSTRACT OF THE DISSERTATION

Engineering bio-inspired microenvironments for stem cell proliferation and skeletal differentiation

by

Yongsung Hwang

Doctor of Philosophy in Materials Science and Engineering

University of California, San Diego, 2011

Professor Shyni Varghese, Chair

Interactions of cells with their extracellular matrix (ECM) play an important role in development, disease progression, and regeneration. The material properties of ECM such as geometry, chemistry, hydrophobicity, mechanics, and microstructure play an important role in regulating various cellular processes and tissue morphogenesis. Thus there is a surge of interest in determining the effect of various material properties on cell fate and tissue formation. Beyond providing fundamental understandings, these efforts can also led to development of effective scaffolds (structural support for cell culture) as scaffold engineering is an integral part of *in vitro* cell cultures, tissue engineering, and transplants/implants.

The central focus of this thesis is design of polymer-based biomaterials as synthetic matrices for cell culture and understands how cell-matrix interactions affect tissue formation, stem cell differentiation and self-renewal. The first two chapters focuses on synthesis and characterization of three dimensional hydrogels having interconnected macroporous network structures of poly(ethylene glycol) using cryogelation techniques, where I have developed a novel, green strategy to create monolithic structures with heterogeneous and homogenous networks. I have also developed a process to create three-dimensional structures with different internal architecture while maintaining the same porosity. These 3D structures were then used to understand effect of scaffold porosity, pore structure, etc play an important role in cell proliferation, differentiation, and tissue formation using cartilage tissue engineering as a model system.

We also harnessed the potential of cell-matrix interactions to develop defined, synthetic matrices to expand human embryonic stem cells in vitro without introducing any detrimental effects. Employing a number of hydrogels I have determined the effect of various physico-chemical cues (bulk and interfacial properties) on adhesion, growth, colony formation, and self-renewal of human embryonic stem cells. Poly[acrylamide-*co*-sodium 4-vinylbenzenesulfonate] hydrogels having a moderate hydrophobicity (water contact angle of 23^{o}) and bulk rigidity of 343.7kPa have supported *in vitro* growth of a number of hPSCs (HUES9, HUES6, and iPSCs) in defined medium (StemPro®) for more than 20 passages. These studies are discussed in chapter 4.

CHAPTER 1: Introduction

"The reason I can see further is that I stand on the shoulders of a giant."

- Sir Isaac Newton

This chapter, in part, is a reprint of the material as it appears in Regenerative Medicine, Volume 6, 2011. Hwang, Yongsung; Phadke, Ameya; Varghese, Shyni. The dissertation author was the primary investigator and author of this paper.

1.1 Motivation and Background

1.1.1 Extracellular matrix and the cell-matrix interaction

During tissue development and remodeling process, cells interact with their surrounding extracellular matrix (ECM), which is dynamic and multifunctional in nature. Interaction of cells with their surrounding ECM plays a pivotal role in maintaining the tight regulation of various cellular behaviors.[1, 2] Emerging studies shows the effects of the architectural and functional properties of ECM on various cell behaviors. In native tissue, ECMs consists of a highly hydrated 3D network of fibrous proteins (collagens, fibronectin, laminin, elastin, and vitronectin), proteoglycans, and glycosaminoglycans (GAGs) and the organizations of these components contribute to both the chemical and mechanical characteristics of tissues. As already well-orchestrated in native tissues, collagen and elastin networks are responsible for the resistance to shear and tensile stress, and osmotic pressure attributed to the presence of the negatively charged GAGs makes

the ECMs highly swollen matrix as well as provides the resistance to the compressive loads by creating interstitial spaces.[3, 4] In addition to this structural support to the cell, ECM has also been shown to bind to growth factors, which allow ECM to store large quantities of various signaling and communication molecules. Moreover, ECM can mediate cell adhesion and proliferation by releasing and activating stored growth factors in a spatio-temporal manner.[5, 6] Therefore, it is important to understand the role of ECM on cellular functions in a systematic manner and the roles of interaction between cells and their ECM are illustrated in Fig. 1.1.

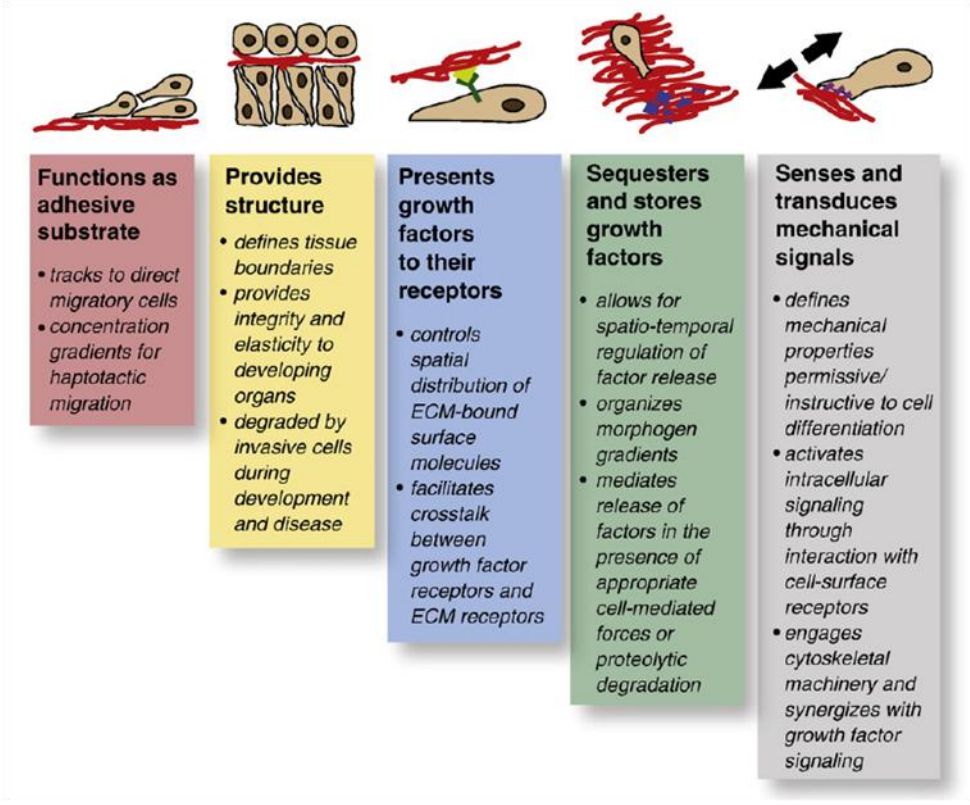


Fig. 1.1 Summary of roles of ECM[1]

1.1.2 Hydrogel-based artificial ECMs for skeletal tissue regeneration

Hydrogels, 3D network of hydrophilic polymers that can imbibe large amounts of water or biological fluids, are an excellent mimic of native ECM and thus a valuable tool to study cell-matrix interactions. The hydrogel networks can be formed either through chemical crosslinking or physical interactions.[7] Recent years have witnessed a surge of interest in employing hydrogels as artificial ECMs for cell cultures where they not only provide structural support but can also provides various physicochemical cues to the embedded cells.[8, 9] The hydrogel-based artificial ECMs can be categorized into two; hydrogels synthesized from natural materials and synthetic materials. Although the naturally-derived systems can provide required biological recognitions, there are still certain limitations, such as poor mechanical properties and batch-to-batch differences.[10, 11] In contrast, synthetic materials (e.g., polymer) based systems can be tuned easily to manipulate various structural, chemical, and mechanical properties. Polymer-based systems can also be tailored to achieve the desired hydrophobicity (or hydrophilicity). All of these factors play important roles in regulating cell-matrix interactions.[12-14] There are a number of synthetic hydrogels that have been shown to support growth and function of embedded cells both *in vitro* and *in vivo*.[15-17] Given the structural similarity of hydrogels with that of soft tissues such as cartilage a large number of studies have employed hydrogels for tissue engineering soft tissues. Among various synthetic hydrogels, photopolymerizable poly(ethylene glycol) (PEG)-based hydrogels as 3D scaffolds have been extensively explored due to their high water content, biocompatibility, and physical tunability modulating proper diffusion of oxygen, nutrients, and bioactive molecules.[18, 19] Bryant *et al*. have characterized physical

properties of poly(ethylene glycol)-based hydrogels having different crosslinking densities and demonstrated their effects on cartilage-specific ECM production.[20, 21] The cells embedded within the hydrogels maintain a round morphology and secret cartilage specific ECM. Kim *et al*. also have demonstrated the optimal amount of a heparin-based polymer for re-differentiating the de-differentiated chondrocytes in vitro culture and demonstrated its potential to regenerate partial-thickness cartilage defects.[22] Recently, cryogelation has emerged as a promising technique to fabricate porous 3D polymeric scaffolds.[23-25] This technique utilizes the formation of ice crystals at sub-zero temperature as porogens while polymerization is undergoing within liquid/semi-liquid phases. Upon completion of cryogelation at sub-zero temperature, subsequent equilibrium at room temperature gives rise to interconnected macroporous structures within the scaffold. Due to their high degree of porosity and the interconnected macropore structures, these scaffolds can promote effective mass transports as well as cell infiltrations throughout the scaffold. Bolgen *et al*. have synthesized biodegradable cryogel scaffolds with 2-hydroxyethyl methacrylate (HEMA)-lactate-dextran and evaluated their potential as cell scaffolds using osteoblast-like cell line (MG63). Seeded cells were successfully proliferated with time and they secreted a significant amount of extracellular matrices within the scaffolds.[26]

1.1.3 Role of physico-chemical cues on self-renewal of human pluripotent stem cells

Although many studies investigating numerous cell behaviors have been performed on monolayer cell culture using commercially available tissue culture plates (TCPS) in the absence/presence of exogenous extracellular matrices, there are very

limited spaces to modulate the physical and chemical properties of these substrates. Therefore, there has been a surge of interest in controlling the physical and chemical properties of synthetic matrix substrates for cell culture.[27] By introducing hydrogel-based biomaterials as a novel cell culture substrate, recent advantages include investigations of the combinatory effects of chemical and physical properties on maintaining self-renewal and pluripotency of human pluripotent stem cells (hPSCs) and controlling stem cell fates.

Synthetic materials devoid of bioactive moieties or ligands support cell adhesion through non-specific adsorption of ECM components. A recent study by Mei *et al*. showed that synthetic hydrogels that selectively adsorb proteins such as vitronectin from the cell culture medium could support adhesion and growth of hESCs while maintaining their pluripotency.[28] Note that in this study the authors have used a combinatorial approach and have screened 496 different combinations of 22 acrylate monomers. Using the array technology, the authors have also screened the crosslinked polymers for various physico-chemical properties, such as hydrophobicity, surface topology, surface chemistry, and elastic modulus. Their study demonstrated that matrices with moderate hydrophobicity (water contact angle of 65-80^{o}) supported colony formation and self-renewal of hESCs in mTeSR medium. The authors suggested the adsorption of vitronectin on these matrices as a potential mechanism behind their ability to support hESC culture through engagement of $\alpha_v\beta_3$ and $\alpha_v\beta_5$ integrins.[29] In another study, Brafman *et al*. utilized a similar high-throughput screening approach and examined the effect of various linear polymers having different chemical structures, functional groups, and molecular weights on *in vitro* self-renewal of hPSCs. Of the 90 linear polymers

tested, 16 supported adhesion and proliferation of hESCs. However, among these polymers, only one polymer, viz. poly(methyl vinyl ether-alt-maleic anhydride) (PMVE-alt-MA) could support long-term culture of hESCs. PMVE-alt-MA was found to be optimal for long-term self-renewal and proliferation of a number of hPSC cell lines like Hues1, Hues9 and iPSCs in Stempro medium.[30] HPSCs cultured on PMVE-alt-MA showed increased expression of α_5 and α_v integrins as well as a number of endogenous ECM proteins. Beyond chemical structure, the molecular weight (M_n) of PVME-alt-MA was found to play a significant role on supporting proliferation and pluripotency of hPSCs. The potential of synthetic materials to support self-renewal of hPSCs was further supported by Villa-Diaz *et al*., which demonstrated that TCPS coated with poly[2-(methacryloyloxy)ethyl dimethyl-(3-sulfopropyl)ammonium hydroxide] (PMEDSAH), having a water contact angle of 17^o supports long-term growth of BG01 and H9 hESCs while maintaining their pluripotency and normal karyotype using MEF-conditioned medium and StemPro.[31] Moreover, hESCs cultured on these materials showed population-doubling times similar to those cultured on Matrigel surfaces.

1.1.4 Role of chemical cues on stem cell behaviors

The effect of surface chemistry on the differentiation of stem cells also has been well-studied. For instance, different modifications in surface chemistry via plasma treatment have been demonstrated to control chondrogenic and osteogenic differentiation of MSCs.[32, 33] Keselowsky *et al*. mechanistically studied the effect of substrate surface chemistry on osteogenic differentiation by using calvarial osteoblasts cultured on

self-assembled monolayers in a 2D culture.[34] They demonstrated that scaffold chemistry can affect the conformation of adsorbed proteins (specifically, fibronectin) which can in turn lead to the activation of cell surface integrins like $\alpha_5\beta_1$ and $\alpha_v\beta_3$; integrins α_5 and β_1 have been implicated in the osteogenic differentiation of MSCs.[35, 36] Lan *et al.* have also demonstrated the influence of surface chemistry as presented by self-assembled monolayers (SAMs), on the differentiation of C2C12 skeletal myoblasts.[37] Monolayers presenting –OH and $–CH_3$ surface functionalities were found to engage α5β1 integrin and promoted myogenesis. Benoit *et al*. demonstrated the effect of small functional groups on the differentiation of hMSCs in both 2D and 3D culture conditions using synthetic polymer-based matrices.[38] The authors reported the ability of poly(ethylene glycol) methacrylate hydrogels modified with phosphate, carboxyl, and t-butyl groups to induce differentiation of hMSCs into osteogenic, chondrogenic, and adipogenic differentiation, respectively. Under 2D culture conditions, cells on the phosphate-, carboxyl-, and t-butyl-functionalized matrices showed morphology and gene expressions characteristic of osteogenic, chondrogenic, and adipogenic lineages, respectively. In order to decouple the effect of cell morphology or cell shape on stem cell differentiation from that of chemical functional groups, the cells were also encapsulated in phosphate- and t-butyl-functionalized materials. Consistent with 2D culture conditions, cells encapsulated within phosphate- and t-butyl-functionalized hydrogels underwent osteogenic and adipogenic differentiation, respectively, despite the similar round morphology in both materials due to encapsulation. Functional group-dependent stem cell differentiation was also demonstrated by using self-assembled monolayers: amine (-

NH2)- and silane (-SH)-modified surfaces promoted osteogenesis, while hydroxyl (-OH)- and carboxyl (-COOH)-modified surfaces promoted chondrogenesis.[39, 40]

1.1.5 Role of physical cues on stem cells behaviors

Along with chemistry of the surface, synthetic extracellular matrices can be imparted with various other physical properties that can affect their cellular response. One such a property is interfacial hydropbobicity. Indeed, variation in chemical functional groups is known to affect hydrophobicity, which in turn affects protein adsorption and conformation [41-43], subsequently affecting various cellular responses. In an effort to decouple matrix hydrophobicity from surface chemistry, rigidity, and topology, Ayala *et al*. recently developed polyacrylamide hydrogels containing N-acryloyl amino acids with varying side chain lengths.[44] This allowed for the synthesis of hydrogels with pendant side chains containing varying numbers of methylene groups (from 1-10) but with an identical terminal carboxyl group, thereby allowing for systematic, subtle variation in matrix hydrophobicity without altering the bulk mechanical and chemical properties, as well as the surface roughness of the synthetic matrices. HMSCs showed optimal attachment and spreading to hydrogels with pendant side chains containing 5 methylene groups (water contact angle of 50-60^{o}). These hydrogels also promoted differentiation of the hMSCs into osteogenic and myogenic lineages in osteogenic and myogenic induction medium, respectively. Furthermore, osteogenic differentiation of hMSCs on these matrices with optimal hydrophobicity (or hydrophilicity) was observed in regular growth medium. This matrix hydrophibicity-

mediated cellular response was attributed to hydrophobicity-dependent conformation of the pendant side chains, leading to differential binding to proteins and their conformations. Similarly, matrix hydrophobicity was also shown to affect various other biological processes like biomineralization.[45] Such biomineralized materials could be used as a bone-mimicking microenvironment to direct osteogenic differentiation of stem cells.[46-48]

Matrix hydrophobicity has also been employed as a tool to modulate embryoid body (EBD) formation for the differentiation of ESCs.[49] Valamehr *et al*. utilized self-assembled monolayers of varying hydrophobicity to study its effect on formation of EBDs by using murine LW1, Rosa, B6 C57 ESCs, and human HSF1 ESCs. The authors demonstrated that surfaces functionalized with octadecanethiol (water contact angle: 103^{o}) promoted the formation of EBDs of 100-300 μm in diameter compared to low-adhesion plates. These EBDs of intermediate size were found to have lower cell death and enhanced expression of the ectodermal markers: nestin and tau, mesodermal markers: Brachyury and fetal liver kinase 1 (Flk1), and endodermal markers: Insulin promoter factor 1 (Pdx1) and (Sox17), when compared to small (<100μm) and large (>300 μm)-sized EBDs. This suggests that hydrophobic surfaces can be used to create EBDs with sizes optimal for their viability and differentiation. The authors also observed that mouse and human ESCs cultured on hydrophobic poly(dimethylsiloxane)-based surfaces (water contact angle: 111^{o}) showed improved neurogenesis (ectodermal differentiation), hematopoesis (mesodermal differentiation) as well as endodermal differentiation, further emphasizing the role of hydrophobicity in differentiation of pluripotent cells.

Another important consideration in the engineering of the stem cell niche is the mechanical properties of the ECM. This has been shown to profoundly affect differentiation of MSCs.[50-53] Engler *et al*. demonstrated that tissue-specific matrix rigidity can be harnessed to direct differentiation of hMSCs into tissue-specific phenotypes under two-dimensional culture conditions.[50] Recently, Huebsch *et al*. investigated the effect of matrix rigidity on stem cell fate in three dimensions.[54] Upon probing three-dimensional matrices with a variety of elastic moduli (ranging from 1.5 kPa to 160 kPa), they determined that softer matrices (with elastic moduli ranging from 2.5 kPa to 11 kPa) and stiffer matrices (with elastic moduli ranging from 20 kPa to 110 kPa) promoted adipogenic and osteogenic differentiation, respectively, in murine MSCs. The authors also suggest that differences in adhesion-ligand presentation due to differences in matrix mechanics may be one of the modes through which cells sense matrix stiffness. An interesting study by Rowlands *et al*. demonstrated that along with matrix mechanics, the chemical components of the matrix itself play an important role in directing stem cell differentiation.[55] The authors observed interplay between the type of ECM protein presented and the matrix stiffness on hMSC differentiation. Collagen I-coated, highly stiff (80 kPa) substrates optimally promoted osteogenesis, while fibronectin coated, 25 kPa gels as well as the 80 kPa collagen I coated gels optimally supported myogenesis. This suggests that an integrative approach considering both the mechanics and chemical cues in the matrix is vital for targeted stem cell differentiation.

Another important aspect of engineered matrices is the role of topographical cues in stem cell differentiation.[56, 57] Curran *et al*. have demonstrated the nanoscale control of surface functionality of matrices using nanolithography and the resultant effect on

stem cell adhesion and fate.[58] Similarly, Dalby *et al*. demonstrated the effect of nanoscale topography and symmetry on the osteogenic differentiation of hMSCs.[59] They cultured hMSCs on arrays constructed by embossing a poly(methylmethacrylate) substrate with 120 nm diameter, 100 nm deep indentations over an area of 1 cm^2. Five specific patterns were tested, viz. hexagonal array (HEX), square array (SQ), disordered square array with random displacement of dots by up to 50 nm on both axes from their position in a true square (DSQ50), disordered square array with random displacement of dots of up to 20 nm on both axes from their position in a true square (DSQ20) and pits placed randomly over a 150 μm x 150 μm field, repeated over 1 cm^2 area (RAND). Indeed, DSQ50 topography was found to optimally promote osteogenesis even in the absence of dexamethasone and L-ascorbic acid. These results suggest that nanoscale control of the synthetic stem cell niche can possibly be used to create highly controlled arrangement of cues presented to stem cells within engineered matrices, providing increased control over their fate.

1.2 Thesis objective

The central focus of this thesis is to gain insight into the design of polymer-based biomaterials that can mimic the native extracellular matrix and to understand the roles of cell-matrix interaction on various cell behaviors, such as proliferation, extracellular matrix production, stem cell differentiation, and self-renewal.

To achieve these goals, the following issues were addressed:

- To develop and optimize the cryogelation processes to manipulate cell-matrix interactions by tailoring specific scaffold parameters affecting microstructural architecture, namely pore size, pore network geometry, hierarchical microstructures, and anisotropy of internal pore structures.
- To design tunable synthetic materials capable of promoting long-term expansion of human pluripotent stem cells while maintaining their pluripotency and to investigate the role of various physicochemical factors on the ability of these hydrogels to support such expansion.

1.3 Overview of the dissertation

Chapter 1 provides a brief introduction to the role of cell-matrix interaction on cellular response and current progress in the development of biomimetic hydrogel scaffolds recapitulating these cues.

Chapter 2 describes the design, development and characterization of 3D hydrogels (referred to as cryogels) with varying pore size and architecture using ice-templating to impart porosity.

Chapter 3 further extends the application of poly(ethylene glycol) cryogels as cell scaffolds for cartilage tissue engineering.

Chapter 4 describes the design of synthetic hydrogels that can support long-term expansion of human pluripotent stem cells, as well as insights into the effect of various physicochemical factors on the ability of these hydrogels to support this expansion.

Chapter 5 concludes the dissertation and describes potential future directions.

1.4 References

1. Rozario, T. and D.W. DeSimone, *The extracellular matrix in development and morphogenesis: a dynamic view.* Dev Biol, 2010. **341**(1): p. 126-40.

2. Daley, W.P., S.B. Peters, and M. Larsen, *Extracellular matrix dynamics in development and regenerative medicine.* J Cell Sci, 2008. **121**(Pt 3): p. 255-64.

3. Pradhan, S. and M.C. Farach-Carson, *Mining the extracellular matrix for tissue engineering applications.* Regen Med. **5**(6): p. 961-70.

4. Escobedo-Lucea, C., et al., *Development of a Human Extracellular Matrix for Applications Related with Stem Cells and Tissue Engineering.* Stem Cell Rev.

5. Taipale, J. and J. KeskiOja, *Growth factors in the extracellular matrix.* Faseb Journal, 1997. **11**(1): p. 51-59.

6. Mooney, D.J. and P. Tayalia, *Controlled Growth Factor Delivery for Tissue Engineering.* Advanced Materials, 2009. **21**(32-33): p. 3269-3285.

7. Elisseeff, J., et al., *The role of biomaterials in stem cell differentiation: Applications in the musculoskeletal system.* Stem Cells and Development, 2006. **15**(3): p. 295-303.

8. Drury, J.L. and D.J. Mooney, *Hydrogels for tissue engineering: scaffold design variables and applications.* Biomaterials, 2003. **24**(24): p. 4337-51.

9. Ma, P.X., *Biomimetic materials for tissue engineering.* Adv Drug Deliv Rev, 2008. **60**(2): p. 184-98.

10. Prestwich, G.D., et al., *Controlled chemical modification of hyaluronic acid: synthesis, applications, and biodegradation of hydrazide derivatives.* J Control Release, 1998. **53**(1-3): p. 93-103.

11. Kim, B.S. and D.J. Mooney, *Development of biocompatible synthetic extracellular matrices for tissue engineering.* Trends Biotechnol, 1998. **16**(5): p. 224-30.

12. Shin, H., S. Jo, and A.G. Mikos, *Biomimetic materials for tissue engineering.* Biomaterials, 2003. **24**(24): p. 4353-64.

13. Sakiyama-Elbert, S.E. and J.A. Hubbell, *Functional biomaterials: Design of novel biomaterials.* Annual Review of Materials Research, 2001. **31**: p. 183-201.

14. Ayala, R., et al., *Engineering the cell-material interface for controlling stem cell adhesion, migration, and differentiation.* Biomaterials. **32**(15): p. 3700-11.

15. Elisseeff, J., et al., *Effects of three-dimensional culture and growth factors on the chondrogenic differentiation of murine embryonic stem cells.* Stem Cells, 2006. **24**(2): p. 284-291.

16. Roy, K. and H. Liu, *Biomimetic three-dimensional cultures significantly increase hematopoietic differentiation efficacy of embryonic stem cells.* Tissue Engineering, 2005. **11**(1-2): p. 319-330.

17. Langer, R., et al., *Differentiation of human embryonic stem cells on three-dimensional polymer scaffolds.* Proceedings of the National Academy of Sciences of the United States of America, 2003. **100**(22): p. 12741-12746.

18. Elisseeff, J., et al., *The effect of incorporating RGD adhesive peptide in polyethylene glycol diacrylate hydrogel on osteogenesis of bone marrow stromal cells.* Biomaterials, 2005. **26**(30): p. 5991-5998.

19. Elisseeff, J., N.S. Hwang, and S. Varghese, *Controlled differentiation of stem cells.* Advanced Drug Delivery Reviews, 2008. **60**(2): p. 199-214.

20. Bryant, S.J. and K.S. Anseth, *Hydrogel properties influence ECM production by chondrocytes photoencapsulated in poly(ethylene glycol) hydrogels.* J Biomed Mater Res, 2002. **59**(1): p. 63-72.

21. Bryant, S.J., K.L. Durand, and K.S. Anseth, *Manipulations in hydrogel chemistry control photoencapsulated chondrocyte behavior and their extracellular matrix production.* J Biomed Mater Res A, 2003. **67**(4): p. 1430-6.

22. Kim, M., et al., *The use of de-differentiated chondrocytes delivered by a heparin-based hydrogel to regenerate cartilage in partial-thickness defects.* Biomaterials. **32**(31): p. 7883-96.

23. Plieva, F., et al., *Macroporous elastic polyacrylamide gels prepared at subzero temperatures: control of porous structure.* Journal of Materials Chemistry, 2006. **16**(41): p. 4065-4073.

24. Plieva, F.M., et al., *Characterization of polyacrylamide based monolithic columns.* Journal of Separation Science, 2004. **27**(10-11): p. 828-836.

25. Plieva, F.M., et al., *Monolithic cryogels with open porous structure and unique double-continuous macroporous networks.* Soft Matter, 2008. **4**(12): p. 2418-2428.

26. Bolgen, N., et al., *Three-Dimensional Ingrowth of Bone Cells Within Biodegradable Cryogel Scaffolds in Bioreactors at Different Regimes.* Tissue Engineering Part A, 2008. **14**(10): p. 1743-1750.

27. Hwang, Y., A. Phadke, and S. Varghese, *Engineered microenvironments for self-renewal and musculoskeletal differentiation of stem cells.* Regenerative Medicine, 2011. **6**(4): p. 505-524.

28. Mei, Y., et al., *Mapping the Interactions among Biomaterials, Adsorbed Proteins, and Human Embryonic Stem Cells.* Advanced Materials, 2009. **21**(27): p. 2781-86.

29. Mei, Y., et al., *Combinatorial development of biomaterials for clonal growth of human pluripotent stem cells.* Nat Mater, 2010. **9**(9): p. 768-78.

30. Brafman, D.A., et al., *Long-term human pluripotent stem cell self-renewal on synthetic polymer surfaces.* Biomaterials, 2010. **31**(34): p. 9135-44.

31. Villa-Diaz, L.G., et al., *Synthetic polymer coatings for long-term growth of human embryonic stem cells.* Nat Biotechnol, 2010. **28**(6): p. 581-3.

32. Mwale, F., et al., *Suppression of Genes Related to Hypertrophy and Osteogenesis in Committed Human Mesenchymal Stem Cells Cultured on Novel Nitrogen-Rich Plasma Polymer Coatings.* Tissue Engineering, 2006. **12**(9): p. 2639-2647.

33. Mwale, F., et al., *The effect of glow discharge plasma surface modification of polymers on the osteogenic differentiation of committed human mesenchymal stem cells.* Biomaterials, 2006. **27**(10): p. 2258-2264.

34. Keselowsky, B.G., D.M. Collard, and A.J. Garcia, *Integrin binding specificity regulates biomaterial surface chemistry effects on cell differentiation.* PNAS, 2005. **102**(17): p. 5953-5957.

35. Moursi, A.M., R.K. Globus, and C.H. Damsky, *Interactions between integrin receptors and fibronectin are required for calvarial osteoblast differentiation in vitro.* J Cell Sci, 1997. **110**(18): p. 2187-2196.

36. Hamidouche, Z., et al., *Priming integrin α5 promotes human mesenchymal stromal cell osteoblast differentiation and osteogenesis.* Proceedings of the National Academy of Sciences, 2009. **106**(44): p. 18587-18591.

37. Lan, M.A., et al., *Myoblast proliferation and differentiation on fibronectin-coated self assembled monolayers presenting different surface chemistries.* Biomaterials, 2005. **26**(22): p. 4523-31.

38. Benoit, D.S.W., et al., *Small functional groups for controlled differentiation of hydrogel-encapsulated human mesenchymal stem cells.* Nat Mater, 2008. **7**(10): p. 816-823.

39. Curran, J.M., R. Chen, and J.A. Hunt, *The guidance of human mesenchymal stem cell differentiation in vitro by controlled modifications to the cell substrate.* Biomaterials, 2006. **27**(27): p. 4783-4793.

40. Phillips, J.E., et al., *Human mesenchymal stem cell differentiation on self-assembled monolayers presenting different surface chemistries.* Acta Biomaterialia, 2010. **6**(1): p. 12-20.

41. Roach, P., D. Farrar, and C.C. Perry, *Interpretation of protein adsorption: surface-induced conformational changes.* Journal of the American Chemical Society, 2005. **127**(22): p. 8168-8173.

42. Xu, L.-C. and C.A. Siedlecki, *Effects of surface wettability and contact time on protein adhesion to biomaterial surfaces.* Biomaterials, 2007. **28**(22): p. 3273-3283.

43. Allen, L.T., et al., *Surface-induced changes in protein adsorption and implications for cellular phenotypic responses to surface interaction.* Biomaterials, 2006. **27**(16): p. 3096-3108.

44. Ayala, R., et al., *Engineering the cell-material interface for controlling stem cell adhesion, migration and differentiation.* Biomaterials, 2011. **(accepted)**.

45. Phadke, A., et al., *Templated Mineralization of Synthetic Hydrogels for Bone-Like Composite Materials: Role of Matrix Hydrophobicity.* Biomacromolecules, 2010. **11**(8): p. 2060-2068.

46. Bhumiratana, S., et al., *Nucleation and growth of mineralized bone matrix on silk-hydroxyapatite composite scaffolds.* Biomaterials, 2011. **32**(11): p. 2812-2820.

47. Wang, H., et al., *Biocompatibility and osteogenesis of biomimetic nano-hydroxyapatite/polyamide composite scaffolds for bone tissue engineering.* Biomaterials, 2007. **28**(22): p. 3338-3348.

48. Gkioni, K., et al., *Mineralization of Hydrogels for Bone Regeneration.* Tissue Engineering Part B: Reviews, 2010. **16**(6): p. 577-585.

49. Valamehr, B., et al., *Hydrophobic surfaces for enhanced differentiation of embryonic stem cell-derived embryoid bodies.* Proceedings of the National Academy of Sciences, 2008. **105**(38): p. 14459-14464.

50. Engler, A.J., et al., *Matrix elasticity directs stem cell lineage specification.* Cell, 2006. **126**(4): p. 677-689.

51. Discher, D.E., P. Janmey, and Y.-l. Wang, *Tissue Cells Feel and Respond to the Stiffness of Their Substrate.* Science, 2005. **310**(5751): p. 1139-1143.

52. Pek, Y.S., A.C.A. Wan, and J.Y. Ying, *The effect of matrix stiffness on mesenchymal stem cell differentiation in a 3D thixotropic gel.* Biomaterials, 2010. **31**(3): p. 385-391.

53. Khatiwala, C.B., et al., *ECM Compliance Regulates Osteogenesis by Influencing MAPK Signaling Downstream of RhoA and ROCK.* Journal of Bone and Mineral Research, 2008. **24**(5): p. 886-898.

54. Huebsch, N., et al., *Harnessing traction-mediated manipulation of the cell/matrix interface to control stem-cell fate.* Nat Mater, 2010. **9**(6): p. 518-526.

55. Rowlands, A.S., P.A. George, and J.J. Cooper-White, *Directing osteogenic and myogenic differentiation of MSCs: interplay of stiffness and adhesive ligand presentation.* American Journal of Physiology - Cell Physiology, 2008. **295**(4): p. C1037-C1044.

56. Stevens, M.M. and J.H. George, *Exploring and engineering the cell surface interface.* Science, 2005. **310**(5751): p. 1135-1138.

57. Leong, K.W., E.K.F. Yim, and S.W. Pang, *Synthetic nanostructures inducing differentiation of human mesenchymal stem cells into neuronal lineage.* Experimental Cell Research, 2007. **313**(9): p. 1820-1829.

58. Curran, J.M., et al., *Introducing dip pen nanolithography as a tool for controlling stem cell behaviour: unlocking the potential of the next generation of smart materials in regenerative medicine.* Lab on a Chip, 2010. **10**(13): p. 1662-1670.

59. Dalby, M.J., et al., *The control of human mesenchymal cell differentiation using nanoscale symmetry and disorder.* Nat Mater, 2007. **6**(12): p. 997-1003.

CHAPTER 2: Development and optimization of creating 3D architectures with controlled internal microstructures

"Imagination is more important than knowledge. For knowledge is limited to all we now know and understand, while imagination embraces the entire world, and all there ever will be to know and understand."

Albert Einstein

This chapter, in full, is a reprint of the material as it appears in Journal of Materials Chemistry, Volume 20, 2010. Hwang, Yongsung; Zhang, Chao; Varghese, Shyni. The dissertation author was the primary investigator and author of this paper.

2.1 Introduction

Hydrogels are three-dimensional, insoluble, cross-linked networks of polymers that can imbibe large quantities of aqueous solutions. Hydrogels are excellent candidates for tissue engineering scaffolds because of their hydrophilic nature and mass transfer properties.[1, 2] Factors affecting microstructure of the scaffolds such as pore size and inter connectivity of pores play an important role in determining cell proliferation, differentiation, and subsequent tissue formation. Macroporous hydrogels with interconnected pores not only provide sufficient surface area for cell attachment and proliferation but also allow enhanced mass transfer of oxygen, nutrients and waste removal.[3, 4]

Various methods have been used in the past to produce macroporous hydrogels such as gas foaming[4, 5], fiber bonding[6], micro-emulsion formation[7], phase separation[8], freeze-drying[9], and porogen leaching.[10, 11] More recently, cryogelation technique has been explored as a green process to synthesize three-dimensional (3D) hydrophilic structures with highly interconnected macroporous networks, termed as cryogels. Cryogels are synthesized at subzero temperature where the reactants concentrated in the unfrozen/semi-frozen phase undergo polymerization to form a crosslinked network, while ice crystals start nucleating from the aqueous phase. These ice crystals function as porogens to produce interconnected macroporous network structures. The cryogels are characterized for their highly interconnected macroporous network structures with enhanced mechanical properties.[12, 13]

Previously, there have been limited investigations into the potential of cryogels as cell scaffolds. Kathuria et al. synthesized chitosan-gelatin cryogels and characterized their mechanical stability under various cyclic compressions. They also showed the cell viability and proliferation of fibroblasts within these cryogels.[14] Another study by Bolgen et al. reported the formation of 2-hydroxyethyl methacrylate (HEMA)-lactate-dextran cryogels, and their *in vitro* biocompatibility.[15] Beyond tissue engineering applications, cryogels have also been investigated in separation techniques.[16, 17] Although these studies suggest the potential application of cryogels, a detailed characterization of cryogel structures has not been carried out as yet. One of the attractive features of cryogels is their network microstructure, and in this study we evaluate the parameters that affect the microstructure of cryogels using poly(ethylene glycol) (PEG) as a model system. The choice of PEG is based on their widespread use in tissue

engineering and other biomedical applications. While PEG hydrogels have been extensively explored as cell scaffolds and delivery vehicles[1, 18-20], there have been no reports on formation and characterization of PEG cryogels. In addition to PEG cryogels as a model system, we also evaluate another possible parameter that can affect internal microstructures of cryogels using N-acryloyl 6-aminocaproic acid (A6ACA), as A6ACA has been demonstrated to promote templated mineralization as well as cell attachment and differentiation on polymeric substrates.[21]

Previous studies have demonstrated the effect of monomer concentration, degree of crosslinking, and solvent type on the pore structures of acrylamide cryogels.[22] Studies have also shown the effect of freezing temperature on microstructure of cryogels.[23] In this study, we evaluate the role of polymerization rate on cryogel formation without altering the concentration of precursors/monomers or solvent. The cryogels were synthesized using diacrylated PEG (PEGDA) as a precursor. The rate of polymerization/gelation was controlled by varying the concentration of TEMED (N,N,N',N'-tetramethethylenediamine), which functions as an accelerator in a redox initiator-mediated polymerization. We also investigate the effect of freezing temperature and degree of supercooling on cryogelation since these parameters have a significant effect on both the formation of ice crystals and the rate of gelation. Lastly, we investigate the effects of preferential nucleation sites to control the directionality and geometry of internal pore structures.

2.2 Materials and Methods

2.2.1 Materials

Toluene and triethylamine were purchased from Fisher Scientific, and dichloromethane and diethyl ether were purchased from Sigma-Aldrich. Polyethylene glycol (PEG) (Mn=3400) and acryloyl chloride were purchased from Aldrich and they were used to synthesize poly(ethylene glycol) diacrylate (PEGDA) oligomer without any further purification. Ammonium persulfate (APS) and N, N, N', N'-tetramethethylenediamine (TEMED) were obtained from Sigma. For cell viability test, Live/Dead Viability/Cytotoxicity Kit (Molecular Probes, Cat#L-3224) was purchased from Molecular Probes.

2.2.2 Synthesis of PEGDA oligomer

PEGDA oligomer was prepared according to the reported method.[24] Briefly, 18.0 gram of PEG was dissolved in 300 mL of toluene in a 500 mL round bottom flask in an oil bath heated at 125℃. The solution was then refluxed for 4 hours under vigorous stirring. Traces of water in the reaction mixture were removed by azeotropic distillation. Upon cooling the solution to room temperature, 3.262 gram (32.2 mmol, 4.493 mL) of triethylamine was added to it under vigorous stirring. Then the flask was moved to an ice bath and stirred for 30 minutes. 2.918 gram (32.2 mmol, 2.452 mL) of acryloyl chloride in 15 mL of anhydrous dichloromethane was then added to the reaction mixture dropwise for 30 minutes. After keeping the reaction mixture in the ice bath for another 30 minutes, the flask was heated at 45℃ overnight. The reaction mixture was then cooled to room temperature and the quaternary ammonium salt was removed from the reaction mixture

by filtering through diatomaceous earth (2-3 cm) on a fritted glass funnel. The filtrate was condensed using a rotary evaporator and then precipitated in excessive diethyl ether. The white precipitate was collected by filtration and vacuum dried at 40℃ for 24 hours. The resultant PEGDA oligomer was purified by precipitation followed by column chromatography and dialysis prior to its usage.

2.2.3 Synthesis of A6ACA monomer

N-acryloyl 6-aminocaproic acid (A6ACA) was synthesized from 6-aminocaproic acid (Acros Organics Inc.) as described elsewhere.[25, 26] Briefly, 13.1 gram of 6-aminocaproic acid and 4.4 gram of sodium hydroxide (NaOH) were dissolved in 80 mL of deionized water in an ice bath under vigorous stirring. Then 9.97 gram of acryloyl chloride in 15 mL of tetrahydrofuran (THF) was then added to the reaction mixture dropwise and the pH of reaction mixture was maintained at 7.5-7.8 until the reaction was complete. The reaction mixture was then separated using ethyl acetate. The organic phase containing dissolved the A6ACA was collected, combined, and dried using sodium sulfate. Finally, the solution was then filtered, concentrated, and precipitated in petroleum ether.

2.2.4 Synthesis of PEG cryogels

PEGDA oligomers were dissolved in Phosphate Buffered Saline (PBS) to prepare a solution of 10% w/v. To this solution at 4℃, the initiator-accelerator mixture {0.5% w/v of ammonium persulfate (APS) and either 0.05% or 0.1% w/v of N,N,N’,N’-Tetramethylethylenediamine (TEMED)} was added, and the reaction mixture was

polymerized at -14℃ or -20℃ for 20 hours. Two cooling rates were used to evaluate the effect of degree of supercooling and onset of the nucleation of ice crystals on cryogel formation and their microstructure.

2.2.5 Synthesis of A6ACA cryogels

Similarly, 0.5 M (9.25% w/v) of A6ACA monomer and 20% w/v of PEGDA oligomers (Mn=3400) were dissolved in 0.5 M of NaOH. To this solution at 4℃, the initiator-accelerator mixture {0.5% w/v of ammonium persulfate (APS) and 0.15% w/v of N,N,N',N'-Tetramethylethylenediamine (TEMED)} was added, and the reaction mixture was polymerized at -20℃ for 20 hours with or without thin ice layer, which was prepared by freezing 40 μl of DI water, at the bottom of the mold. This thin icy layer was used to introduce preferential nucleation sites to create directionality of internal pore structures.

2.2.6 Scanning electron microscopy (SEM)

The microstructures of PEG cryogels and hydrogels were examined using a scanning electron microscopy (SEM, Philips XL30 ESEM). Briefly, the samples were dehydrated in 50%, 75% and 100% ethanol and dried using a critical point dryer (Tousimis AutoSamdri 815). After samples were completely dried, they were gold-coated using sputter coater (Emitech K575X Sputter Coater) for 30 seconds prior to SEM imaging.

2.2.7 Swelling ratio measurement

The swelling ratios of each sample were measured using a gravimetric method. After removing unreacted monomer by washing in excess water, cryogels were dried using hot air sterilizer oven (Fisher Scientific 525D) at 60℃, followed by vacuum oven (Shel Lab 1410) until a constant dried weight was reached. Each sample was immersed in PBS at 37℃ for 48 hours and their swollen weights were measured immediately after removal of excess water from the surface using a slightly wet tissue paper. The equilibrium swelling ratio of samples was determined as a ratio of weights of equilibrium swollen gels to dried gels.[27]

2.2.8 Mechanical testing

Prior to compression test, the cryogels were immersed in PBS for 24 hours to reach equilibrium swelling. Compression tests were performed using Instron 3342 Universal Testing System (Instron, Norwood, MA, USA) equipped with a Model 2519-104 force transducer. Samples were compressed by two parallel plates at the maximum loading of 250N with a compression rate of 1mm/min. The compressive modulus was calculated from the linear region of stress-strain curve (0-10% strain). All measurements were carried out as quadruplicates for each set of parameters.

2.2.9 Mercury intrusion porosimetry (MIP)

Pore size distributions and internal pore surface area of two different types of A6ACA cryogels were evaluated by using mercury intrusion porosimetry (Micromertitics Autopore IV 9500 porosimeter). Briefly, the samples were dehydrated in 50%, 75% and

100% ethanol and dried using a critical point dryer (Tousimis AutoSamdri 815) and they were subjected to a pressure cycle starting at approximately 0.5 psia, increasing to 60000 psia.

2.2.10 Microcomputed tomography (MicroCT)

Spongy and columnar cryogels were prepared and washed for 24 hours in phosphate-buffered saline. Samples were then immersed in excess of a 5% solution of ferric chloride for 12 hours. Following immersion, cryogels were frozen at -80℃ for 1 hour and lyophilized for 24 hours. Internal microstructure was visualized by micro computed tomography (microCT) using 1076 Skycan High Resolution Micro CT Scanner (Skyscan, Belgium) at 9 μm pixel size. Reconstruction was carried out using NRecon software (Skyscan, Belgium), and coronal sections of 3D microstructure were constructed using DataViewer software (Skyscan, Belgium).

2.2.11 Cyrogels as cell scaffolds

The potential application of PEG cryogels as cell scaffolds has been evaluated using bovine chondrocytes (bCCs) and human mesenchymal stem cells (hMSCs). Prior to seeding cells, cryogels were sterilized with 70% ethanol and were washed with fresh PBS. The rinsed cryogels were coated with collagen type I solution (50μg/mL, BD bioscience, Cat# 354231) to improve cell adhesion prior to cell seeding. The cells were seeded onto the cryogels at a seeding density of 1×10^6 cells/cryogel. The cell-loaded cryogels having dimensions of 10 mm diameter and 5 mm height were incubated in a

growth medium (Dulbecco's Modified Eagle Medium [DMEM] containing 10% Fetal Bovine Serum [FBS]).

2.2.12 Cell viability test

Live/Dead assay was performed to evaluate the cell viability after 36 hours of cell seeding.[28] Briefly, cell-laden cryogels were cut into thin slices and incubated with the Live/Dead assay dye solution (Molecular Probes, Cat#L-3224), which contains 0.5µl of Calcein-AM and 2µl of Ethidium homodimer-1 in 1ml of DMEM. After 30 minutes of incubation, the slices were rinsed with PBS and images were obtained using fluorescence microscope.

2.2.13 Statistical analysis

All data are presented as mean ± standard deviation (SD). Single factor analysis of variance (ANOVA) with Tukey's Multiple Comparison Test was performed to determine statistical significance ($p < 0.05$).

2.3 Results and Discussion

2.3.1 Influence of polymerization conditions on cryogel structures

PEG cryogels were synthesized by radical polymerization of PEGDA having molecular weight (Mn) of 3400 using redox initiators APS/TEMED. In this study, we have used two different concentrations of TEMED, 0.05% and 0.1% w/v, to vary the rate of polymerization. Previous studies have demonstrated that high concentration of redox initiators in the reaction mixture enhances their rate of polymerization.[23, 29] In addition to TEMED concentration, we have also varied temperatures of cryogelation (-14℃ and -20℃), and degree of supercooling. We have chosen to vary the freezing temperature and degree of supercooling as they play a critical role in determining the network structure of cryogels due to their influence on both formation of polymer network and ice crystals.[22]

First the effect of TEMED mediated polymerization rate on formation of cryogels and their network structure was studied by varying the concentration of TEMED in the reaction mixture. Varying the rate of polymerization resulted in PEG cryogels with different microstructures. The PEGDA reaction mixture containing 0.1% w/v TEMED upon thawing after 20 hours at -20℃ formed a crosslinked network. The physical appearance of these networks along with their swelling/deswelling behavior suggests that they exhibit a heterogeneous microstructure. Our first observation was that only the top regions of these cryogels exhibited rapid absorption and release of water molecules, while maintaining a different swelling behavior for the bottom region. Additionally, at equilibrium swollen state these cryogels showed a heterogeneous shape; expanded top region with higher diameter compared to the bottom region (Fig. 2.1a). The

heterogeneous structure of these cryogels synthesized at -20℃ became more apparent in their dried state (Fig. 2.1b). These observations clearly suggest a heterogeneous network structure in which the top layer has a highly interconnected macroporous structure (cryogel-like structure) while the bottom layer has a closed network structure with small pores (hydrogel-like structure). Hereafter we refer to these heterogeneous cryogels as $I_{0.1}T_{-20}C_S$, where $I_{0.1}$ represents the amount of TEMED, T_{-20} represents the freezing temperature and C_S represents the slow cooling rate. The nomenclature used for various cryogels discussed in this study is tabulated in Table 2.1. The layered heterogeneous network structure of $I_{0.1}T_{-20}C_S$ was further confirmed by scanning electron microscopy (SEM) analysis (Fig. 2.1c-f). Fig. 2.1c and 1e-f show the side view of the $I_{0.1}T_{-20}C_S$ cryogel containing both cryogel-like and hydrogel-like structures within the same network, while Fig. 2.1d shows their internal network structure.

Table 2.1 Compositions and nomenclature of the cryogels.

Sample code	Amount (w/v) of TEMED	Temperature (^oC) of polymerization	Rate of Cooling
$I_{0.1}T_{-14}C_F$	0.1%	-14	Fast
$I_{0.1}T_{-20}C_F$	0.1%	-20	Fast
$I_{0.1}T_{-20}C_S$	0.1%	-20	Slow
$I_{0.05}T_{-14}C_F$	0.05%	-14	Fast
$I_{0.05}T_{-20}C_F$	0.05%	-20	Fast
$I_{0.05}T_{-20}C_S$	0.05%	-20	Slow
Conventional Hydrogels	0.05%	20	N/A

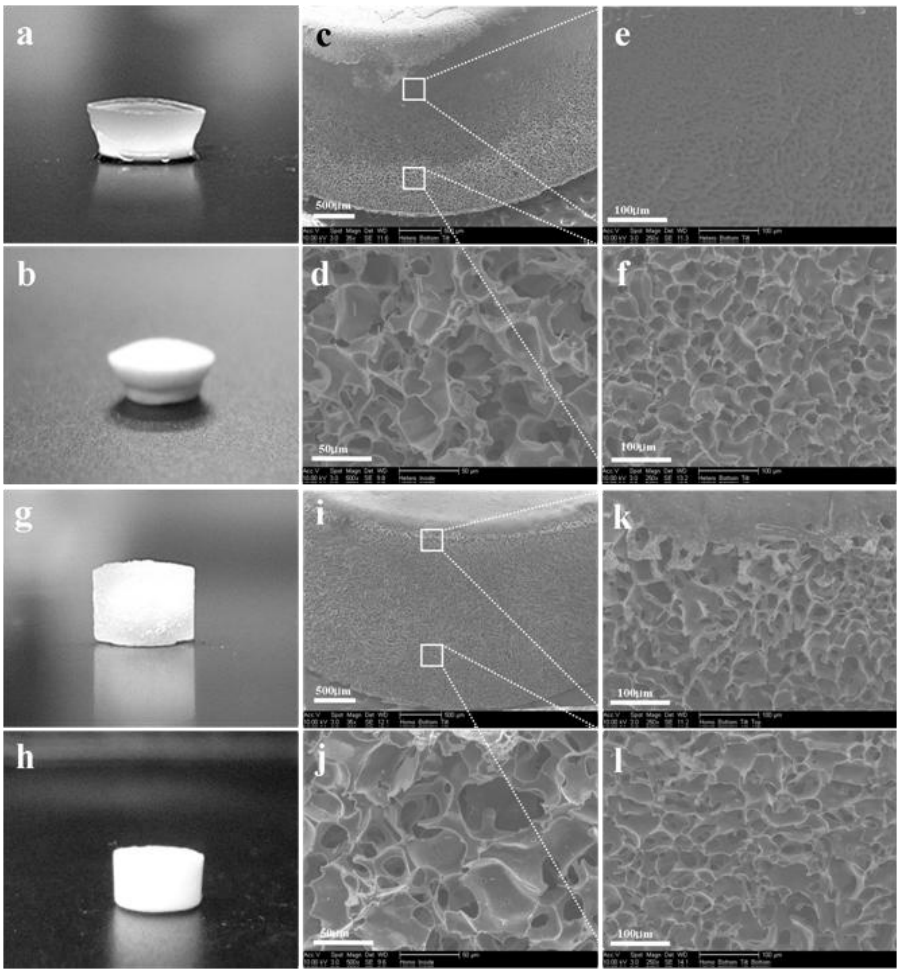


Fig. 2.1 Photographs (a, b, g, h) and SEM images (c-f, i-l) of heterogeneous cryogel ($I_{0.1}T_{-20}C_S$) and homogeneous cryogel ($I_{0.05}T_{-20}C_S$): (a, g) equilibrium swollen cryogels; (b, h) dried cryogels; (c, i), (e-f, k-l) side view of cryogels; and (d, j) internal fracture surface of cryogels.

In contrast, PEGDA reaction mixtures containing low amounts of TEMED concentration (0.05% w/v) resulted in a homogeneous network structure as indicated by their physical appearance and swelling behavior (Fig. 2.1g-h). These cryogels (referred to as $I_{0.05}T_{-20}C_S$) showed homogeneous swelling in PBS solution unlike their heterogeneous counterparts, $I_{0.1}T_{-20}Cs$. SEM analysis of these cryogels showed a highly interconnected macroporous structures with pore sizes ranging 30-100μm throughout the network (Fig. 2.1i). These pore sizes are slightly higher than those observed in $I_{0.1}T_{-20}C_S$ cryogel which has pore sizes in the range of 30-70μm in the cryogel layer. Figs. 2.1i-l show the internal network structures and the side view of $I_{0.05}T_{-20}C_S$. As seen from Figs. 2.1c and 2.1i, a thin layer of hydrogel of the order of 5-10μm at the bottom of the cryogel adjacent to the plastic mold was always observed irrespective of the experimental conditions. The corresponding thermogram for the cryogelation at -20^oC is shown in Fig. 2.2a, which shows that the cryogelation of $I_{0.05}T_{-20}C_S$ involved a degree of supercooling of 10.9°C with an onset of nucleation of ice after 12 minutes of incubation.

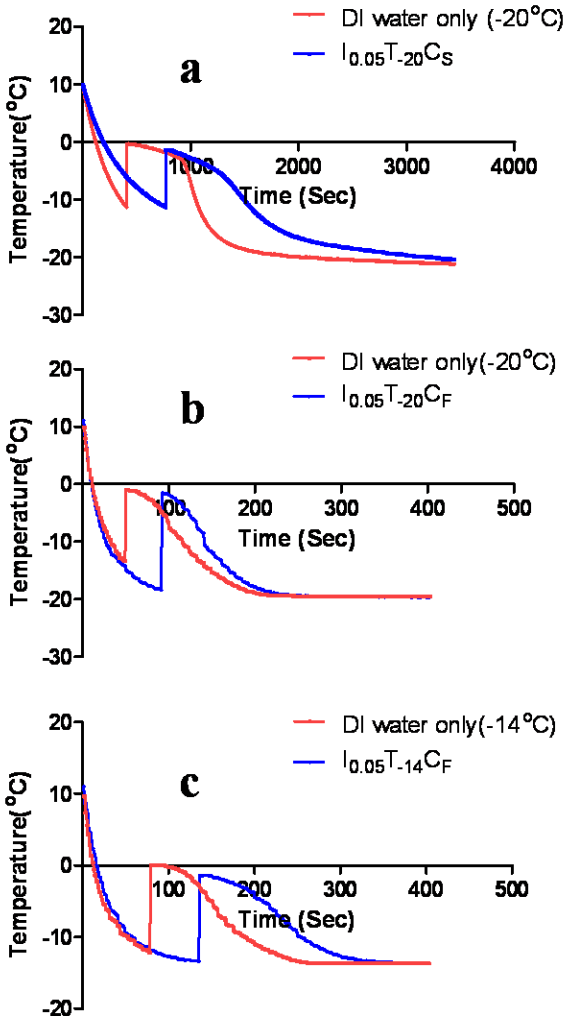


Fig. 2.2 Thermograms of cryogelation at different temperatures with reference to DI water. (a) $I_{0.05}T_{-20}C_S$ (b) $I_{0.05}T_{-20}C_F$ (c) $I_{0.05}T_{-14}C_F$.

The formation of heterogeneous network at high TEMED concentration could be explained based on a competition between rate of the nucleation of ice crystals and the rate of gelation. The process of cryogelation involves polymerization/gelation of the reaction mixture (unfrozen liquid phase containing high concentration of reactants) and the nucleation of ice crystals; the microstructures of cryogels are strongly dependent upon the kinetics of these two processes.[14, 22] In the case of heterogeneous cryogels, the presence of hydrogel-like structure is a result of gelation process proceeding at a faster rate than the nucleation of ice crystals.

The tight network formed due to faster gelation prevents distribution of the ice crystals formed, which acts as porogens to produce macroporous and interconnected pore structures, throughout the gel network. As a result, the few ice crystals formed float on the top due to their lower density compared to the liquid phase, thus yielding a layered network structure comprising of cryogel-like structure on the top and hydrogel-like structure at the bottom.

Since the degree of supercooling and onset of nucleation of ice crystals have critical roles in determining the microstructure of cryogels, we evaluated the effect of these parameters on microstructure of cryogels synthesized at -20^{o}C. As seen from Fig. 2.2b, we have used a faster cooling rate compared to the one described above for creating $I_{0.1}T_{-20}C_S$ and $I_{0.05}T_{-20}C_S$. The thermogram exhibits a degree of supercooling of 16.3°C and the nucleation of ice initiates at around 1.5 mins after their incubation (Fig. 2.2b). Irrespective of the faster cooling, the precursors containing higher amounts of TEMED again resulted in a heterogeneous cryogel exhibiting a layer of cryogel-like structure at the top and another layer of hydrogel-like structure at the bottom similar to $I_{0.1}T_{-20}C_S$

(Fig. 2.3). We refer to these cryogels as $I_{0.1}T_{-20}C_F$, where C_F indicates faster cooling rate. A close observation of the resulted cryogels indicates that the hydrogel layer of $I_{0.1}T_{-20}C_F$ is thinner as compared to s $I_{0.1}T_{-20}C_S$. The SEM analysis of $I_{0.1}T_{-20}C_F$ cryogel also shows a different internal structure where the cryogel-like structure exhibits a much smaller pore size (20-40μm) as compared to $I_{0.1}T_{-20}C_S$. A similar trend was observed in the case of cryogels synthesized using low TEMED concentration, where the internal structure of these homogeneous cryogels, $I_{0.05}T_{-20}C_F$, showed a more interconnected network structure with pore size of 20-50μm (Figs. 2.4-5). These smaller pore size could be attributed to the higher degree of supercooling, which results in ice crystals with smaller sizes.

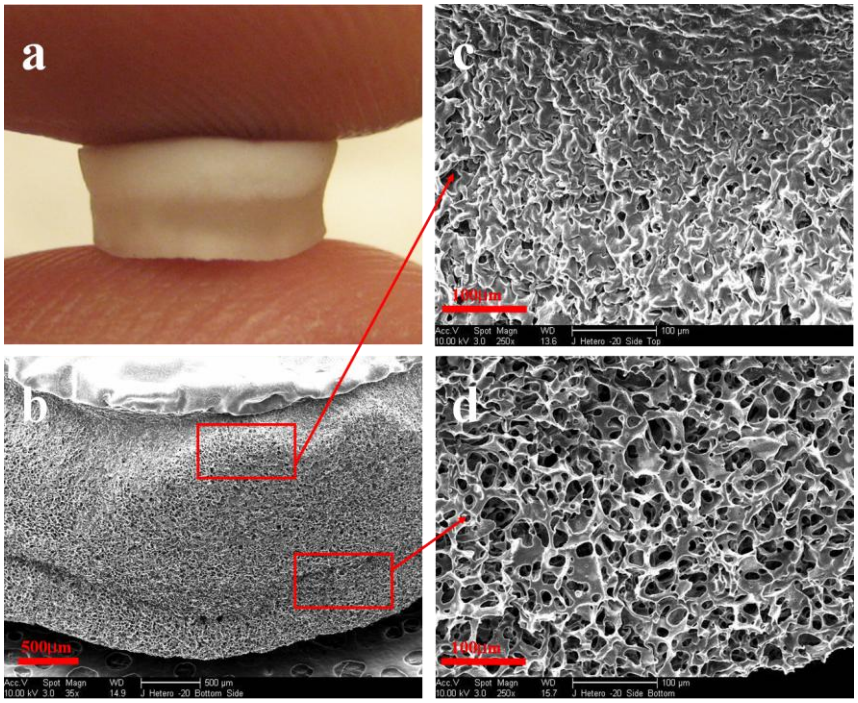


Fig. 2.3 Photograph (a) and SEM images (b-d) of $I_{0.1}T_{-20}C_F$.

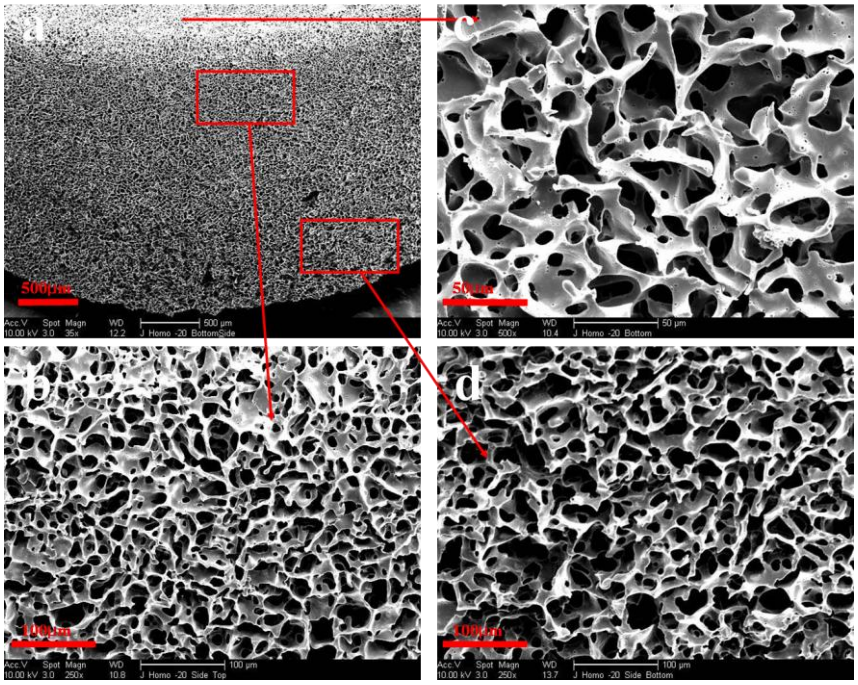


Fig. 2.4 SEM images of bottom and side view of $I_{0.05}T_{-20}C_F$.

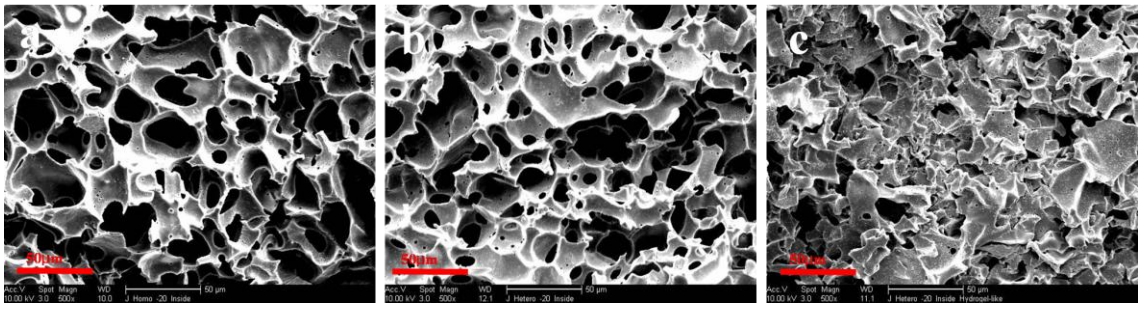


Fig. 2.5 SEM images of $I_{0.05}T_{-20}C_F$ and $I_{0.1}T_{-20}C_F$; (a) internal fracture surface of $I_{0.05}T_{-20}C_F$, (b) internal fracture surface of cryogel-like structure of $I_{0.1}T_{-20}C_F$, and (c) internal fracture surface of hydrogel-like structure of $I_{0.1}T_{-20}C_F$.

Having established the effect of the rate of gelation and degree of supercooling on cryogelation and their microstructure, we then evaluated the effect of freezing temperature on cryogel formation using two temperatures: -14℃ and -20℃. The reaction mixtures containing 0.1% w/v TEMED failed to form a cryogel at -14℃ unlike -20℃, but instead formed a conventional hydrogel-like structure (Fig. 2.6a). However, reaction mixtures containing low TEMED concentrations (0.05% w/v) resulted in cryogels with homogeneous network structures at -14℃ as shown in Fig. 2.6b. Fig. 2.6e-f show the side view of this homogeneous cryogel, $I_{0.05}T_{-14}C_F$. The pore sizes were observed to be in the range of 30-100μm and were bigger than those of $I_{0.05}T_{-20}C_{F,}$ but they were very similar to those of $I_{0.05}T_{-20}C_S$ (Fig. 2.6c). The similar pore size observed between $I_{0.05}T_{-14}C_F$ and $I_{0.05}T_{-20}C_S$ could be attributed to their similar degree of supercooling (12^oC) and the corresponding thermogram for $I_{0.05}T_{-14}C_F$ is shown in Fig. 2.2c. One of the significant differences between the cryogels formed at -14℃ and -20℃ ($I_{0.05}T_{-14}C_F$ and $I_{0.05}T_{-20}C_F$) is that the former appeared to have somewhat closed or disconnected structures while the latter showed continuous interconnected microstructures (Fig. 2.6d and Fig. 2.5a).

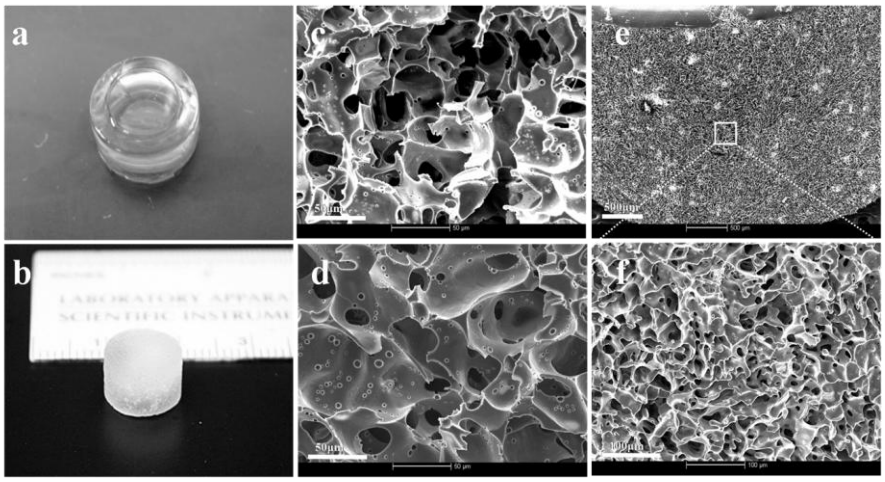


Fig. 2.6 Photographs (a-b) and SEM images (c-f) of hydrogels and homogeneous cryogels: (a) equilibrium swollen network, synthesized at -14^{o}C using 0.1% w/v TEMED; exhibited a hydrogel like appearance (b) equilibrium swollen homogeneous cryogel ($I_{0.05}T_{-14}C_F$), synthesized at -14^{o}C using 0.05% w/v TEMED (c) internal fracture surface of $I_{0.05}T_{-14}C_F$ exhibiting interconnected pores, and (d) internal fracture surface of $I_{0.05}T_{-14}C_F$ shows a closed pore structure (e-f) side view of $I_{0.05}T_{-14}C_F$.

Numerous studies have been attempted to understand the phenomena at the solid-liquid interface, where cellular or dendritic ice crystal structures were formed.[30-32] To create the directionality of internal pore structures, in this study, we have introduced the thin icy layer at the bottom of the mold as preferential nucleation sites without changing the precursor concentrations. In the presence of these preferential nucleation sites, the icy layer might provide higher amount of temperature gradient from top to the bottom than their counterparts which having the exact same precursor but more uniform temperature gradient. As a result, it promoted the growth of icy columns which were perpendicular to the solid-liquid interface as shown in Fig. 2.7a-d. Fig 2.7a-d showing top view and internal pore structures clearly demonstrated that A6ACA cryogels synthesized on top of icy layer have larger pore sizes at the top surface and also they have unidirectional columnar structures from top the bottom. On the other hand, their counterparts synthesized without preferential nucleation sites have more randomly oriented uniform pore structures throughout the constructs as shown in Fig. 2.7e-h. The different internal pore structures were also evaluated by using microCT analysis (Fig. 2.7i-j). In accordance with previous reports[33, 34], compared to spongy-like A6ACA cryogels (Fig. 2.7j), the presence and orientation of columnar pore structures were distinctively demonstrated as shown in Fig. 2.7i. To further investigate the internal pore structures, such as pore sizes and pore surface areas, we characterized their internal pore structures by mercury intrusion porosimetry. Although we columnar and spongy A6ACA cryogels have similar porosity (≈70%), we have observed larger pore sizes in columnar A6ACA cryogels, which correlates to SEM analysis (Fig. 2.8 and Table 2.2).

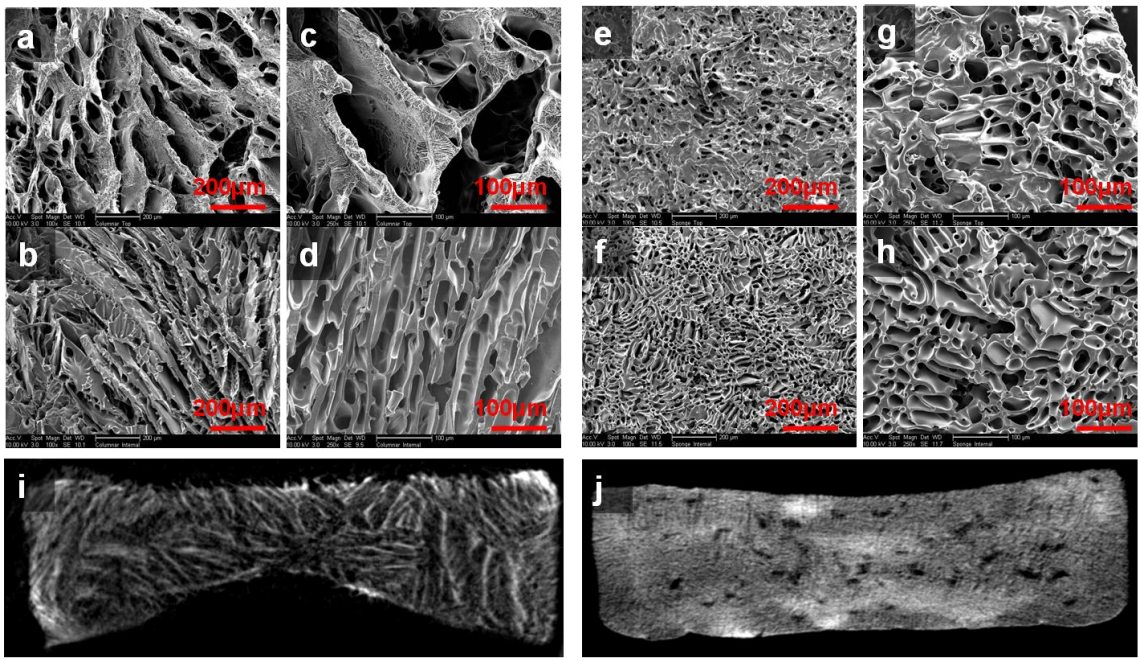


Fig. 2.7 SEM images (a-h) and microCT image (i-j) of columnar (a-d) and spongy (e-h) A6ACA cryogels: (a, c, e, g) top view of cryogels and (b, d, f, h) internal fracture surface of cryogels, and microCT images describing columnar (i) and spongy (j) internal pore structure.

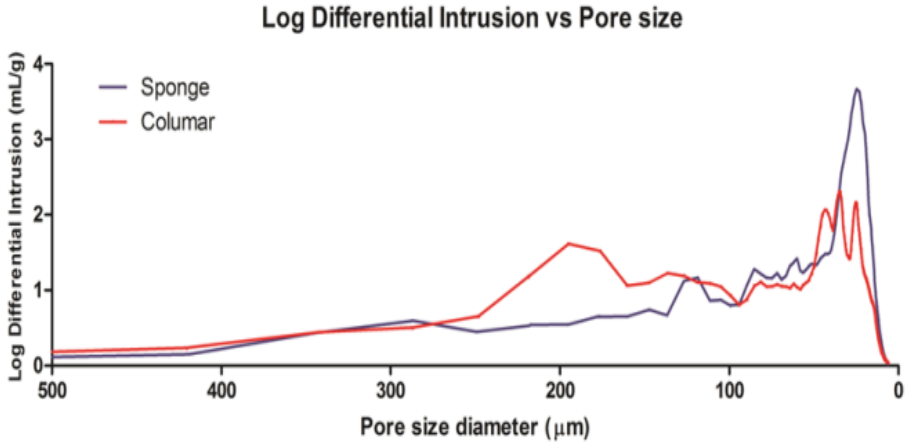


Fig. 2.8 Pore size distributions of sponge A6ACA (blue) and columnar A6ACA (red) cryogels.

Table 2.2 Physical properties of sponge A6ACA and columnar A6ACA cryogels obtained by MIP.

Properties	Sponge A6ACA	Columnar A6ACA
Total Pore Area	0.37±0.18m²/g	0.17±0.05m²/g
Median Pore Diameter (Volume)	28.27±11.99µm	60.07±16.36µm
Median Pore Diameter (Area)	19.27±6.88µm	30.37±7.75µm
Average Pore Diameter (4V/A)	26.69±10.59µm	45.56±9.93µm
Porosity	70.00±0.43%	69.58±4.51%

2.3.2 Swelling properties of cryogels

Synthesis of macroporous network structures has been adopted previously to improve the swelling-deswelling kinetics of various hydrogels.[35, 36] As seen from Fig. 2.3, the homogeneous cryogels, $I_{0.05}T_{-20}C_S$ and $I_{0.05}T_{-14}C_F$, undergo faster swelling kinetics than conventional hydrogels which show a gradual swelling over the time. These homogeneous cryogels ($I_{0.05}T_{-20}C_S$ and $I_{0.05}T_{-14}C_F$), irrespective of their differences in cryogelation procedure, had similar equilibrium swelling and exhibited similar swelling kinetics (Table 2.3 and Fig. 2.9). The cryogels reached equilibrium swelling within 1−2 minutes. In contrast, corresponding conventional hydrogels synthesized at room temperature, took almost 12 hours to reach the equilibrium swelling and showed much smaller equilibrium swelling ratios than homogeneous cryogels (Table 2.3). The equilibrium swelling ratios of heterogeneous cryogels, $I_{0.1}T_{-20}C_S$, were found to be higher than conventional hydrogels but lower than homogeneous cryogels ($I_{0.05}T_{-20}C_S$ and $I_{0.05}T_{-14}C_F$). Further probing of the swelling kinetics of heterogeneous cryogels, $I_{0.1}T_{-20}C_S$, showed that they exhibit a two step swelling. Upon immersion of dried $I_{0.1}T_{-20}C_S$ in PBS

solution, the cryogel-like top region was found to undergo rapid swelling, while the hydrogel-like bottom region underwent slow swelling. To further clarify this, we dissected the two layers of these heterogeneous cryogels and evaluated their swelling independently. Indeed the cryogel-like top structure showed a rapid swelling, characteristic of macroporous cryogel structure, while the bottom layer having hydrogel-like structure showed slower swelling similar to the conventional hydrogels. Therefore, the observed swelling behavior of heterogeneous cryogels is a combination of swelling behaviors from cryogel-like structure and hydrogel-like structures.

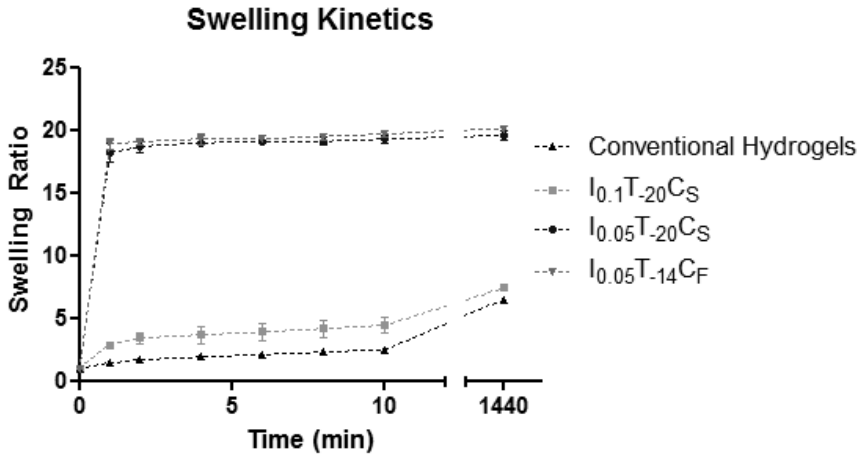


Fig. 2.9 Swelling kinetics of conventional hydrogels, and the heterogeneous ($I_{0.1}T_{-20}C_S$) and homogeneous cryogels ($I_{0.05}T_{-20}C_S$ and $I_{0.05}T_{-14}C_F$). (From t=1min to t=1440min, * $p < 0.05$ for all cryogels compared to conventional hydrogels; ** $p < 0.05$ for comparison between $I_{0.05}T_{-20}C_S$ and $I_{0.1}T_{-20}C_S$ for whole period of time)

Table 2.3 Mechanical properties of conventional hydrogels, heterogeneous ($I_{0.1}T_{-20}C_S$) and homogeneous cryogels ($I_{0.05}T_{-20}C_S$ and $I_{0.05}T_{-14}C_F$). (* $p < 0.05$ for $I_{0.05}T_{-20}C_S$ and $I_{0.05}T_{-14}C_F$ compared to conventional hydrogels; † $p > 0.05$ for comparison between $I_{0.1}T_{-20}C_S$ and conventional hydrogels; ** $p < 0.05$ for comparison between $I_{0.05}T_{-20}C_S$ and $I_{0.1}T_{-20}C_S$; †† $p > 0.05$ for comparison between $I_{0.05}T_{-20}C_S$ and $I_{0.1}T_{-20}C_S$)

Entry	Toughness (kJ/m^3)	Stress at break (MPa)	Strain at break (%)	Compressive modulus (kPa)	Equilibrium swelling ratio
Conventional Hydrogel	21.93±5.50	0.14±0.04	53.74±4.02	57.04±3.48	6.49±0.17
$I_{0.1}T_{-20}C_S$	38.95±12.33$^{\dagger, **}$	0.39±0.14$^{\dagger, **}$	72.94±9.24$^{*, **}$	24.17±3.16$^{*, \dagger\dagger}$	7.43±0.26$^{*, **}$
$I_{0.05}T_{-20}C_S$	71.33±9.12$^{*, **}$	1.62±0.16$^{*, **}$	91.70±0.64$^{*, **}$	18.60±1.13$^{*, \dagger\dagger}$	19.60±0.42$^{*, **}$
$I_{0.05}T_{-14}C_F$	61.64±7.34*	1.30±0.19*	85.86 ±1.17*	25.60±1.33*	20.14±0.07*

2.3.3 Mechanical properties of cryogels

We then evaluated the effect of network microstructure on their mechanical properties. Compared to conventional hydrogels, heterogeneous and homogeneous cryogels exhibited lower compressive moduli (Table 2.3). Among the homogeneous cryogels, $I_{0.05}T_{-14}C_F$ had a higher compressive modulus than that of $I_{0.05}T_{-20}C_S$. The compressive moduli of these cryogels were very close to those of heterogeneous cryogels, $I_{0.1}T_{-20}C_S$. Conventional hydrogels showed 53.74% of deformation and 0.14 MPa of maximum stress thereby exhibiting brittle mechanical properties. In contrast, heterogeneous and homogeneous cryogels showed larger deformations and fracture stress (Table 2.3). The $I_{0.05}T_{-14}C_F$ cryogels exhibited a deformation of 85.86% and a fracture stress of 1.30 MPa, whereas deformation and fracture stress of $I_{0.05}T_{-20}C_S$ cryogels were measured to be 91.70% and 1.62 MPa, respectively. The $I_{0.1}T_{-20}C_S$ cryogels exhibited a large deformation of up to 72.94% with a fracture stress of 0.39 MPa. The higher compressive modulus of $I_{0.05}T_{-14}C_F$ over $I_{0.05}T_{-20}C_S$ could be attributed to their closed macroporous network structure. The higher compressive modulus of $I_{0.1}T_{-20}C_S$ could be

attributed to the hydrogel like structure of the bottom region of these cryogels. During the mechanical measurements, we consistently observed that the cracks were initiated at the hydrogel-like layer and not at the cryogel-like layer. While the hydrogel-like structure contributes to the higher compressive modulus of heterogeneous cryogels, the cryogel-like structure contributes to their larger deformations, which were lower than those of homogeneous cryogels ($I_{0.05}T_{-20}C_S$ and $I_{0.05}T_{-14}C_F$) but significantly higher than that of conventional hydrogels.

The equilibrium swollen cryogels were easily compressed during which the cryogels expelled the imbibed PBS. The rapid deswelling of these networks under stress is attributed to their highly interconnected macroporous structure. In the case of heterogeneous cryogels, rapid deswelling was observed only in the top region while the bottom region retained the imbibed water (data not shown).

2.3.4 Cytocompatibility of cryogels

In order to investigate the potential of the PEG cryogels as cell scaffolds for tissue engineering, we evaluated the response of cells to the scaffold using both bovine chondrocytes (bCCs) and human mesenchymal stem cells (hMSCs). As seen in Fig. 2.10a, the PEG cryogels coated with collagen type I provided structural support for the attachment of chondrocytes and most of the chondrocytes were viable after 36 hours of culture. The seeded cells migrated and homogeneously distributed within the homogeneous cryogels like $I_{0.05}T_{-20}C_S$. A similar behavior was observed in the case of hMSCs (data not shown). In the case of heterogeneous cryogels ($I_{0.1}T_{-20}C_S$), the cells were found to be confined within the cryogel layer, unlike homogenous cryogels where

the cells were distributed within the entire network. The distribution of seeded cells within the cryogels was observed even in the absence of collagen type 1 coating. However the number of cells distributed after 36 hours of cell seeding was found to be lower than that of the corresponding collagen type 1 coated cryogels. As seen from Fig. 2.10b, a time dependent increase in chondrocyte proliferation was observed in cryogels, and it could be due to the high surface area and available pore size.

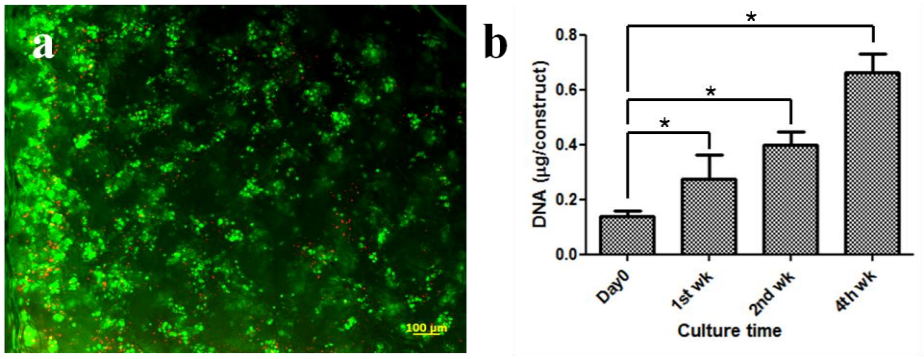


Fig. 2.10 (a) Live/Dead assay of chondrocyte-loaded cryogel ($I_{0.05}T_{-20}C_S$) after 36 hours of cell seeding (b) Results of DNA assay showing the amount of DNA with culture time using $I_{0.1}T_{-20}C_S$ cryogels as cell scaffolds. (* $p < 0.05$ for 1st, 2nd and 4th week of DNA amount compared to Day0)

2.4 Conclusion

PEG cryogels with similar chemical composition but distinctly different microstructures were synthesized by manipulating the kinetics of polymerization. The effect of freezing temperature and degree of supercooling on cryogel formation and their microstructure was also evaluated. We showed for the first time that monolithic heterogeneous networks containing both cryogel-like and hydrogel-like structures can be synthesized using cryogelation techniques by manipulating the polymerization kinetics. The ability to control the microstructure of cryogels via concentration of the initiator (accelerator) introduces a new "knob" to manipulate the structural properties of such materials. Using the same approach with slight modification, i.e., introduction of preferential nucleation sites, we have successfully controlled the directionality and geometry of internal pore structures without altering precursor concentrations. We also found that the mechanical and swelling properties of the cryogels were strongly dependent upon their network microstructure. These highly elastic interconnected macroporous structures could undergo large deformation without altering their structural properties. The tunable structural and mechanical properties, high elasticity, swelling behavior favoring enhanced mass transport of PEG cryogels along with their ability to support cell growth make them excellent scaffolds for cell and tissue engineering.

2.5 Acknowledgments

This chapter, in full, is a reprint of the material as it appears in Journal of Materials Chemistry, Volume 20, 2010. Hwang, Yongsung; Zhang, Chao; Varghese, Shyni. The dissertation author was the primary investigator and author of this paper.

2.6 References

1. Varghese, S. and J.H. Elisseeff, *Hydrogels for musculoskeletal tissue engineering.* Polymers for Regenerative Medicine, 2006: p. 95-144.

2. Hoffman, A.S., *Hydrogels for biomedical applications.* Adv Drug Deliv Rev, 2002. **54**(1): p. 3-12.

3. Peters, M.C. and D.J. Mooney, *Synthetic extracellular matrices for cell transplantation.* Porous Materials for Tissue Engineering, 1997. **250**: p. 43-52.

4. Kim, B.S. and D.J. Mooney, *Development of biocompatible synthetic extracellular matrices for tissue engineering.* Trends in Biotechnology, 1998. **16**(5): p. 224-230.

5. Mooney, D.J., et al., *Novel approach to fabricate porous sponges of poly(D,L-lactic-co-glycolic acid) without the use of organic solvents.* Biomaterials, 1996. **17**(14): p. 1417-22.

6. Mikos, A.G., et al., *Preparation of poly(glycolic acid) bonded fiber structures for cell attachment and transplantation.* J Biomed Mater Res, 1993. **27**(2): p. 183-9.

7. Bennett, D.J., et al., *Synthesis of Porous Hydrogel Structures by Polymerizing the Continuous-Phase of a Microemulsion.* Polymer International, 1995. **36**(3): p. 219-226.

8. Nam, Y.S. and T.G. Park, *Biodegradable polymeric microcellular foams by modified thermally induced phase separation method.* Biomaterials, 1999. **20**(19): p. 1783-1790.

9. O'Brien, F.J., et al., *The effect of pore size on cell adhesion in collagen-GAG scaffolds.* Biomaterials, 2005. **26**(4): p. 433-41.

10. Mikos, A.G., et al., *Preparation and Characterization of Poly(L-Lactic Acid) Foams.* Polymer, 1994. **35**(5): p. 1068-1077.

11. Mikos, A.G., et al., *Laminated three-dimensional biodegradable foams for use in tissue engineering.* Biomaterials, 1993. **14**(5): p. 323-30.

12. Plieva, F.M., et al., *Cryogel applications in microbiology.* Trends in Microbiology, 2008. **16**(11): p. 543-551.

13. Lozinsky, V.I., et al., *Polymeric cryogels as promising materials of biotechnological interest.* Trends in Biotechnology, 2003. **21**(10): p. 445-451.

14. Kathuria, N., et al., *Synthesis and characterization of elastic and macroporous chitosan-gelatin cryogels for tissue engineering.* Acta Biomater, 2009. **5**(1): p. 406-18.

15. Bolgen, N., et al., *Three-Dimensional Ingrowth of Bone Cells within Biodegradable Cryogel Scaffolds in Bioreactors at Different Regimes.* Tissue Eng Part A, 2008.

16. Arvidsson, P., et al., *Direct chromatographic capture of enzyme from crude homogenate using immobilized metal affinity chromatography on a continuous supermacroporous adsorbent.* Journal of Chromatography A, 2003. **986**(2): p. 275-290.

17. Plieva, F.M., et al., *Characterization of polyacrylamide based monolithic columns.* Journal of Separation Science, 2004. **27**(10-11): p. 828-836.

18. Bryant, S.J. and K.S. Anseth, *Hydrogel properties influence ECM production by chondrocytes photoencapsulated in poly(ethylene glycol) hydrogels.* Journal of Biomedical Materials Research, 2002. **59**(1): p. 63-72.

19. Bryant, S.J., et al., *Crosslinking density influences chondrocyte metabolism in dynamically loaded photocrosslinked poly(ethylene glycol) hydrogels.* Annals of Biomedical Engineering, 2004. **32**(3): p. 407-417.

20. Bryant, S.J., C.R. Nuttelman, and K.S. Anseth, *The effects of crosslinking density on cartilage formation in photocrosslinkable hydrogels.* Biomed Sci Instrum, 1999. **35**: p. 309-14.

21. Phadke, A., et al., *Templated Mineralization of Synthetic Hydrogels for Bone-Like Composite Materials: Role of Matrix Hydrophobicity.* Biomacromolecules, 2010. **11**(8): p. 2060-2068.

22. Plieva, F., et al., *Macroporous elastic polyacrylamide gels prepared at subzero temperatures: control of porous structure.* Journal of Materials Chemistry, 2006. **16**(41): p. 4065-4073.

23. Yao, K.J., et al., *Preparation of polyacrylamide-based supermacroporous monolithic cryogel beds under freezing-temperature variation conditions.* Chemical Engineering Science, 2006. **61**(20): p. 6701-6708.

24. Hern, D.L. and J.A. Hubbell, *Incorporation of adhesion peptides into nonadhesive hydrogels useful for tissue resurfacing.* Journal of Biomedical Materials Research, 1998. **39**(2): p. 266-276.

25. Varghese, S., et al., *Role of hydrophobicity on structure of polymer-metal complexes.* Journal of Physical Chemistry B, 2001. **105**(23): p. 5368-5373.

26. Ayala, R., et al., *Engineering the cell-material interface for controlling stem cell adhesion, migration, and differentiation.* Biomaterials, 2011. **32**(15): p. 3700-11.

27. Bhalerao, V.S., et al., *Thermoreversible hydrogel based on radiation induced copolymerisation of poly(N-isopropyl acrylamide) and poly(ethylene oxide).* Polymer, 1998. **39**(11): p. 2255-2260.

28. Hwang, N.S., S. Varghese, and J. Elisseeff, *Cartilage tissue engineering: Directed differentiation of embryonic stem cells in three-dimensional hydrogel culture.* Methods Mol Biol, 2007. **407**: p. 351-73.

29. Duan, S.F., et al., *Negative cooperative effect of cytotoxicity of a di-component initiating system for a novel injectable tissue engineering hydrogel.* Chinese Science Bulletin, 2005. **50**(11): p. 1093-1096.

30. Rubinsky, B., *Solidification Processes in Saline Solutions.* Journal of Crystal Growth, 1983. **62**(3): p. 513-522.

31. Rubinsky, B., C. Lee, and M. Chaw, *Experimental-Observations and Theoretical-Studies on Solidification Processes in Saline Solutions.* Experimental Thermal and Fluid Science, 1993. **6**(2): p. 157-167.

32. Wegst, U.G.K., et al., *Biomaterials by freeze casting.* Philosophical Transactions of the Royal Society a-Mathematical Physical and Engineering Sciences, 2010. **368**(1917): p. 2099-2121.

33. Butler, M.F., *Instability formation and directional dendritic growth of ice studied by optical interferometry.* Crystal Growth & Design, 2001. **1**(3): p. 213-223.

34. Butler, M.F., *Growth of solutal ice dendrites studied by optical interferometry.* Crystal Growth & Design, 2002. **2**(1): p. 59-66.

35. Chen, J. and K. Park, *Superporous hydrogels: Fast responsive hydrogel systems.* Journal of Macromolecular Science-Pure and Applied Chemistry, 1999. **A36**(7-8): p. 917-930.

36. Bolgen, N., et al., *Cryogelation for preparation of novel biodegradable tissue-engineering scaffolds.* Journal of Biomaterials Science-Polymer Edition, 2007. **18**(9): p. 1165-1179.

CHAPTER 3: Interconnected macroporous poly(ethylene glycol) (PEG) cryogels as a cell scaffold for cartilage tissue engineering

"Knowledge cultivates your seeds and does not sow in your seeds."

- Kahlil Gibran

This chapter, in full, is a reprint of the material as it appears in Tissue Engineering Part C, Volume 16, 2010. Hwang, Yongsung; Sangaj, Nivedita; Varghese, Shyni. The dissertation author was the primary investigator and author of this paper.

3.1 Introduction

Articular cartilage provides low-friction load-bearing surfaces for smooth function of joints but has a limited intrinsic regeneration and self-healing capacity due to its innate avascular nature.[1, 2] Tissue engineering approaches have been touted to play an important role in the treatment of articular cartilage defects, where both scaffolds and cells are critical for the regeneration of functional tissues.[3-7] Hydrogel-like structures are considered as ideal scaffolds for cartilage tissue engineering mainly due to their structural similarities with native cartilage tissue.[8, 9] However, hydrogels typically exhibit a closed network structure, and it would be advantageous to utilize hydrophilic networks with interconnected macroporous structures to promote mass transfer properties and provide increased surface areas for cell attachment and proliferation.[10-13] As a result, macroporous hydrogel scaffolds have been developed using various techniques

such as fiber bonding, gas foaming, micro-emulsion formation, phase separation, freeze-drying, and porogen leaching.[11, 14-20]

More recently, gelation technique at subzero temperatures, known as ‘cryogelation’ has been employed to create hydrogels with macroporous interconnected microstructures. During cryogelation at subzero temperatures, the reactants restricted to the unfrozen/semi-frozen phases form the crosslinked network, while ice crystals nucleated from the aqueous phase (formed by the freezing of water at low temperatures) function as porogens. The melting of these ice crystals at temperature above the freezing temperature (e.g. room temperature) gives rise to interconnected macroporous networks.[21] The resultant cryogels show enhanced mechanical properties and swelling kinetics.[22, 23] Recent studies have shown the potential application of cryogels as scaffolds, owing to their hydrophilicity and macroporous interconnected microstructures.[24] For instance, Kathuria *et al.* reported that chitosan-gelatin cryogels promoted the attachment and proliferation of fibroblasts (Cos-7).[25] Bolgen *et al.* have demonstrated the ingrowth and biosynthetic activity of osteoblast-like cells (MG63) within biodegradable 2-hydroxyethyl methacrylate (HEMA)-lactate-dextran cryogels.[26]

Recently, we have synthesized interconnected macroporous PEG cryogels with varying microstructures by manipulating either the rate of polymerization, freezing temperature, or degree of supercooling.[27] In this study, we evaluated the potential of these PEG cryogels as scaffold for engineering cartilage tissue using primary bovine chondrocytes.

3.2 Materials and Methods

3.2.1 Materials

Toluene and triethylamine were purchased from Fisher Scientific and dichloromethane and diethyl ether were purchased from Sigma-Aldrich. Poly(ethylene glycol) (PEG) (Mn 3400) and acryloyl chloride were purchased from Aldrich and were used without further purification. Ammonium persulfate (APS) and N, N, N', N'-tetramethylethylenediamine (TEMED) were obtained from Sigma. Live/Dead Viability/Cytotoxicity Kit (Molecular Probes, Cat#L-3224) for cell viability test and Quanti-iT^{TM} PicoGreen® dsDNA Assay Kit (Molecular Probes, Cat# P7589) for DNA assay were purchased from Molecular Probes. Collagenase type II (Cat# 4177) and papain (Cat# LS003126) were purchased from Worthington Biochemical Corporation.

3.2.2 Synthesis of PEGDA oligomer

Poly(ethylene glycol) diacrylate (PEGDA) oligomers were prepared as described elsewhere.[28] Briefly, 18.0g of PEG was dissolved in 300mL of toluene in a 500mL round bottom flask in an oil bath at 150℃. The solution was then refluxed for 4 hours under vigorous stirring. Trace amounts of water in the reaction mixture were removed by azeotropic distillation. Upon cooling the solution to room temperature, 3.262g (32.2mmol) of triethylamine was added with vigorous stirring. The flask was then moved to an ice bath and stirred for 30 minutes. 2.918g (32.2mmol) of acryloyl chloride in 15mL of anhydrous dichloromethane was then added to the reaction mixture drop wise for 30 minutes. After keeping the reaction mixture in an ice bath for another 30 minutes, the

flask was heated to 45℃ overnight. The reaction mixture was then cooled to room temperature and the quaternary ammonium salt was removed from the reaction mixture by filtering through diatomaceous earth (2-3cm) on a fritted glass funnel. The filtrate was condensed using a rotary evaporator and then precipitated in excess diethyl ether. The white precipitate was collected and vacuum dried at 40℃ for 24 hours. The resultant PEGDA oligomer was purified by precipitation followed by column chromatography and dialysis prior to its usage.

3.2.3 Preparation of PEG cryogels

PEGDA oligomers were dissolved in Phosphate Buffered Saline (PBS) to prepare a solution of 10%w/v. At 4℃, the initiator-accelerator mixture [0.5%w/v of ammonium persulfate (APS) and 0.05%w/v of N,N,N’,N’-tetramethylethylenediamine (TEMED)] were added to this solution, and the reaction mixture was polymerized at -20℃ for 20 hours. The gelled reaction mixture was thawed at room temperature that resulted in the formation of interconnected macroporous network (cryogels). The cryogels were washed with excess water to remove the unreacted reactants. Cryogels were synthesized in cylindrical forms having diameter and height of 10 mm and 5 mm, respectively.

3.2.4 Scanning electron microscopy (SEM) of cryogels

The microstructures of PEG cryogels were examined using a scanning electron microscopy (SEM, Philips XL30 ESEM). Briefly, thin slices of constructs were cut vertically from the center of the construct. The slices were then dehydrated serially in 50%, 75% and 100% ethanol and dried using a critical point dryer (Tousimis AutoSamdri

815). The dried sections were gold-coated using a sputter coater (Emitech K575X Sputter Coater) for 30 seconds prior to SEM imaging.

3.2.5 Isolation of chondrocytes

Chondrocytes were isolated as described elsewhere.[29] In brief, full thickness articular cartilage (AC) was dissected from the patellofemoral groove and distal femoral condyles of 6-8 week old bovine legs. The cartilage pieces were dissected and incubated in Dulbecco's Modified Eagle's Medium (DMEM, GIBCO, Grand Island, NY, U.S.A.) containing 0.2% collagenase (Worthington Biochemical Corporation, Lakewood, NJ, U.S.A) and 5% fetal bovine serum (Atlanta Biologicals, GA, USA) for 16 hours at 37℃ with 5% CO_2 to isolate chondrocytes. The cell suspension was then filtered through a 70µm nylon cell strainer (BD Falcon, CA, USA) and washed with PBS containing 100U/ml penicillin and 100µg/ml streptomycin. The isolated chondrocytes (primary chondrocytes) were used without any further *ex vivo* expansion.

3.2.6 Chondrocytes seeding and culture on PEG cryogels

Before seeding chondrocytes, cryogels were sterilized with 70% ethanol and washed with fresh PBS. The cryogels were then coated with collagen type I by immersing them in 50µg/mL of collagen type I solution (BD Bioscience, Cat# 354231) to improve cell adhesion prior to cell seeding. The cryogels were partially dehydrated under sterile conditions for 3 hours before cell seeding. The partially dehydrated cryogels had a swelling ratio of 10.07±0.77 (g/g) compared to their equilibrium swelling ratio of 19.93 ±0.03 (g/g). Cell seeding on the cryogels was done by adding cell suspension in drop-

wise manner. Briefly, isolated chondrocytes were suspended in chondrocyte medium (2.5 x 10^7 cells/mL) [DMEM supplemented with 10% FBS, 0.04mM L-proline (Sigma), 50μg/ml ascorbic acid (Sigma), 0.1mM non-essential aminoacid (GIBCO), and 100U/ml penicillin and 100μg/ml streptomycin]. 40μL of cell suspension containing 1 x 10^6 cells was seeded on the top surface of the partially hydrated cryogel at various spots, and incubated for two hours to allow their infiltration. The cell-loaded cryogels were then cultured in 2mL of chondrocyte medium, and the medium was changed every two days. All the cell cultures were done at 37^{o}C in 5% CO_2 environment.

3.2.7 Cell viability test

A Live/Dead assay was performed to evaluate the cell viability after 36 hours of *in vitro* cultivation.[30] Briefly, the cell-laden cryogels were vertically cut into thin slices from the center of the construct and incubated with the Live/Dead assay dye solution (Molecular Probes, Cat#L-3224) containing 0.5μL of Calcein-AM and 2μL of Ethidium homodimer-1 in 1mL of DMEM. After 30 minutes of incubation, the slices were rinsed with PBS and cell viability was examined using a fluorescence microscope (Carl Zeiss, Axio Observer A1).

3.2.8 Biochemical Assays

Biochemical assays were performed on cell-laden cryogels as a function of culture time (1st, 2nd and 4th week). At each time point, constructs were lyophilized for 24 hours and then digested with 1mL of papain solution [125μg/mL papain (Worthington biochemical corporation, Cat# LS003126), 10mM $_L$-cysteine (Sigma, Cat# 7352),

100mM phosphate, and 10mM EDTA at pH 6.3] for 16 hours at 60^{o}C as previously reported.[31] The deoxyribonucleic acid (DNA) content was measured by PicoGreen DNA assay as described by Dadsetan *et al*.[32] and the amount of DNA was converted into the number of chondrocytes using conversion factor of 7.7pg of DNA per chondrocyte.[33] The glycosaminoglycan (GAG) content was determined using dimethylmethylene blue (DMMB) spectrophotometric assay at 525nm, in which chondroitin sulfate C was used to establish the standard curve as previously described.[34] The collagen content was determined by measuring the hydroxyproline content of samples by following an established method.[35] The collagen content for acellular cryogels coated with collagen type I was also investigated; however, it was below the detection level.

3.2.9 Histological and immunohistochemical analysis

The chondrocyte-laden cryogels were divided into two vertical halves, fixed overnight with 4% paraformaldehyde, and embedded in paraffin. The paraffin embedded constructs were processed into 20 μm sections and the sections corresponding to the center of the constructs were used for staining. Before staining, paraffin-embedded sections were deparaffinized with xylene, rehydrated with graded series of ethanol and washed with fresh Millipore water. For histological analysis, sections were stained with Safranin-O and Hematoxylin & Eosin (H&E). Immunohistochemical staining for collagen type II was also performed by following a previously reported method.[36] Briefly, rehydrated samples were blocked with 0.5% Triton X-100 in 3% Bovine Serum Albumin (BSA, Sigma, Cat# A7906) in PBS for 1 hour and incubated with rabbit

polyclonal antibodies against type I and type II collagen (Fitzgerald, Cat# 70R-CR007X and Cat# 70R-CR008X, respectively) at 1:300 dilution. These sections were incubated with goat anti-rabbit IgG secondary antibodies (Alexa Fluor® 488) at 1:250 dilution for 1 hour and then the nuclei were counterstained with 4',6-diamidino-2-phenylindole (DAPI) (Vector laboratories, Inc., Burlingame, CA) for 30 minutes. Images were observed using a fluorescent microscope.

3.2.10 Statistical Analysis

The data obtained from all biochemical assays of quadruplicate samples were presented as mean ± standard deviation (SD). Single factor analysis of variance (ANOVA) with Tukey's Multiple Comparison Test was performed to determine statistical significance ($p < 0.05$).

3.3 Results and Discussion

3.3.1 Synthesis and Characterization of PEG cryogels

Interconnected macroporous network structures have been known to support cell growth and matrix production.[10-13] Previously, we have reported the development and characterization of interconnected macroporous PEG cryogels using cryogelation techniques. Such cryogels can withstand larger deformation, exhibit higher fracture stresses, and undergo rapid re-swelling upon immersion in aqueous solution.[27] Similar to hydrogels, cryogels also have hydrophilic networks; however, they have interconnected porous network structures unlike conventional hydrogels that exhibit closed pores. Although the studies we reported previously showed the ability of PEG cryogels to support cell culture[27], their ability to function as tissue engineering scaffolds remains to be explored. In the present study, we have investigated the potential of PEG cryogel scaffolds for cartilage tissue engineering using primary bovine chondrocytes.

Fig. 3.1 shows the gross image of a PEG cryogel. The equilibrium swollen PEG cryogels were easily compressed by fingers without breaking and imbibed PBS could be expelled (Fig. 3.1a-b). Completely compressed cryogels showed a sponge-like appearance and could re-swell immediately upon immersion in PBS (Fig. 3.1c-d).

The internal morphology of PEG cryogels is presented in Fig. 3.2. As seen from the SEM image, PEG cryogels have an interconnected pore structure with pore sizes in the range of 30-80µm (Fig. 3.2a). The interconnected macroporous structure was further investigated by a phase contrast microscope using a cryosectioned, cell-laden cryogel section of 20 µm thick (Fig. 3.2b). Live/dead assay showed that the seeded chondrocytes

were distributed throughout the cryogel network and majority of these cells were viable (Fig. 3.2c).

The dropwise addition of cell suspension along with the interconnected macroporous network structures and the ability of cryogels to rapidly imbibe aqueous solutions (Fig. 3.1 and 3.2) promoted the homogeneous distribution of cells within the cryogel upon seeding with minimal detrimental effects to cells. The high cell survivability observed is in agreement with previously reported studies involving dropwise seeding of cells.[37]

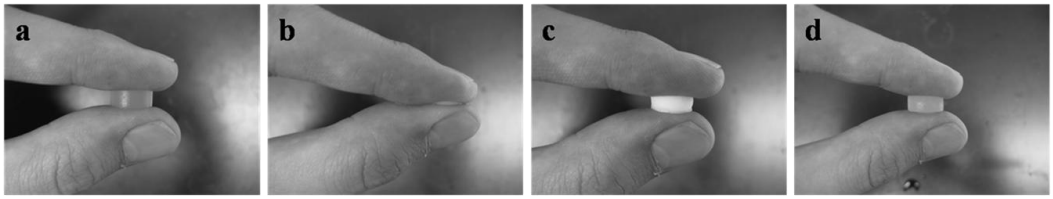


Fig. 3.1 Photographs of PEG cryogels: (a) equilibrium swollen cryogel (b) cryogel compressed between fingers (c) compressed cryogel showing a sponge-like appearance upon removal of force (d) re-swollen cryogel upon immersion in PBS.

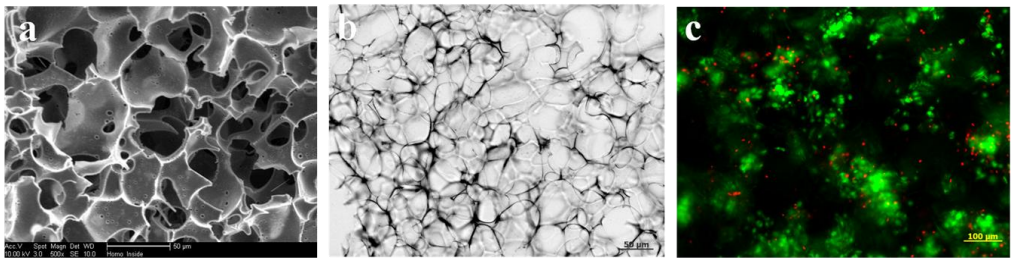


Fig. 3.2 (a) SEM image of internal fracture surface of cryogel (scale bar = 50µm) (b) phase contrast microscope image (scale bar = 50µm) (c) live/dead assay of chondrocyte-laden cryogel after 36 hours of *in vitro* cultivation, section is taken vertically from the center of the construct (scale bar = 100µm).

3.3.2 Cell proliferation and extracellular matrix (ECM) synthesis in PEG cryogels

In addition to promoting the adhesion of chondrocytes, cryogels supported their proliferation. The proliferation of seeded cells within the cryogels was examined by DNA content as a function of culture time (Fig. 3.3). Of the 1.0 x 10^6 cells seeded, around 7.5 (± 0.8) x 10^5 cells were found to be in the cryogels after 24 hours of seeding. The chondrocytes proliferated with culture time, where the highest increase in cell number (88.5%) was observed during the first week of culture. Interestingly, the chondrocytes exhibited different growth rates: an initial rapid growth for 1 week, followed by a period of slower growth between 1-2 weeks, which then almost plateaued. This trend in proliferation could be attributed to the large pore size available at initial culture times, which decreases with culture time because of ECM matrix accumulation. However, this rapid cell growth slowed down during the following weeks of culture, showing marginal increases in cell number of 47.8% (between 1st and 2nd week) and 18.3% (between 2nd and 4th week) respectively. The decrease in proliferation could also be due to the increased biosynthetic activity of chondrocytes. The proliferation is similar to a previously reported trend describing the three-stage proliferation of chondrocytes on porous poly(DL-lactide)-chitosan scaffolds.[38] Chondrocytes seeded on porous poly(DL-lactide)-chitosan scaffolds underwent a rapid growth at the first week of cultivation, followed by a slight proliferation during weeks 2-4.

The pore size and interconnectivity of macroporous 3D scaffolds have been shown to play important roles in cell adhesion, migration, viability, metabolism and growth of cells.[39] For instance, Griffon *et al.* have demonstrated a pore size dependent distribution, attachment and proliferation of the chondrocytes within the three

dimensional hydrogels.[40] In another study, Oh *et al*. have demonstrated that the chondrocytes, osteoblasts and fibroblasts cultured in polycaprolactone scaffolds with varying pore size exhibited enhanced cell growth in scaffolds having larger pore sizes.[41]

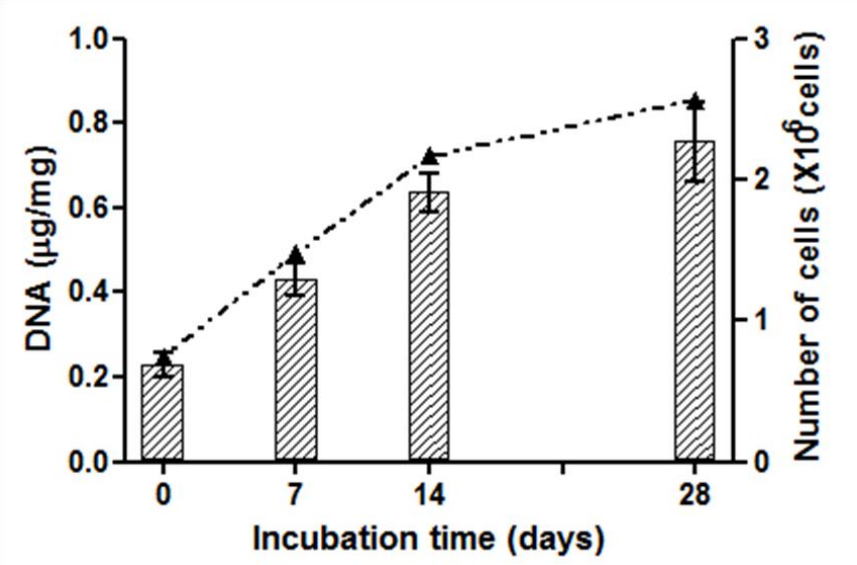


Fig. 3.3 Results of DNA assay showing DNA content normalized to the dry weight of the cryogel after 4 weeks of *in vitro* cultivation (represented by line hatched bars) and the converted number of chondrocytes in constructs after 4 weeks of *in vitro* cultivation (presented by a dotted line) (* $p < 0.05$ for all comparisons among cultivation periods).

Next, we investigated the secretion and accumulation of major cartilage-specific matrix components such as proteoglycans and collagen. Although, a culture time dependent increase in accumulation of GAG per construct was observed, there was no significant increase in GAG accumulation measured between week 2 and week 4 (Fig. 3.4a). In contrast to GAG accumulation normalized to dry weight of cryogels, GAG accumulation normalized to DNA content was found to decrease by 20.3% (2^{nd} week, as compared to GAG content measured at 1^{st} week) and 11.4% (4^{th} week, as compared to GAG content measured at 2^{nd} week) (Fig. 3.4c). Accumulation of collagen content was

estimated by spectrophotometric measurement of hydroxyproline content.[35] The collagen content per construct increased to 91.4% (2nd week as compared to collagen content measured at 1st week) and 37.5% (4th week as compared to collagen content measured at 2nd week) in four weeks of culture time as compared to previously measured time points (Fig. 3.4b). Similarly, we also observed a culture time dependent increase in collagen accumulation normalized to the amount of corresponding DNA (Fig. 3.4d).

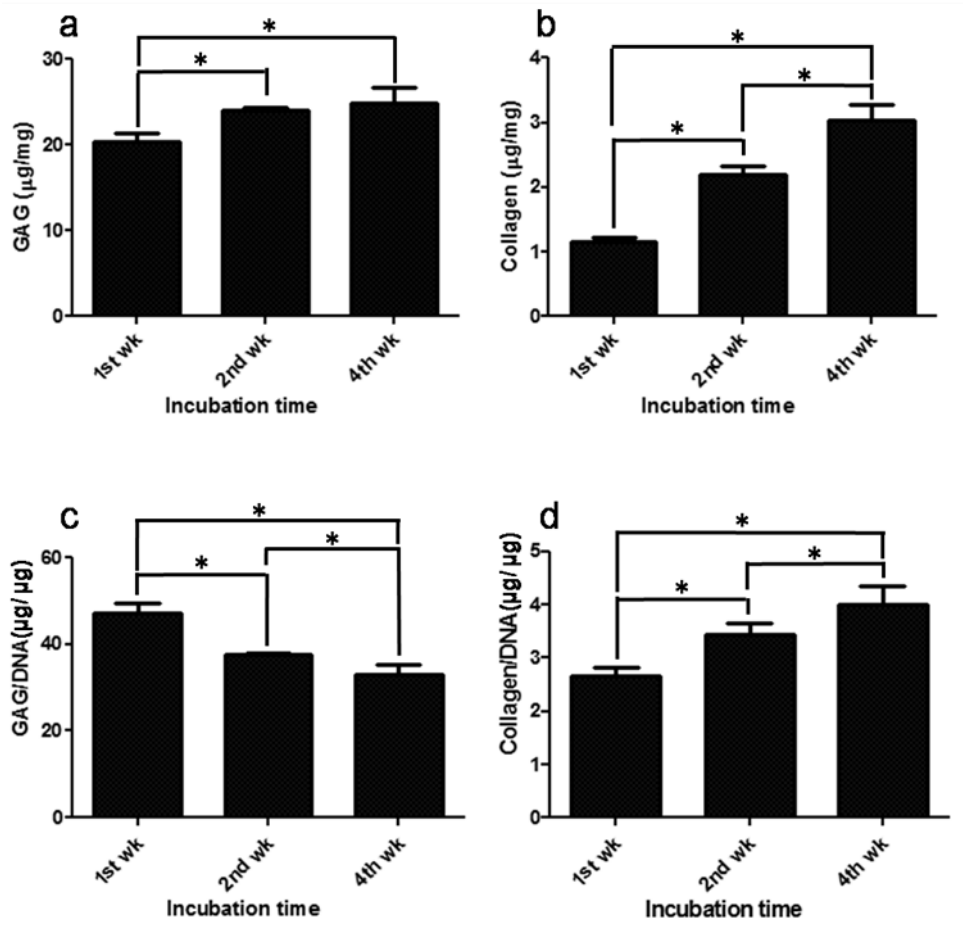


Fig. 3.4 Results of biochemical assays (a) GAG content normalized to the dry weight of the cryogel (b) collagen content normalized to the dry weight of the cryogel (c) amount of GAG normalized to the corresponding DNA values (d) amount of collagen normalized to the corresponding DNA values (* $p < 0.05$ for comparisons among cultivation periods).

The increased matrix accumulation could adversely affect the effective mass transport associated with the large pore size as with increasing matrix accumulation the pore size is decreasing. Hence, incorporating degradable moieties along with macroporous network would be highly advantageous for engineering large tissues, where the space created by scaffold erosion compensates the decrease in scaffold pore size due to matrix accumulation.[40, 42] However, there are few reports showing long term cell survival in interconnected macroporous non-degradable scaffolds as well.[37]

In addition to proliferating, chondrocytes secreted cartilage-specific ECM components. Interconnected macroporous networks in the cryogels enabled uniform distribution of cell secreted GAG molecules throughout the entire scaffold as further observed in histological and immunuhistological evaluation (Fig. 3.6c-d).

This is in agreement with previous findings, which showed the effect of crosslink density of hydrogels on diffusion and the distribution of GAG molecules.[43] Due to their high solubility in water, GAG can easily diffuse out of the gel prior to their polymerization into larger molecules.[44, 45] This along with the large pore size of croygels could also explain the observed reduction in GAG content (normalized to the corresponding DNA values) from week 1 to week 2. However, with increasing culture time the diffusion of GAG molecules from the cryogels would decrease as the seeded chondrocytes deposit more matrices. Previously reported studies have also shown that cell secreted GAG diffuses out of loosely crosslinked hydrogels. [46] The ability of GAG molecules to diffuse within the cryogel has been also seen from Safranin-O staining at week 1 to week 4; the larger Safranin-O stained regions were observed in week 4 as compared to week 1.

In contrast to GAG, collagen content within the cryogel was found to increase with culture time. This may be due to the fact that the high molecular weight of collagen molecules along with their intermolecular forces significantly increases their confinement within the cryogel network.[47, 48] This confinement could also be attributed to the collagen type I coating of cryogels, even though collagen content of the acellular cryogels was found to be below the detectable range by hydroxyproline assay. Although the hydroxypoline assay does not distinguish specific collagen type, findings from the immunohistological staining (for collagen type I and II) indicate that the majority of the cartilage matrix was collagen type II specific further supporting the maintenance of chondrocyte phenotype on the matrix.

3.3.3 SEM analysis on chondrocyte-laden PEG cryogels

After 1 and 4 weeks of *in vitro* cultivation, we performed SEM analysis of the chondrocyte-laden PEG cryogels to investigate cell distribution and ECM accumulation. SEM analysis indicated the presence of chondrocyte secreted ECM within the cryogels (Fig. 3.5). The extent of ECM accumulation appeared to increase from week one to four. A closer observation of the ECM indicates the presence of fibrous material, possibly collagen (Fig. 3.5b, d) within the cryogel section.

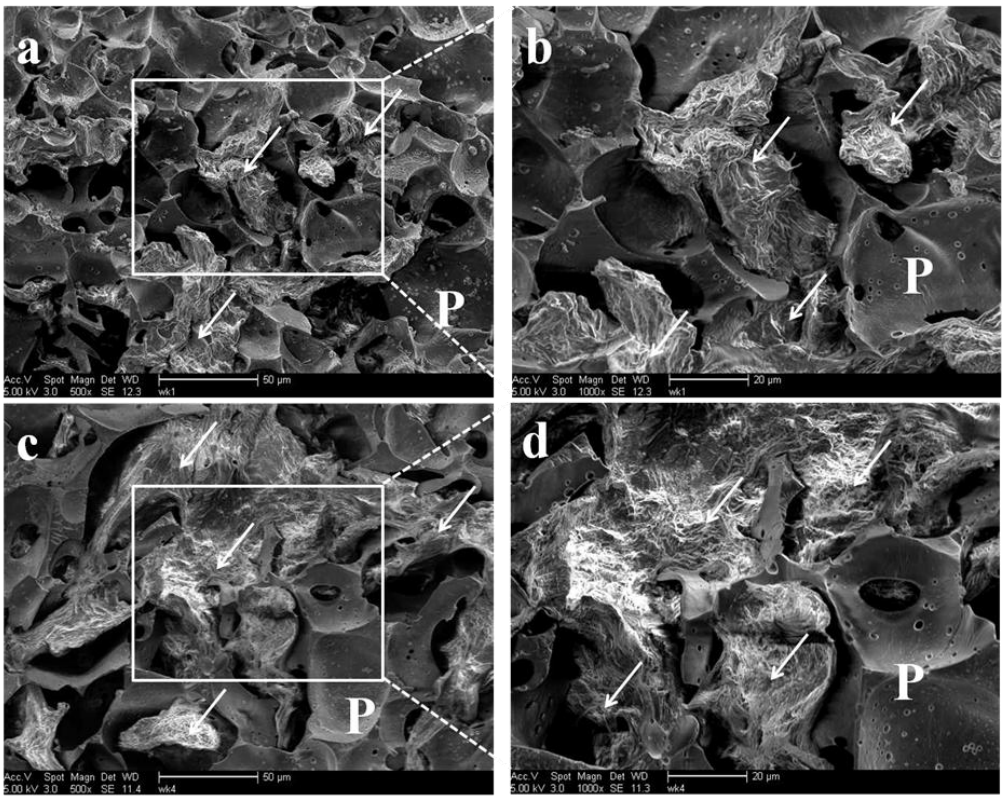


Fig. 3.5 SEM images of chondrocytes seeded on PEG cryogels at different magnifications (a, c) (scale bar = 50µm) and (b, d) (scale bar = 20µm): (a, b) after 1 week of *in vitro* cultivation (c, d) after 4 weeks of *in vitro* cultivation (P represents a polymer network and an arrow indicates ECM).

3.3.4 Histological and immunohistochemical analysis

In addition to biochemical analysis, we also examined the cartilage tissue formati on by histochemical and immunohistochemical studies to observe newly synthesized prot eoglycans and collagen type II after the 1st and 4th week of cultivation, and the histologica l analysis further supported the infiltration of cells and their homogenous distribution wit hin the cryogels. H&E staining of the cell-laden cryogels after week 1 and 4 clearly indic ated cell proliferation, confirming the data obtained through DNA quantification (Fig. 3.6). Basophilic ECM surrounding the chondrocytes was notably increased at week 4 of cult

ure. Moreover, it was observed that chondrocytes within the interconnected macroporous networks had rounded or somewhat elongated morphology (Fig. 3.6a-b). Safranin-O stain ing for negatively charged proteoglycans showed matrix production by the chondrocytes within the cryogels. Areas of larger and more intense Safranin-O staining were observed after 4 weeks compared to 1 week of culture (Fig. 3.6c-d). A similar trend was observed f or collagen type II production for the chondrocyte-laden cryogels with culture time (Fig. 3.6e-f). The cell-secreted ECM was found to be distributed throughout the cryogel. Immu nostaining for collagen type I showed absence of collagen type I proteins after week 1 an d 4 of culture indicating that the chondrocytes cultured within the cryogels maintained th eir phenotype (Fig. 3.6g-h).

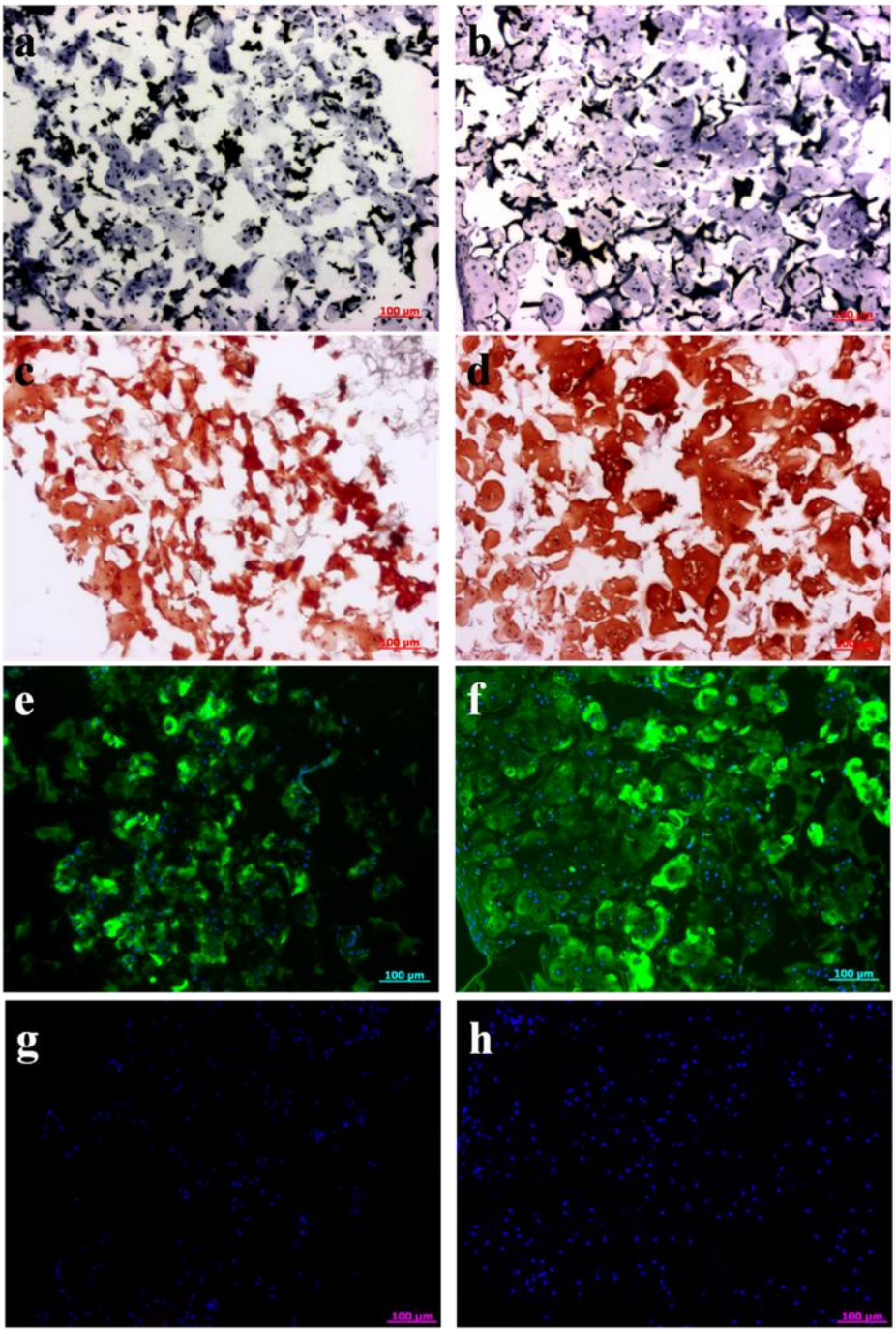


Fig. 3.6 Results of H&E staining (a-b), Safranin-O staining (c-d), collagen type II immunostaining (e-f), and collagen type I immunostaining (g-h) of cell-laden done after 1st week of culture (a, c, e, g) and 4th week of culture (b, d, f, h) (scale bar = 100µm).

3.4 Conclusion

This study demonstrates the potential of macroporous PEG cryogels as a cell scaffold for cartilage tissue engineering using primary bovine chondrocytes. We evaluated the highly interconnected and macroporous internal morphology of cryogels by various microscopic analyses. The seeded chondrocytes were found to be successfully distributed within the macroporous network. The seeded chondrocytes proliferated, maintained chondrocyte phenotype and secreted cartilage-specific matrix within the cryogels. Our findings described in this manuscript demonstrate that the PEG cryogels can successfully support cell proliferation and cartilage-specific ECM production, showing their promising application as scaffolds for cartilage tissue engineering.

3.5 Acknowledgments

This chapter, in full, is a reprint of the material as it appears in Tissue Engineering Part C, Volume 16, 2010. Hwang, Yongsung; Sangaj, Nivedita; Varghese, Shyni. The dissertation author was the primary investigator and author of this paper.

3.6 References

1. Hunziker, E.B., *Articular cartilage repair: basic science and clinical progress. A review of the current status and prospects.* Osteoarthritis Cartilage, 2002. **10**(6): p. 432-63.

2. Buckwalter, J.A. and H.J. Mankin, *Articular cartilage: degeneration and osteoarthritis, repair, regeneration, and transplantation.* Instr Course Lect, 1998. **47**: p. 487-504.

3. Langer, R. and J.P. Vacanti, *Tissue engineering.* Science, 1993. **260**(5110): p. 920-6.

4. Chung, C. and J.A. Burdick, *Engineering cartilage tissue.* Adv Drug Deliv Rev, 2008. **60**(2): p. 243-62.

5. Temenoff, J.S. and A.G. Mikos, *Review: tissue engineering for regeneration of articular cartilage.* Biomaterials, 2000. **21**(5): p. 431-440.

6. Steinert, A.F., U. Noth, and R.S. Tuan, *Concepts in gene therapy for cartilage repair.* Injury-International Journal of the Care of the Injured, 2008. **39**: p. S97-S113.

7. Kuo, C.K., et al., *Cartilage tissue engineering: its potential and uses.* Current Opinion in Rheumatology, 2006. **18**(1): p. 64-73.

8. Varghese, S. and J.H. Elisseeff, *Hydrogels for musculoskeletal tissue engineering.* Polymers for Regenerative Medicine, 2006: p. 95-144.

9. Hoffman, A.S., *Hydrogels for biomedical applications.* Adv Drug Deliv Rev, 2002. **54**(1): p. 3-12.

10. Peters, M.C. and D.J. Mooney, *Synthetic extracellular matrices for cell transplantation.* Porous Materials for Tissue Engineering, 1997. **250**: p. 43-52.

11. Kim, B.S. and D.J. Mooney, *Development of biocompatible synthetic extracellular matrices for tissue engineering.* Trends in Biotechnology, 1998. **16**(5): p. 224-230.

12. Woodfield, T.B.F., et al., *Design of porous scaffolds for cartilage tissue engineering using a three-dimensional fiber-deposition technique.* Biomaterials, 2004. **25**(18): p. 4149-4161.

13. Hollister, S.J., *Porous scaffold design for tissue engineering.* Nature Materials, 2005. **4**(7): p. 518-524.

14. Mooney, D.J., et al., *Novel approach to fabricate porous sponges of poly(D,L-lactic-co-glycolic acid) without the use of organic solvents.* Biomaterials, 1996. **17**(14): p. 1417-22.

15. Mikos, A.G., et al., *Laminated three-dimensional biodegradable foams for use in tissue engineering.* Biomaterials, 1993. **14**(5): p. 323-30.

16. Bennett, D.J., et al., *Synthesis of Porous Hydrogel Structures by Polymerizing the Continuous-Phase of a Microemulsion.* Polymer International, 1995. **36**(3): p. 219-226.

17. Nam, Y.S. and T.G. Park, *Biodegradable polymeric microcellular foams by modified thermally induced phase separation method.* Biomaterials, 1999. **20**(19): p. 1783-1790.

18. Mikos, A.G., et al., *Preparation and Characterization of Poly(L-Lactic Acid) Foams.* Polymer, 1994. **35**(5): p. 1068-1077.

19. O'Brien, F.J., et al., *The effect of pore size on cell adhesion in collagen-GAG scaffolds.* Biomaterials, 2005. **26**(4): p. 433-41.

20. Mikos, A.G., et al., *Preparation of poly(glycolic acid) bonded fiber structures for cell attachment and transplantation.* J Biomed Mater Res, 1993. **27**(2): p. 183-9.

21. Plieva, F.M., et al., *Pore structure in supermacroporous polyacrylamide based cryogels.* Soft Matter, 2005. **1**(4): p. 303-309.

22. Plieva, F., et al., *Macroporous elastic polyacrylamide gels prepared at subzero temperatures: control of porous structure.* Journal of Materials Chemistry, 2006. **16**(41): p. 4065-4073.

23. Savina, I.N., et al., *Cryogels from poly(2-hydroxyethyl methacrylate): macroporous, interconnected materials with potential as cell scaffolds.* Soft Matter, 2007. **3**(9): p. 1176-1184.

24. Plieva, F.M., et al., *Cryogel applications in microbiology.* Trends in Microbiology, 2008. **16**(11): p. 543-551.

25. Kathuria, N., et al., *Synthesis and characterization of elastic and macroporous chitosan-gelatin cryogels for tissue engineering.* Acta Biomater, 2009. **5**(1): p. 406-18.

26. Bolgen, N., et al., *Three-Dimensional Ingrowth of Bone Cells within Biodegradable Cryogel Scaffolds in Bioreactors at Different Regimes.* Tissue Eng Part A, 2008.

27. Hwang, Y., Zhang C, Varghese S., *Poly (ethylene glycol) cryogels as potential cell scaffolds: Effect of polymerization conditions on cryogel microstructure and properties. J. Mater. Chem., 2010, 20, 345–351.* 2010.

28. Hern, D.L. and J.A. Hubbell, *Incorporation of adhesion peptides into nonadhesive hydrogels useful for tissue resurfacing.* Journal of Biomedical Materials Research, 1998. **39**(2): p. 266-276.

29. Kim, T.K., et al., *Experimental model for cartilage tissue engineering to regenerate the zonal organization of articular cartilage.* Osteoarthritis Cartilage, 2003. **11**(9): p. 653-64.

30. Hwang, N.S., S. Varghese, and J. Elisseeff, *Cartilage tissue engineering: Directed differentiation of embryonic stem cells in three-dimensional hydrogel culture.* Methods Mol Biol, 2007. **407**: p. 351-73.

31. Kim, M.S., et al., *Musculoskeletal differentiation of cells derived from human embryonic germ cells.* Stem Cells, 2005. **23**(1): p. 113-23.

32. Dadsetan, M., et al., *Effect of hydrogel porosity on marrow stromal cell phenotypic expression.* Biomaterials, 2008. **29**(14): p. 2193-2202.

33. Kim, Y.J., et al., *Fluorometric Assay of DNA in Cartilage Explants Using Hoechst-33258.* Analytical Biochemistry, 1988. **174**(1): p. 168-176.

34. Farndale, R.W., D.J. Buttle, and A.J. Barrett, *Improved quantitation and discrimination of sulphated glycosaminoglycans by use of dimethylmethylene blue.* Biochim Biophys Acta, 1986. **883**(2): p. 173-7.

35. Stegeman.H and K. Stalder, *Determination of Hydroxyproline.* Clinica Chimica Acta, 1967. **18**(2): p. 267-&.

36. Hwang, N.S., et al., *Effects of three-dimensional culture and growth factors on the chondrogenic differentiation of murine embryonic stem cells.* Stem Cells, 2006. **24**(2): p. 284-291.

37. Keskar, V., et al., *In Vitro Evaluation of Macroporous Hydrogels to Facilitate Stem Cell Infiltration, Growth, and Mineralization.* Tissue Engineering Part A, 2009. **15**(7): p. 1695-1707.

38. Wu, H., et al., *Proliferation of chondrocytes on porous poly(DL-lactide)/chitosan scaffolds.* Acta Biomaterialia, 2008. **4**(1): p. 76-87.

39. Lien, S.M., L.Y. Ko, and T.J. Huang, *Effect of pore size on ECM secretion and cell growth in gelatin scaffold for articular cartilage tissue engineering.* Acta Biomaterialia, 2009. **5**(2): p. 670-679.

40. Griffon, D.J., et al., *Chitosan scaffolds: interconnective pore size and cartilage engineering.* Acta Biomater, 2006. **2**(3): p. 313-20.

41. Oh, S.H., et al., *In vitro and in vivo characteristics of PCL scaffolds with pore size gradient fabricated by a centrifugation method.* Biomaterials, 2007. **28**(9): p. 1664-1671.

42. Bryant, S.J. and K.S. Anseth, *Controlling the spatial distribution of ECM components in degradable PEG hydrogels for tissue engineering cartilage.* Journal of Biomedical Materials Research Part A, 2003. **64A**(1): p. 70-79.

43. Bryant, S.J. and K.S. Anseth, *Hydrogel properties influence ECM production by chondrocytes photoencapsulated in poly(ethylene glycol) hydrogels.* J Biomed Mater Res, 2002. **59**(1): p. 63-72.

44. Mahmood, T.A., et al., *Tissue engineering of bovine articular cartilage within porous poly(ether ester) copolymer scaffolds with different structures.* Tissue Engineering, 2005. **11**(7-8): p. 1244-1253.

45. van Susante, J.L.C., et al., *Linkage of chondroitin-sulfate to type I collagen scaffolds stimulates the bioactivity of seeded chondrocytes in vitro.* Biomaterials, 2001. **22**(17): p. 2359-2369.

46. Villanueva, I., et al., *Static and dynamic compressive strains influence nitric oxide production and chondrocyte bioactivity when encapsulated in PEG hydrogels of different crosslinking densities.* Osteoarthritis and Cartilage, 2008. **16**(8): p. 909-918.

47. Riesle, J., et al., *Collagen in tissue-engineered cartilage: types, structure, and crosslinks.* J Cell Biochem, 1998. **71**(3): p. 313-27.

48. Kaab, M.J., I.A. Gwynn, and H.P. Notzli, *Collagen fibre arrangement in the tibial plateau articular cartilage of man and other mammalian species.* Journal of Anatomy, 1998. **193**: p. 23-34.

CHAPTER 4: Engineering cell-material interfaces for long-term expansion of human pluripotent stem cells

"The most beautiful thing we can experience is the mysterious.

It is the source of all true art and science."

- Albert Einstein

This chapter, in full, is currently being prepared for submission for publication of the material. *Chang, Chien-Wen; *Hwang, Yongsung; Brafman, David; Hagan, Thomas; Lin, Susan; Varghese, Shyni. The dissertation author was the primary investigator and author of this paper.

4. 1 Introduction

Due to the large number of cells required for cell-based therapies, extensive expansion of pluripotent cells is essential while maintaining their pluripotency. As a result, there has been tremendous interest in developing defined, scalable *in vitro* culture conditions that can support their growth.[1, 2] These efforts have led to the development of multiple growth media having defined compositions.[3-5] Even with the emergence of these media however, expansion of human pluripotent stem cells (hPSCs) still require relatively undefined substrates such as feeder cell layers of mouse embryonic fibroblasts (MEF) or ECM-based Matrigels.[6-11] These approaches present challenges for the clinical application of hPSCs due to their undefined composition as well as the risk of

xenogenic contamination (such as with Neu5GC, a non-human sialic acid expressed on Matrigel and by MEF feeder layers).[12] Development of chemically defined matrices is a challenging task because of the myriad of signals that Matrigel and MEF provide, and the complexity associated with deconvoluting the effect of these signals on hPSC expansion and pluripotency. Despite these challenges, recent advances in the field have lead to identification of matrices—both naturally-derived and synthetic—capable of supporting self-renewal of hPSCs.[13-21] High throughput screening technologies have contributed significantly towards the development of these chemically defined culture conditions.[22, 23]

Emerging studies demonstrate the role of heparin molecules on maintaining self-renewal of hPSCs.[24, 25] Harnessing the beneficial effect of heparin moieties on modulating self-renewal of hPSCs, Klim *et al.* have developed synthetic matrices displaying heparin-binding peptides to support long-term self-renewal of human embryonic stem cells (hESCs).[26] The role of heparin moieties on self-renewal of hPSCs is not surprising given that heparin molecules can bind to soluble fibroblast growth factor (FGF) molecules and modulate FGF signaling; FGF-2 is an important signaling molecule in maintaining self-renewal of hPSCs and in fact, basic fibroblast growth factor (bFGF) is an inherent component of hPSC culture medium.[27] Additionally, heparin molecules have been shown to protect bFGF from denaturation and proteolytic degradation, thereby increasing their longevity and function during *in vitro* culture.[28-30]

Synthetic heparin mimics such as poly(sodium-4-styrenesulfonate) (PSS) have been shown to bind to soluble bFGF and regulate FGF signaling amenable to heparin

molecules.[31-33] Leveraging these findings in conjunction with the prominent role of bFGF molecules on maintaining self-renewal of hPSCs, we developed synthetic hydrogel matrices containing PSS moieties and evaluated their ability to support long-term culture of hPSCs while maintaining their pluripotency. We further elucidate the role of various physicochemical cues of the matrix on self-renewal of hPSCs by employing a number of hydrogels with varying functional groups, matrix rigidity, and hydrophobicity. We also gain insight into the mechanisms by which PSS-based hydrogels support self-renewal of hPSCs. Such easy-to-synthesize, defined synthetic matrices could potentially accelerate the translational applicability of hPSCs. In addition, such finely tunable hydrogel-based systems could also provide a platform to dissect the role of bulk and interfacial properties of extracellular matrices on self-renewal of hPSCs and also to identify the myriad of molecular and signaling pathways dictating stem cell fate and commitment.

4.2 Materials and methods

4.2.1 Materials

N-acryloyl amino acid (AA) monomers, such as N-acryloyl 2-glycine (A2AGA), N-acryloyl 4-aminobutyeric acid (A4ABA), N-acryloyl 6-aminocaproic acid (A6ACA), and N-acryloyl 8-aminocaprylic acid (A8ACA), were synthesized from glycine (Fisher Scientific, Inc.), 4-aminobutyeric acid, 6-aminocaproic acid, and 8-aminocaprylic acid (Acros Organics Inc.), respectively, as described elsewhere.[34, 35] Sodium 4-vinylbenzenesulfonate (SS), 3-sulfopropyl acrylate potassium salt (SPA), and [2-(methacryloyloxy)ethyl]dimethyl-(3-sulfopropyl)ammonium hydroxide (MEDSAH) were purchased from Aldrich. Acrylamide (Am) was purchased from Invitrogen and N,N'-methylenebisacrylamide (BisAm), ammonium persulfate (APS) and N,N,N',N'-tetramethylethylenediamine (TEMED) were obtained from Sigma. The monomers used in this study are summarized in Table 4.1.

Table 4.1 Lists of monomers.

Acronym	Full name
Am	Acrylamide
A2AGA	N-Acryloyl 2-glycine
A4ABA	N-Acryloyl 4-aminobutyeric acid
A6ACA	N-Acryloyl 6-aminocaproic acid
A8ACA	N-Acryloyl 8-aminocaprylic acid
SPA	3-Sulfopropyl acrylate potassium salt
MEDSAH	2-(Methacryloyloxy)ethyl]dimethyl-(3-sulfopropyl) ammonium hydroxide
SS	Sodium 4-vinylbenzenesulfonate
BisAm	N,N'-Methylenebisacrylamide

4.2.2 Hydrogel preparation

PSS-based hydrogelswere synthesized by copolymerizing acrylamide (Am, 7.5 mmol) with sodium 4-vinylbenzenesulfonate (SS, 2.5 mmol) monomers at 6:2, 6:1, and 6:0.5 molar ratios. The monomers were dissolved in deionized (DI) water, and polymerized in BioRad 1 mm spacer glass plates at room temperature using 0.26, 0.19, and 0.10 mmol BisAm as a crosslinker and 1.3%w/v APS/TEMED (redox initiator/accelerator). SPA and MEDSAH-based hydrogels were synthesized by copolymerizing Am (7.5 mmol) with SPA (2.5 mmol) or MEDSAH (2.5 mmol) at 6:2 mol ratio. They were dissolved in DI water and were polymerized using 0.26 mmol BisAm and 1.3%w/v APS/TEMED. Lastly, AA-based hydrogels were synthesized by copolymerizing Am (7.5 mmol) with AA monomers (2.5 mmol) at 6:2 mol ratio. They were dissolved in 1M NaOH and were polymerized using 0.26 mmol BisAm and 1.3%w/v APS/TEMED. Their compositions and nomenclature of the hydrogels are summarized in Table 4.2. Prior to seeding cells, hydrogels were sterilized with 70% ethanol and were washed with fresh phosphate buffered saline (PBS) solution for 72 hours. The rinsed hydrogels were incubated in culture media containing 10% fetal bovine serum for overnight before plating cells.

Table 4.2 Compositions and nomenclature of hydrogels were summarized, and their elastic modulus and water contact angle were tabulated.

Sample code	Comonomer (B)	Molar ratio of Am_x:B_y (BisAm)	Elastic modulus (kPa)	Water contact angle (^{o})
PAm_6-*co*-$PA2AGA_2$	A2AGA (2.5mmol)	6:2 (0.26)	353.0±13.9	20.9±1.4
PAm_6-*co*-$PA4ABA_2$	A4ABA (2.5mmol)	6:2 (0.26)	N/A	36.1±1.9
PAm_6-*co*-$PA6ACA_2$	A6ACA (2.5mmol)	6:2 (0.26)	N/A	53.8±2.7
PAm_6-*co*-$PA8ACA_2$	A8ACA (2.5mmol)	6:2 (0.26)	N/A	67.3±1.6
PAm_6-*co*-$PSPA_2$	SPA (2.5mmol)	6:2 (0.26)	342.5±19.7	32.6±1.2
PAm_6-*co*-$PMEDSAH_2$	MEDSAH (2.5mmol)	6:2 (0.26)	378.8±36.6	66.3±2.3
PAm_6-*co*-$PSS_{0.5}$	SS (0.625mmol)	6:0.5 (0.26)	327.8±7.1	N/A
PAm_6-*co*-PSS_1	SS (1.25mmol)	6:1 (0.26)	382.9±5.1	N/A
PAm_6-*co*-PSS_2	SS (2.5mmol)	6:2 (0.26)	343.7±5.1	23.0±2.0
PAm_6-*co*-PSS_2-M	SS (2.5mmol)	6:2 (0.19)	137.6±6.9	N/A
PAm_6-*co*-PSS_2-L	SS (2.5mmol)	6:2 (0.10)	53.5±2.8	N/A

4.2.3 Surface roughness measurements

Surface roughness was evaluated using a Multimode AFM equipped with a Nanoscope IIIA controller from Veeco Instruments (Santa Barbara, CA) run by Nanoscope software v5.30 as previous reported.[34] AFM images were acquired in contact mode at forces of ~4 nN with an "E" scanner (maximum scan area 12 x 12 mm^2) using Si3N4 cantilevers (Veeco) with 0.06 N/m nominal spring constants. Hydrogels were prepared as described above. Upon synthesis, hydrogels were washed in PBS for 36 hour to leach out the unreacted monomers and to reach their equilibrium swelling. For a given scan area, the reported roughness value is the average root mean square (RMS) roughness obtained from two different spots of triplicate specimens. Data was analyzed using the nanoscope software. Using the manufacturer's software, flattening order 3 was applied to all images to correct for tilt and bow before roughness analysis.

4.2.4 Elastic modulus measurements

Prior to compression test, the hydrogels were immersed in PBS for 24 hours to reach equilibrium swelling. Compression tests were performed using Bose ElectroForce 3200 Test Instrument (*Bose*, Minnesota, USA). Samples were compressed by two parallel plates at the maximum loading of 225N load cell with a compression rate of 0.1mm/min. The compressive modulus was calculated from the linear region of stress-strain curve (0-5% strain). All measurements were carried out as quadruplicates for each set of parameters.

4.2.5 Water contact angle measurements

The water contact angles of the hydrogels were determined by a sessile drop method at room temperature using contact angle meter (CAM100, KSV Instruments Ltd.). A 5 μl droplet of water was placed on the surface of hydrogels. All samples were prepared as triplicates and results were shown as a mean value with standard deviation.

4.2.6 OCT4-GFP reporter line

The lenti construct that was used to generate the OCT4-GFP reporter line was kindly provided by Dr. Alexey Terskikh. High titer lenti was produced as previously reported.[36, 37] HUES9 cells were infected overnight with lenti Oct4-GFP and single clones were isolated and screened for (i) stable GFP expression levels, (ii) low GFP expression levels after EB formation, and (iii) rapid decrease in GFP expression upon removal of MEF conditioned medium.

4.2.7 HPSCs culture

HPSCs, including HUES9, HUES9-Oct4-GFP, HUES6, and human induced pluripotent stem cells (hiPSCs), were expended in defined medium (StemPro® ; DMEM/F-12 supplemented with StemPro supplement, 2% bovine serum albumin (BSA), 55 μM 2-mercaptoethanol, and 1% Gluta-MAX) and MEF conditioned medium, which was collected after conditioning MEF for 24 hour using Knockout DMEM supplemented with 10% Knockout Serum Replacement, 10% human plasmonate (Talecris Biotherapeutics), 1% non-essential amino acids, 1% penicillin/streptomycin, 1% Gluta-MAX, 55 μM 2-mercaptoethanol as previous described elsewhere.[20] Cells were

manually passaged using a pipette when they reached ~80% confluency and the medium was changed every day supplemented with 30ng/ml of bFGF (Life Technologies).

4.2.8 Population doubling time (PDT)

Population doubling time (PDT) for HUES9 grown on Matrigel and PAm_6-*co*-PSS_2 hydrogel was calculated as below:

$$PDT(hr) = \frac{(T2 - T1)}{3.32 * (\log N2 - \log N1)}$$

where T1 was day 3, T2 was day 5, N1 was the number of cells at T1, and N2 was the number of cells at T2. The number of cells at each time point was counted using TC10^{TM} Automated Cell Counter (Biorad).

4.2.9 Immunocytochemistry

Immunostaining were performed using the following primary antibodies: Oct4 (1:200; Santa Cruz), Nanog (1:200; Santa Cruz), Sox17 (1:200; R & D systems), SMA (1:500; R & D systems), Nestin (1:50; BD Biosciences). The following secondary antibodies were used: goat anti-rabbit Alexa 647 (1:400; Life Technologies), donkey anti-mouse Alexa 546 (1:250; Life Technologies), and donkey anti-goat Alexa 546 (1:250; Life Technologies). For immunostaining, cells were fixed in 4% PFA for 5 min at 4℃, followed by 10 min at room temperature. Immediately before staining, the cells were permeabilized with 0.2% (v/v) Triton-X-100 and blocked with 1% (w/v) BSA and 3% (w/v) nonfat dry milk for 30 min. Cells were stained with the primary antibodies diluted in 1% BSA overnight at 4℃, washed 3 times with TBS, and incubated with secondary

antibodies for 1 hr at 37℃. Nucleic acids were stained for DNA with Hoechst 33342 (2 μg/ml; Life Technologies) for 5 min at room temperature. Imaging of was performed using an automated confocal microscope (Olympus Fluoview 1000 with motorized stage and incubation chamber).

4.2.10 RNA isolation and quantitative PCR

RNA was isolated from cells using TRIzol (Invitrogen), and treated with DNase I (Invitrogen) to remove traces of DNA. Reverse transcription was performed by means of qScript cDNA Supermix (Quanta Biosciences). Quantitative PCR was carried out using TaqMan probes (Applied Biosystems) and TaqMan Fast Universal PCR Master Mix (Applied Biosystems) on a 7900HT Real Time PCR machine (Applied Biosystems). Taqman gene expression assay primers (Applied Biosystems) were used. Gene expression was normalized to 18S rRNA levels. Delta Ct values were calculated as $C_t^{target} - C_t^{18s}$. All experiments were performed with three technical replicates. The relative fold changes in expression were calculated as $2^{-\Delta\Delta Ct}$.[38] Data are presented as the average of the biological replicates ± standard error of the mean.

Table 4.3 Primer sequences for RT-PCR.

Target gene	Forward (5'-3')	Reverse (5'-3')
Nanog	ACCAGAACTGTGTTCTCTTCCACC	CCATTGCTATTCTTCGGCCAGTTG
Oct4	GGAAGGTATTCAGCCAAACGACCA	CTCACTCGGTTCTCGATACTGGTT
CXCR4	CACTTCAGATAACTACACCG	ATCCAGACGCCAACATAGAC
Sox17	AGTGACGACCAGAGCCAGAC	CCTTAGCCCACACCATGAAA
SMA	ACAACTGGCATCGTGCTGGAC	GATGGCTGGAACAGGGTCTCTGG
ACTC1	CCCTGGAGAAGAGCTATGAAC	GGAAGGTAGATGGAGAGAGAAG
Nestin	AGAGGGGAATTCCTGGAG	CTGAGGACCAGGACTCTCTA
Sox1	CACAACTCGGAGATCAGCAA	GTCCTTCTTGAGCAGCGTCT
Sox2	GGGAAATGGGAGGGGTGCAAAAGAGG	TTGCGTGAGTGTGGATGGGATTGGTG
18s	ACACGGACAGGATTGACAGA	GGACATCTAAGGGCATCACAG

4.2.11 FACS analysis

hPSCs were dissociated with acutase. The cells were resuspended in stain buffer (2% FBS/0.09% sodium azide/DPBS; BD Biosciences) and stained directly with Alexa-647 conjugated Tra-1-81 (Biolgend) or Alexa Fluor 647 mouse IgM,κ isotype control. Cells were stained for 30 min on ice, washed, and resuspended in stain buffer. Samples were analyzed using BD Biosystems FACSCanto.

4.2.12 In vitro differentiation of HUES9 cells grown on PAm_6-co-PSS_2 hydrogel

(1) Endoderm Differentiation. All media components are from Life Technologies unless indicated otherwise. For endoderm differentiation, hPSCs were cultured on Matrigel in mouse embryonic fibroblast (MEF)-conditioned media (CM) supplemented with 30 ng/ml FGF2 until confluency. The medium was then changed to RPMI medium supplemented with 1% (v/v) Gluta-MAX and 100 ng/ml recombinant human Activin A (R&D Systems). Cells were cultured for 3 days, with FBS concentrations at 0% for the first day and 0.2% for the second and third days. Cultures were supplemented with 30 ng/ml purified mouse Wnt3a for the first day.[39] *(2) Ectoderm Differentiation and NPC Formation.* To initiate ectoderm differentiation, hPSCs were cultured on Matrigel in MEF conditioned medium supplemented with 30 ng/ml FGF2. Cells were then detached by treatment with acutase (Millipore) for 5 min and resuspended in neural progenitor cell (NPC) embryoid body (EB) media (10% FBS, 1% N2, 1% B27, DMEM/F-12), 5 μM ROCK inhibitor (Y-27632, Stemgent), 50 ng/ml recombinant mouse Noggin (R&D Systems), 0.5 μM dorsomorphin (Tocris Bioscience). Next, 7.5×10^5 cells were added to each well of several 6-well ultra low attachment plates (Corning). The plates were then

placed on an orbital shaker set at 95 rpm in a 37^{o}C/5% CO_2 incubator. The next day, the cells formed spherical clusters and the media was changed to NPC EB media without FBS supplemented with 50 ng/ml recombinant mouse Noggin and 0.5 µM Dorsomorphin. The media was subsequently changed every other day. After 5 days in suspension culture, the EBs were then transferred to a 10 cm dish coated (3 x 6 wells per 10 cm dish) with growth factor reduced Matrigel (1:25 in KnockOut DMEM; BD Biosciences) for attachment. The plated EBs were cultured in NPC EB media without FBS supplemented with 50 ng/ml recombinant mouse Noggin and 0.5 µM Dorsomorphin. After 7 days of attachment, rosette-forming EBs were cut out by manual dissection. Isolated rosettes were incubated in acutase for 15 minutes in a 37^{O}C/5% CO_2 tissue culture incubator. The rosettes were then plated to poly-L-ornithine (PLO; 10 µg/ml; Sigma) and mouse laminin (Ln; 5 µg/ml) coated plates in NPC expansion media (1% N2, 1% B27, DMEM/F-12) supplemented with 30 ng/ml FGF2 and 30 ng/ml EGF (R & D systems). NPCs were maintained on PLO/Ln plates in NPC media supplemented with 30 ng/ml FGF2 and 30 ng/ml EGF. *(3) Mesoderm Differentiation.* For mesoderm induction, hPSCs were cultured on Matrigel in DMEM supplemented with 20% FBS and 1% penicillin/streptomycin for 21 days.

4.2.13 Karyotype analysis

To monitor genomic integrity, cells grown on PAm_6-*co*-PSS_2 hydrogel with StemPro® medium and MEF conditioned medium were evaluated by cytogenetic analysis at passage 16 using standard protocols for G-banding (Cell Line Genetics).

4.2.14 PCR array analysis for various extracellular matrix and adhesion molecules

Briefly, RNA was isolated from cells using TRIzol (Invitrogen), and treated with DNase I (Invitrogen) to remove traces of DNA. Reverse transcription was performed by using RT^2 First Strand Kit (SABioscience, Cat# 330401) and 200 ng of cDNA was processed for quantitative real-time RT-PCR of 84 genes involved in extracellular matrix and adhesion molecules by using PCR array kit (RT^2 Profiler^{TM} PCR Arrays Extracellular matrix and adhesion molecules, PAHS-013A-2, SABioscience) and ABI Prism 7700 Sequence Detection System (Applied Biosystems). PCR products were quantified by measuring SYBR Green fluorescent dye incorporation with ROX dye reference.

4.2.15 Protein adsorption assay

The amount of various protein adsorptions to PAm_6-*co*-$A2AGA_2$ and PAm_6-*co*-PSS_2 hydrogels was quantified by a modified Bradford protein assay using Bio-Rad Protein Assay kit (Cat# 500-0006) as previously reported.[40] Briefly, dye agent was prepared according to the manufacturer's protocol, and both hydrogels were synthesized, and placed in 96-well plate (n=3).These hydrogels were incubated with 200 μl of bovine serum albumin (Sigma, Cat# A8412), vitronectin (Sigma, Cat# V8379-50UG), collagen type I (BD Biosciences, Cat# 354231), collagen type IV (Sigma, Cat# C5533), laminin (Sigma, L6274), and fibronectin (Gibco, Cat# 33016-015) solutions diluted in PBS at concentrations of 0, 2.5, 5, 10, and 15 μg/ml for 15 hours at 4^oC. After incubating with solutions, 30 μl of each supernatant solution from triplicate samples for each concentration were combined with 200 μl of Bradford dye reagent solution. These solutions were well mixed by gentle pippetting and then transferred into a flat-bottom 96-

well plate to measure their absorbance at 595 nm on Multimode Detector (Beckman Coulter, DTX 880). Standard curves for each protein was also established to calculate the amount of each protein adsorbed by both hydrogels.

4.2.16 Enzyme-Linked Immunosorbent Assay (ELISA)

The amount of bFGF absorbed by PAm_6-*co*-$A2AGA_2$ and PAm_6-*co*-PSS_2 hydrogels was carried out by bFGF ELISA kit (RayBiotech, Inc., cat# ELH-bFGF-001) while following the manufacturer's protocol. The bFGF was immobilized on the surface of these hydrogels and the remaining bFGF in the supernatant of reaction solution was quantified.

4.2.17 Statistical Analysis

All values were presented as mean ± standard deviation and statistical significance was determined by two-tailed unpaired Student's t-test.

4.3 Results and Discussion

4.3.1 Design and characterization of hydrogels

We have synthesized hydrogels with varying chemical functional groups, matrix rigidity, and interfacial hydrophobicity by copolymerizing acrylamide (Am) monomers with anionic monomershaving either pendant -SO_3H or -COOH groups as described in Fig. 4.1 and Table 4.1-2. These hydrogels are referred to as PAm_x-*co*-PB_y, where PAm and PB represent the polymer components of the hydrogel, and 'x' and 'y' denote the mole ratio of the monomers used in hydrogel synthesis, respectively. For instance, the hydrogel synthesized by copolymerizing Am with SS at a mole ratio of 6:2 is denoted as PAm_6-*co*-PSS_2. Additionally, we have also synthesized PAm_6-*co*-PSS_2 hydrogels with different BisAm (crosslinker) contents to vary the hydrogel rigidity. The PAm-*co*-PSS hydrogels with varying charge density were synthesized by copolymerizing Am with varying PSS:Am molar ratios, from 0.5 to 2. Taken together, these hydrogels allow us to examine the effect of functional groups, hydrophobicity, rigidity, and charge density of the hydrogel matrices on hPSC cellular responses.

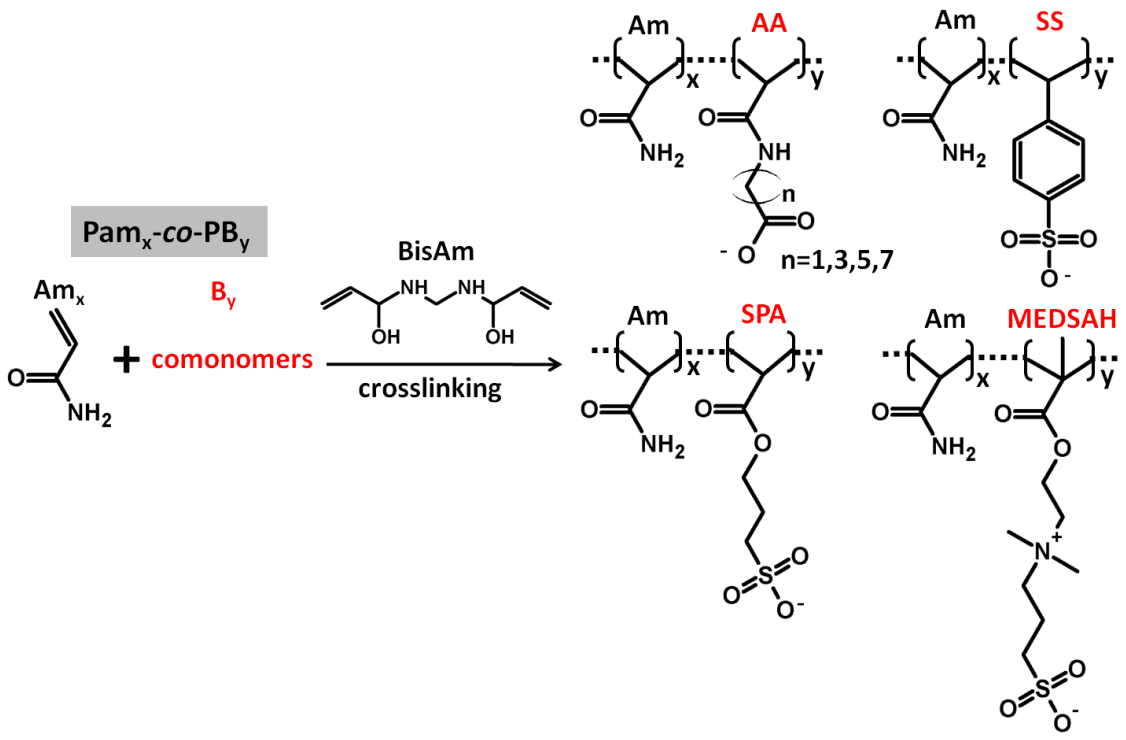


Fig. 4.1 Synthesis of various hydrogels used in this study.

4.3.2 PSS-based hydrogels support self-renewal and long-term expansion of hPSCs

Human pluripotent stem cells (hPSCs), such as human embryonic stem cells (hESCs) and human induced pluripotent stem cells (hiPSCs) are currently expanded by culturing on feeder cells such as MEF or ECM-rich Matrigel.[6, 10] Emerging evidence shows that hPSCs can be grown on synthetic biomaterials.[17, 20] In this study, we demonstrate the potential of synthetic hydrogels containing heparin-mimicking poly(styrene sulfonate) moieties on self-renewal of hPSCs with maintained pluripotency.

Our initial observation was that the human embryonic stem cells (hESCs, HUES9-Oct4-GFP, and HUES9) grown on PAm$_6$-*co*-PSS$_2$ hydrogels maintained bright and compact colonies similar to that observed on Matrigel and MEF supported cultures (Fig. 4.2a-c). Though the number of cells adhered onto the PAm$_6$-*co*-PSS$_2$ hydrogels

were significantly lower compared to those on Matrigel, the adhered cells on PAm_6-*co*-PSS_2 hydrogel surfaces formed compact colonies. The population doubling of hPSCs on PAm_6-*co*-PSS_2 hydrogels was found to be 47.9 hour while that on Matrigel was found to be 23.3 hour (Fig. 4.2d). The finding that the HUES9 cells on PAm_6-*co*-PSS_2 hydrogels maintained pluripotency prompted us to investigate the ability of PAm_6-*co*-PSS_2 hydrogels to support long-term expansion of hPSCs while maintaining their pluripotency.

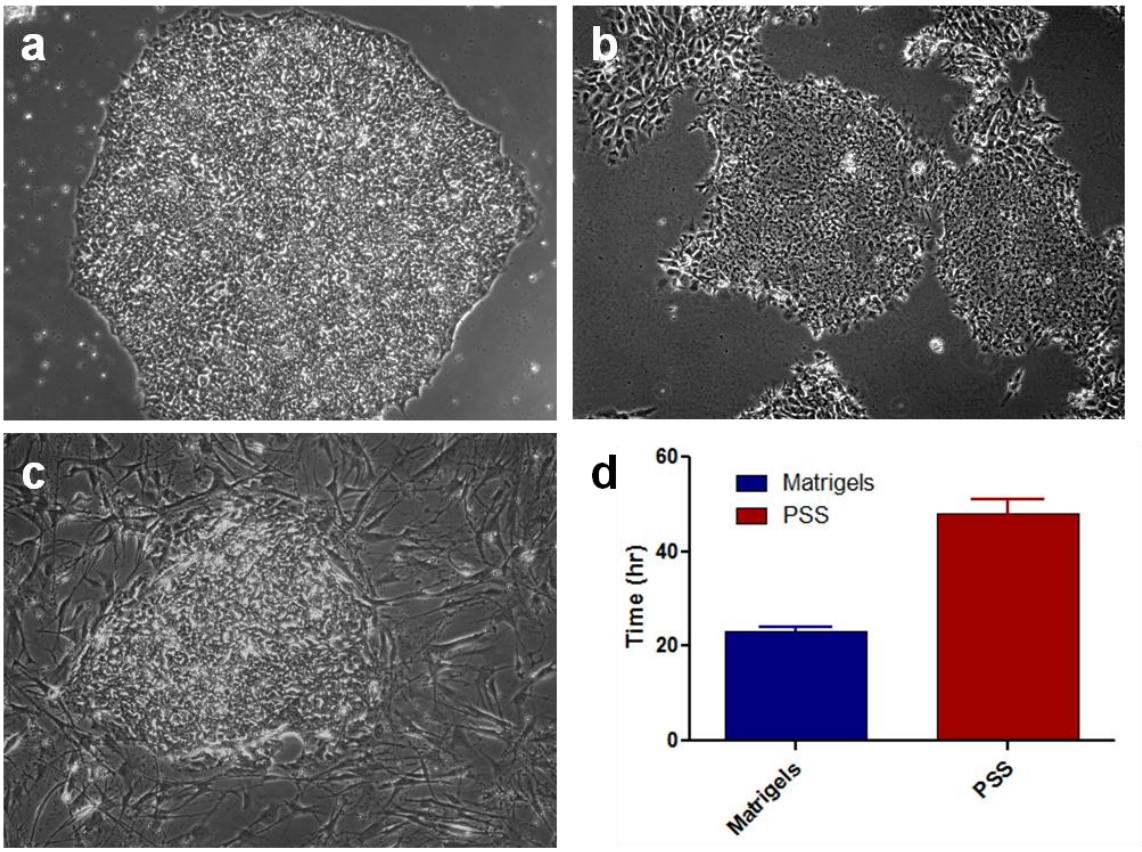


Fig. 4.2 Phase contrast images of undifferentiated HUES9 colonies. (a) HUES9 cells grown on PAm_6-*co*-PSS_2 hydrogel (b) HUES9 cells grown on Matrigel (c) HUES9 cells grown on MEF, and (d) comparison of population doubling time between cells grown on Matrigel (blue) and cells grown on PAm_6-*co*-PSS_2 hydrogel (red).

A significant drawback of several previously developed synthetic matrices for hPSC expansion is their differential efficacy across different hPSC cell lines.[21] To investigate whether this was a concern with PSS-based hydrogels, we have utilized multiple cell lines, namely, HUES9, HUES9-OCT4-GFP, HUES6, and hiPSCs. These cells were cultured in StemPro® medium and compared against those cultured on Matrigel under identical conditions. While we have extensively passaged and characterized HUES9 cells grown on PAm_6-*co*-PSS_2 hydrogel (>20 passages or 8 months), HUES6 and hiPSCs were also cultured 7-9 passages.

The PAm_6-*co*-PSS_2 hydrogel indeed supported adhesion and growth of HUES9 cells both in MEF conditioned medium and chemically defined StemPro® medium without affecting their pluripotency. HUES9 cells expanded on PAm_6-*co*-PSS_2 hydrogel with frequent splitting for over 20 passages using StemPro® medium exhibited characteristic stem cell morphology, colony formation. The pluripotency of the expanded cells was evaluated through immunofluorescent staining for Oct4 and Nanog. Indeed, the HUES9 cells expanded using PAm_6-*co*-PSS_2 hydrogels stained positively for Oct4 and Nanog, suggesting that they maintained pluripotency(Fig. 4.3a). The real-time qRT-PCR results indicate that hPSCs cultured on PAM_6-*co*-PSS_2 hydrogels exhibit similar gene expression level of Oct4 and Nanog to those cultured on Matrigel (Fig. 4.3b). The pluripotency of HUES9 cells expanded on PAm_6-*co*-PSS_2 hydrogel was further confirmed by FACS analysis, which revealed a similar percentage of Oct4 and Tra1-81 positive cells on PAm_6-*co*-PSS_2 hydrogel and Matrigel (Fig. 4.3c). Similar to HUES9 cells, HUES6 and hiPSCs cultured and passaged on PAm_6-*co*-PSS_2 hydrogel in StemPro® medium displayed typical characteristics of hPSCs, such as morphology,

colony formation, and positive Oct4 and Nanog expression (Fig. 4.4). This indicates that the ability of PAm_6-*co*-PSS_2 hydrogels to effectively support the self-renewal and maintained pluripotency of hPSCs is independent of the specific cell line.

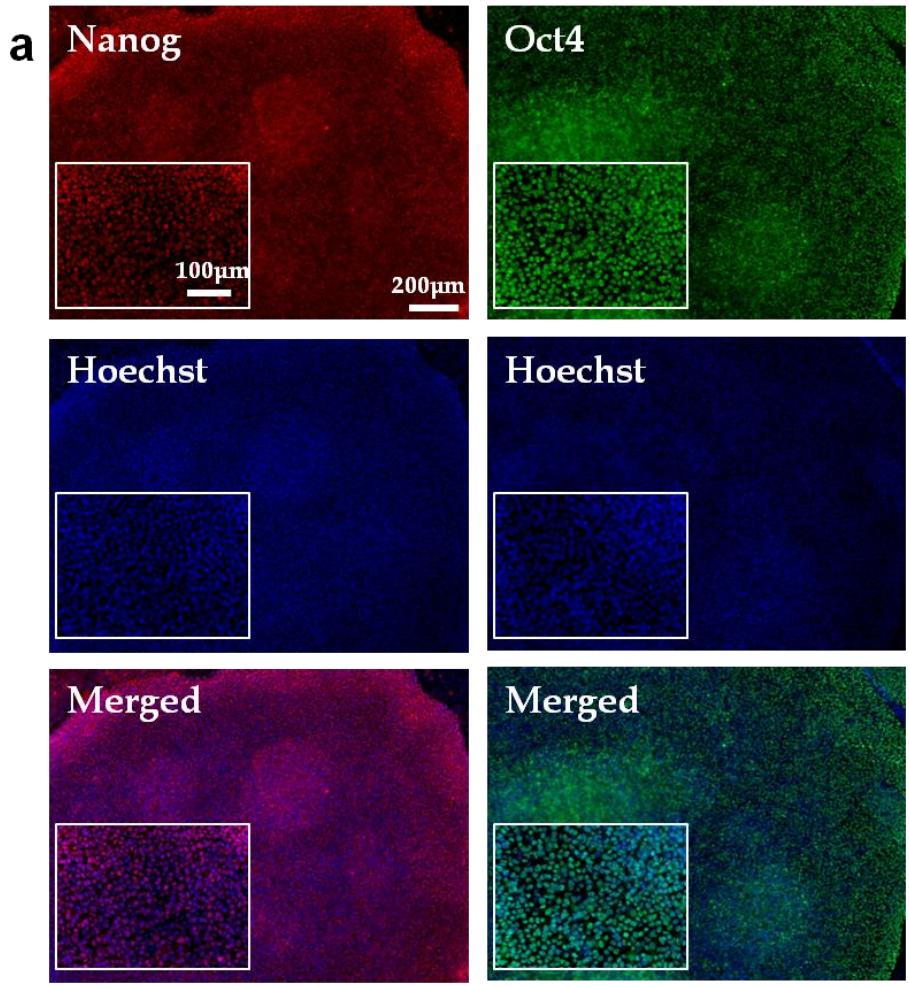


Fig. 4.3 Maintenance of pluripotency of HUES9 cells grown on PAm_6-*co*-PSS_2 hydrogel and Matrigel. (a) immunofluorescence of HUES9 cells grown on PAm_6-*co*-PSS_2 hydrogel for cell nuclei (blue) and pluripotent markers, Nanog (red) and Oct4 (green) (b) results of real-time quantitative RT-PCR for gene expressions of pluripotent markers (Nanog and Oct4) (c) FACS analysis of cells showing the majority of cells were pluripotent. (Continued on next page)

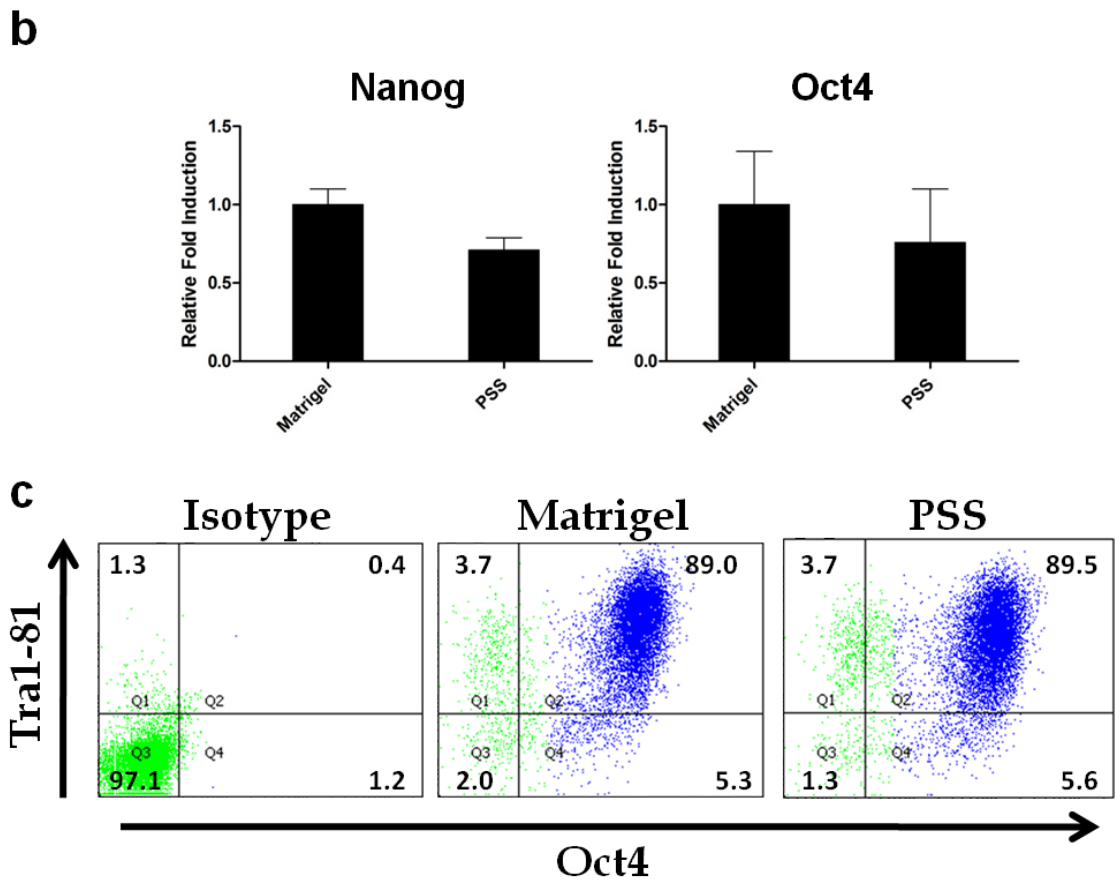


Fig. 4.3 (continued). (Caption shown on previous page)

.

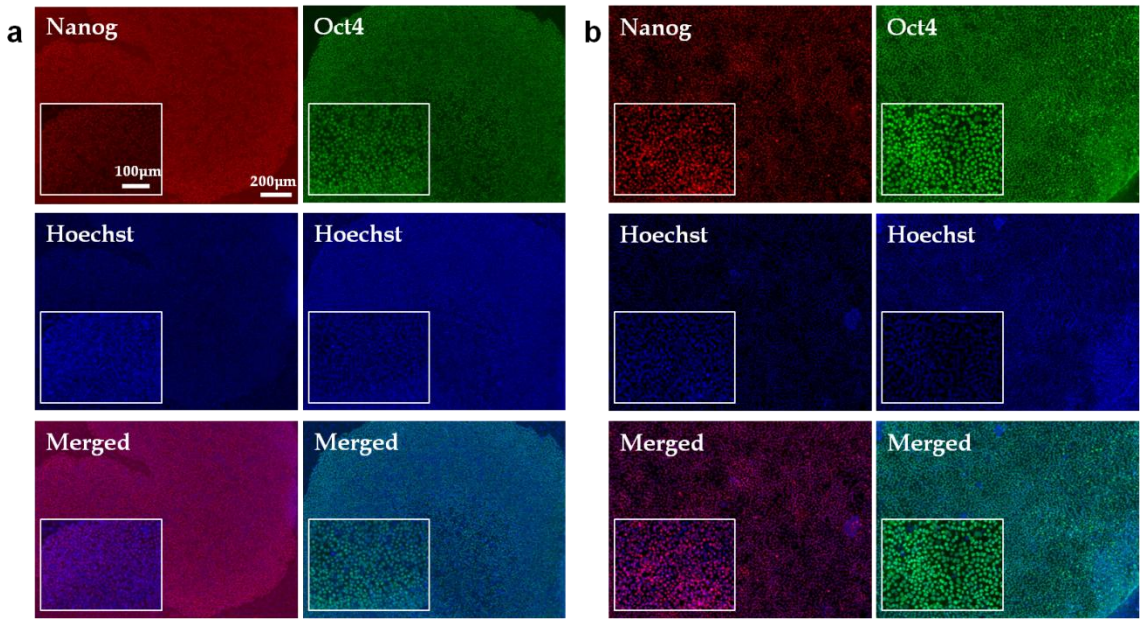


Fig. 4.4 Maintenance of pluripotency of HUES6 cells (a) and hiPSCs (b) grown on PAm_6-*co*-PSS_2 hydrogel demonstrated by immunofluorescence for cell nuclei (blue) and pluripotent markers, Nanog (red) and Oct4 (green).

Pluripotent stem cells are characterized by their ability to differentiate into all the three germ layers. HUES9 cells expanded on PAm_6-*co*-PSS_2 hydrogel were successfully differentiated into all three germ layers (mesoderm, ectoderm, and endoderm), further confirming that the cells grown extensively on these hydrogels maintained their ability to differentiate into multiple germ layers (Fig. 4.5). Additionally, the cells cultured on PAm_6-*co*-PSS_2 hydrogel maintained a normal karyotype (Fig. 4.6). Together these findings suggest that the potential of PAm_6-*co*-PSS_2 hydrogel to support long-term culture of undifferentiated hPSCs while maintaining their pluripotency.

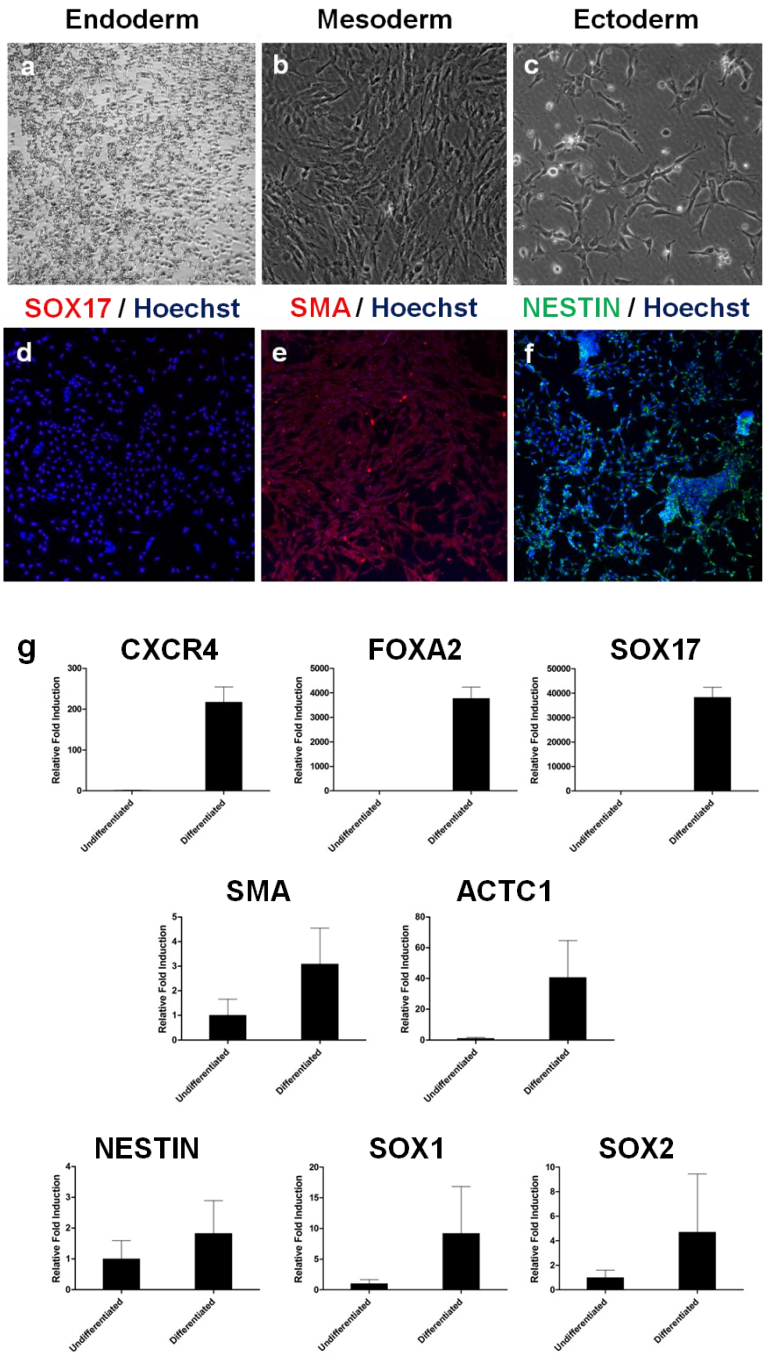


Fig. 4.5 *In vitro* 3 germ layers differentiationof HUES9 cells grown on PAm_6-*co*-PSS_2 hydrogel (a, d) endoderm differentiation (Sox17) (b, e) mesoderm differentiation (smooth muscle actin, SMA) (c, f) ectoderm differentiation (Nestin) (g) endoderm differentiation (CXCR4, FOXA2, Sox17), mesoderm differentiation (SMA, ACTC1), and ectoderm differentiation (Nestin, Sox1, Sox2).

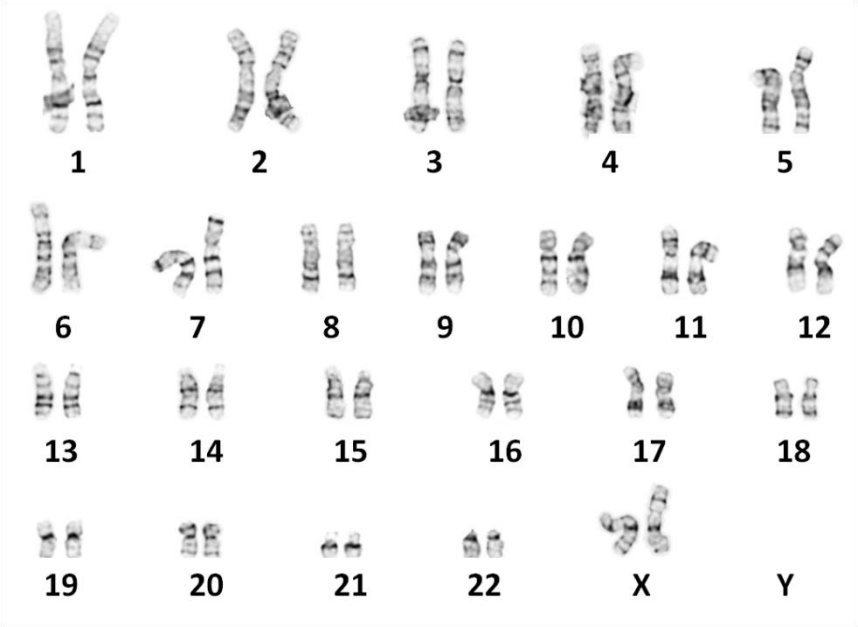


Fig. 4.6 Karyotype analysis of HUES9 cells grown on PAm_6-*co*-PSS_2 hydrogel using StemPro® medium.

4.3.3 Effect of matrix rigidity on hPSCs

Having established the unique ability of PSS-based hydrogels (PAm_6-*co*-PSS_2) to support the culture of hPSCs while maintaining their pluripotency, we next determined the effect of matrix rigidity on hPSCs. It has been well-established that substrate stiffness can have a significant impact on cell behavior.[41, 42] To examine the role that the rigidity of the hydrogel plays in hESC attachment and self-renewal, PSS-based hydrogels with varying matrix rigidity (PAm_6-*co*-PSS_2-L, PAm_6-*co*-PSS_2-M and PAm_6-*co*-PSS_2 having compressive moduli of 54 kPa, 138 kPa, and 344 kPa, respectively) were developed by varying the cross-link density. As seen from Fig. 4.7, increased cell adhesion and colony formation were observed with increasing rigidity of PSS-based hydrogels. Among these hydrogels, PAm_6-*co*-PSS_2 (compressive modulus of 344 kPa) successfully supported adhesion, colony formation, and pluripotency of HUES9-Oct4-

GFP cells. On the other hand, PAm$_6$-*co*-PSS$_2$-L hydrogels supported minimal cell attachment while that on PAm$_6$-*co*-PSS$_2$-M hydrogel exhibited moderate cell attachment, although, the attached cells underwent spontaneous differentiation (Fig. 4.7b and 4.7e).

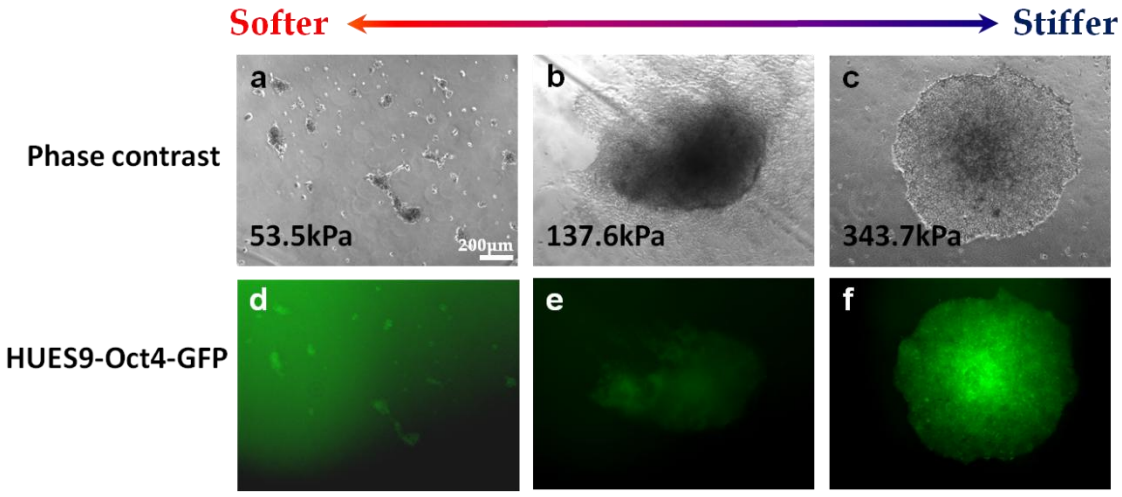


Fig. 4.7 Phase contrast images (a-c) and green fluorescent images (d-f) of HUES9 cells grown on various PSS-based hydrogels having different bulk rigidity (a, d) PAm$_6$-*co*-PSS$_2$-L hydrogel, (b, e) PAm$_6$-*co*-PSS$_2$-M hydrogel, and (c, f) PAm$_6$-*co*-PSS$_2$ hydrogel.

4.3.4 Effect of charge density of hydrogel on hPSC response

Matrix charge density has been implicated to play an important role on mediating cell adhesion;[43] this could in turn have an effect on colony formation, growth and pluripotency of hPSCs on anionic PSS-based hydrogels. PSS-based hydrogels with varying charge density were synthesized by varying the mole fraction of SS moieties within the hydrogels (molar ratio between Am and SS as 6:2 for PAm$_6$-*co*-PSS$_2$, 6:1 for PAm$_6$-*co*-PSS$_1$, and 6:0.5 for PAm$_6$-*co*-PSS$_{0.5}$). No cell adhesion was observed on PAm$_6$-*co*-PSS$_{0.5}$ hydrogels. Although PAm$_6$-*co*-PSS$_1$ hydrogels supported some cell adhesion, they did not yield large colony formation as expected in the case of hPSCs (Fig. 4.8).

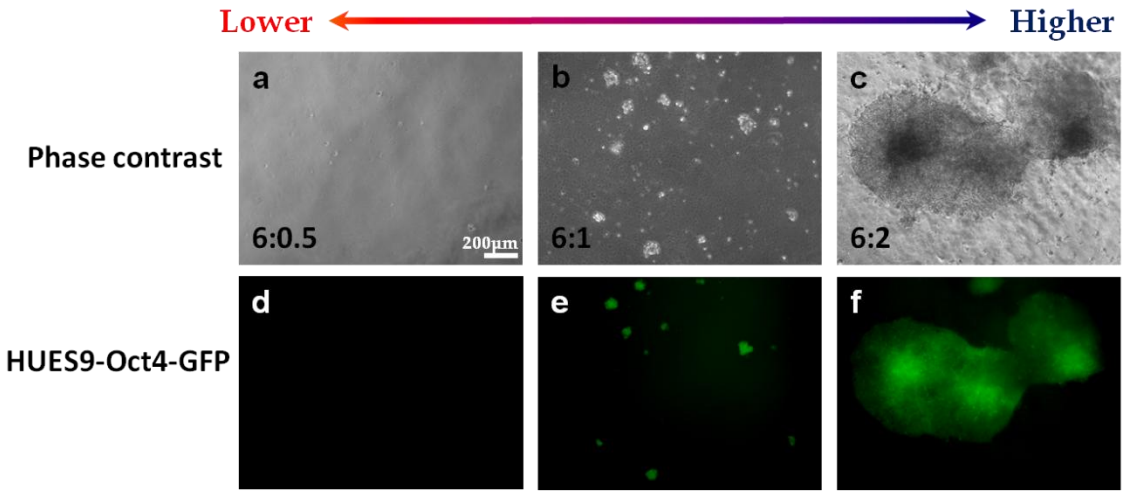


Fig. 4.8 Phase contrast images (a-c) and green fluorescent images (d-f) of HUES9 cells grown on various PSS-based hydrogels with varying charge density (a, d) PAm_6-*co*-$PSS_{0.5}$ hydrogel, (b, e) PAm_6-*co*-PSS_1 hydrogel, and (c, f) PAm_6-*co*-PSS_2 hydrogel.

4.3.5 Effect of chemical functional group(s) and matrix hydrophobicity on hPSCs

Variations in chemical functionality have been demonstrated to affect cell-matrix interactions [20, 44] Similarly, matrix interfacial hydrophobicity also plays an important role in determining cell-matrix interactions.[45] To determine the effect of matrix hydrophobicity on adhesion, colony formation, and pluripotency of hPSCs, we have examined the cellular response of HUES9-Oct4-GFP cultured on various hydrogels, such as PAm_6-*co*-PSS_2, PAm_6-*co*-$PSPA_2$, and PAm_6-*co*-$PMEDSAH_2$. These hydrogels all have pendant side chains terminating with $-SO_3H$ functional group, but they have different hydrophobicities as tabulated in Table 4.2. Similar to PAm_6-*co*-PSS_2 hydrogels, significant cell adhesion was observed on PAm_6-*co*-$PSPA_2$ hydrogels, while minimal to no cell adhesion was observed on PAm_6-*co*-$PMEDSAH_2$ (Fig. 4.9). However, unlike PAm_6-*co*-PSS_2 hydrogels, cells on PAm_6-*co*-$PSPA_2$ hydrogels appeard to lose their

pluripotency, as observed from intensity of GFP fluorescence in GFP-Oct4-HUES9. The observation that the ability of PSS-based hydrogels to support self renewal of hPSCs does not merely require the presence of sulfonate moieties, but rather depends on a combination of physical cues such as hydrophilicity and elastic modulus exemplifies the delicate balance of insoluble cues of the niche on various cellular responses leading to self-renewal of hPSCs. Previous studies by Villa-Diaz *et al*. have shown that PMEDSAH coated dishes having a water contact angle of ~17^{o} and sulfonate groups supported self-renewal of hESCs in Stempro® medium.[21] However, our PAm_6-*co*-$PMEDSAH_2$ hydrogels containing PMEDSAH moieties failed to support hPSCs adhesion and growth; this could be attributed to the differences in chemical composition and/or the interfacial hydrophobicity.

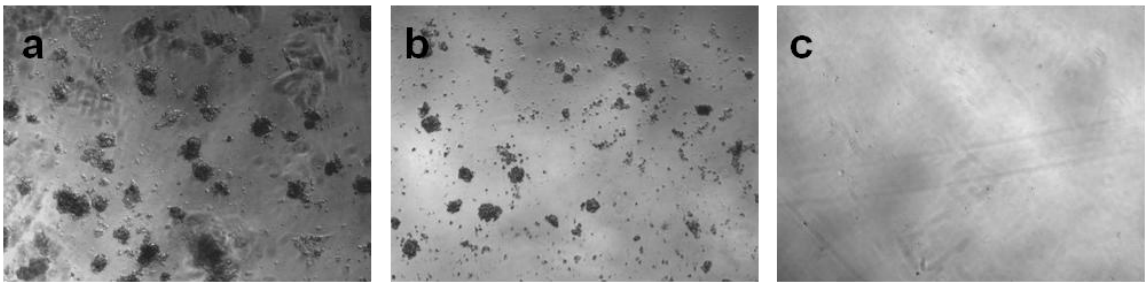


Fig. 4.9 Phase contrast images (a-c) of various hydrogels terminating with -SO_3H functional group (a) initial HUES9 cell attachment on PAm_6-*co*-PSS_2 hydrogel having water contact angle of 23.0^{o} (b) initial HUES9 cell attachment on PAm_6-*co*-$PSPA_2$ hydrogel having water contact angle of 32.6^{o} , and (c) no HUES9 cell attachment on PAm_6-*co*-$PMEDSAH_2$ hydrogel having water contact angle of 66.3^{o}.

We next investigated the effect of chemical functional groups on hPSCs by culturing the HUES9-Oct4-GFP cells on PAm_6-*co*-$PA2AGA_2$ hydrogels having similar interfacial hydrophobicity, matrix rigidity, and surface roughness as PAm_6-*co*-PSS_2, but different functional groups, having carboxyl-terminating pendant side chains rather than the sulfonate-terminating side chains observed for PAm_6-co-PSS_2. (Fig. 4.1 and Table 4.4). Minimal to no cell adhesion was observed on PAm_6-*co*-$PA2AGA_2$. We have further examined the effect of carboxyl functional groups on hPSCs by employing various PAA-based hydrogels having carboxyl functional group but varying hydrophobicity as tabulated in Table 4.2. Similar to PAm_6-*co*-$PA2AGA_2$, no cell adhesion was observed on hydrogels with carboxyl functional groups, such as PAm_6-*co*-$PA4ABA_2$, PAm_6-*co*-$PA6ACA_2$, and PAm_6-*co*-$PA8ACA_2$ (Fig. 4.10).

Table 4.4 Average root mean square (RMS) surface roughness of hydrogels.

Scan area	PAm_6-*co*-$PA2AGA_2$	PAm_6-*co*-PSS_2
400nm x 400nm	0.21 ± 0.024	0.20 ± 0.017
4µm x 4µm	0.45 ± 0.030	0.36 ± 0.017

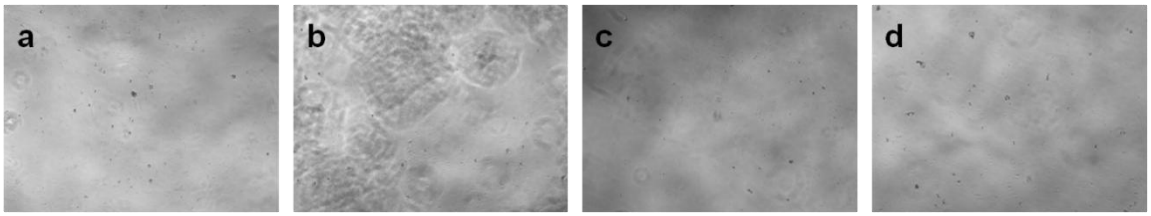


Fig. 4.10 Phase contrast images (a-d) of various hydrogels terminating with -COOH functional group showing no cell adhesion (a) PAm_6-*co*-$PA2AGA_2$ hydrogel having water contact angle of 20.9^o (b) PAm_6-*co*-$PA4ABA_2$ hydrogel having water contact angle of 36.1^o (c) PAm_6-*co*-$PA6ACA_2$ hydrogel having water contact angle of 53.8^o, and (d) PAm_6-*co*-$PA8ACA_2$ hydrogel having water contact angle of 67.3^o.

4.3.6 Cell-matrix interface on adhesion and growth of hPSCs

As the interface of the hydrogels was not functionalized and a short incubation of the hydrogels in medium containing fetal bovine serum prior to cell seeding was needed for initial cell adhesion, we examined adsorption of various extracellular matrix proteins onto the hydrogel surfaces. The effects of matrix interfacial properties (hydrophilicity, functional group, surface roughness, etc.) on protein adsorption and conformation, and their effects on cell adhesion are well known.[46-49] To evaluate the effect of protein adsorption on PSS-mediated expansion of hPSCs, we examined protein adsorption on PAm_6-*co*-PSS_2 hydrogels and compared it against PAm_6-*co*-$PA2AGA_2$. We chose these two hydrogel systems based on our observation that despite having similar hydrophilicty, surface roughness, and rigidity, PAm_6-*co*-PSS_2 hydrogels supports hPSC adhesion and self-renewal while PAm_6-*co*-$PA2AGA_2$ hydrogels did not even support hPSC adhesion. We have also examined the effect of these materials on bFGF binding. While both PAm_6-*co*-PSS_2 and PAm_6-*co*-$PA2AGA_2$ hydrogels supported adsorption of ECM proteins and bFGF, PAm_6-*co*-PSS_2 hydrogels consistently exhibited higher protein adsorption

compared to PAm_6-*co*-$PA2AGA_2$ hydrogels, especially in the case of VN at concentrations expected in medium containing 10% FBS[50, 51], used to precondition the hydrogels prior to hPSC culture; BSA also showed increased adsorption on Am_6-*co*-PSS_2 hydrogels (Fig 4.11a). Notably, previous studies have shown that the adsorption of VN onto hydrogel surfaces can foster adhesion and self-renewal of hPSCs.[40] We also note that both PAm_6-*co*-PSS_2 and PAm_6-*co*-$PA2AGA_2$ exhibits similar bFGF binding abilities possibly due to the presence of anionic functional groups in both hydrogels as previously reported.[31]

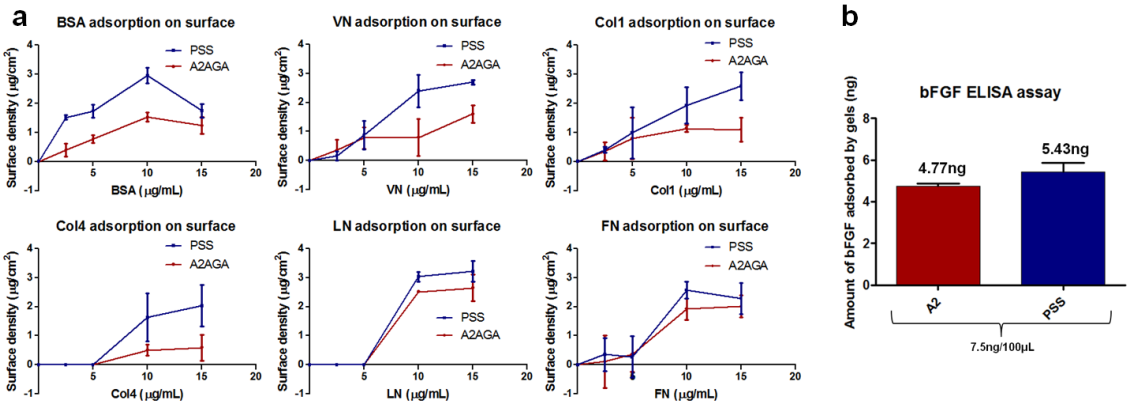


Fig. 4.11 Quantification of (a) various ECM proteins and (b) the amount of bFGF adsorbed to PAm_6-*co*-$PA2AGA_2$ hydrogel (red) and PAm_6-*co*-PSS_2 hydrogel (blue).

Cell surface adhesion molecules such as integrins play an important role in the initial adhesion of hPSCs to the underlying matrix, and also as critical regulator of their self-renewal.[52] Similarly, extracellular matrix (ECM) components secreted by the hPSCs as well as the feeder cells have been shown to play an important role in maintaining the pluripotency of hPSCs.[8] Therefore, we have determined the

endogenous expressions levels of various cell surface adhesion molecules and extracellular matrix components and adhesion molecules of HUES9 cells cultured on PAm_6-*co*-PSS_2, PAm_6-*co*-PPS_2, Matrigel, and compared them against MEF supported culture under identical conditions. An upregulation of a number of ECMs and integrins were observed on hUES9 cells cultured on PAm_6-*co*-PSS_2 hydrogels (Fig. 4.12). Specifically, upregulation on PAm_6-*co*-PSS_2 hydrogels was observed forfibronectin1, laminin (α1, β1, and γ1) and a number cell surface receptors such as integrin α1, integrin α2, integrin α5, integrin α8, integrin αL, integrin αV, and integrin β3, many of which have been shown to play an important role in self-renewal of hESCs.[11, 14, 16, 52-54] We also observed upregulation of CD44, which has been implicated in the mechanism through which hyaluronic acid supports self-renewal of hESCs in MEF condioned medium culture.[55, 56]

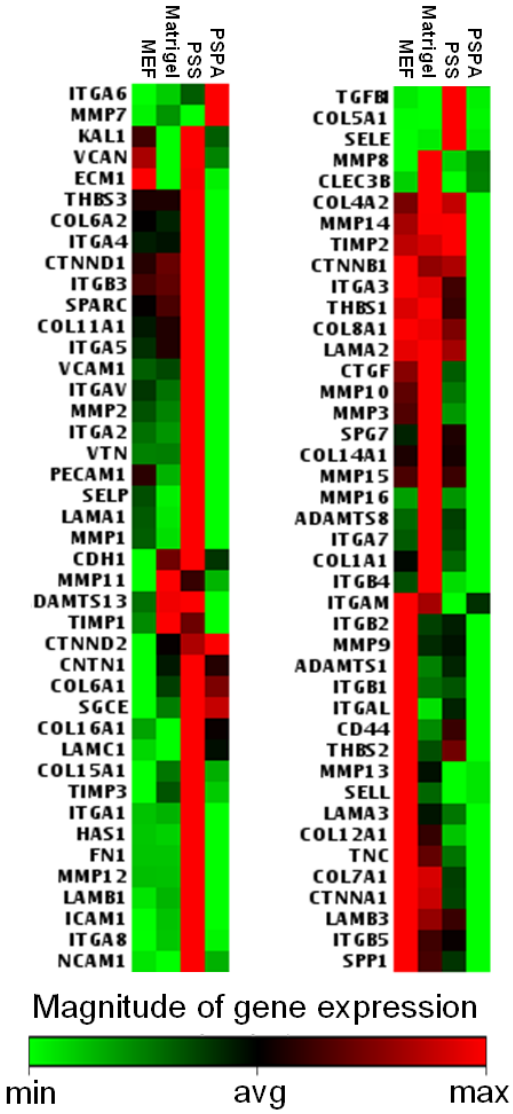


Fig. 4.12 Hierarchical cluster analysis of mapping 84 gene expression profiles of HUES9 cells grown on MEF, Matrigel, PAm$_6$-*co*-PSS$_2$ hydrogel, and PAm$_6$-*co*-PSPA$_2$ hydrogel.

4.4 Conclusion

Developing cost-effective and scalable synthetic matrices for long-term expansion of human pluripotent stem cells (hPSCs) is an important intermediate step to meet the need for large cells required to realize their applications, ranging from drug screening platforms to regenerative medicine. Here, we report the development of a synthetic hydrogel comprising of heparin mimetic moieties, capable of supporting long-term expansion of hPSCs for over 20 passages in chemically defined Stempro® medium. HPSCs expanded on these hydrogels maintained their characteristic morphology, colony forming ability, karyotypic stability, and differentiation potential. HPSCs expanded on this synthetic matrix exhibited pluripotency markers comparable to those cultured on Matrigel. Additionally, we report the correlation between various material properties, such as functional group, hydrophobicity, charge density, and rigidity, on various cellular responses of hPSCs. The observed cellular responses are explained through matrix mediated binding of ECM proteins and growth factors, along with subsequent upregulation of specific adhesion molecules in adhered hPSCs. Such synthetic matrices comprising of "off-the shelf" components are easy to synthesize and do not require any sophisticated processing thus making them cost-effective and translational. Beyond this promising translational application, synthetic matrices with defined bulk and interfacial properties are an ideal tool to probe the molecular mechanisms that control fate and commitment of hPSCs.

4.5 Acknowledgments

This chapter, in full, is currently being prepared for submission for publication of the material. *Chang, Chien-Wen; *Hwang, Yongsung; Hagan, Thomas; Brafman, David; Varghese, Shyni. The dissertation author was the primary investigator and author of this paper.

4. 6 References

1. Couture, L.A., *Scalable pluripotent stem cell culture.* Nat Biotechnol. **28**(6): p. 562-3.

2. Swistowski, A., et al., *Xeno-Free Defined Conditions for Culture of Human Embryonic Stem Cells, Neural Stem Cells and Dopaminergic Neurons Derived from Them.* PLoS ONE, 2009. **4**(7).

3. Ludwig, T.E., et al., *Derivation of human embryonic stem cells in defined conditions.* Nature Biotechnology, 2006. **24**(2): p. 185-187.

4. Lu, J., et al., *Defined culture conditions of human embryonic stem cells.* Proceedings of the National Academy of Sciences of the United States of America, 2006. **103**(15): p. 5688-5693.

5. Yao, S., et al., *Long-term self-renewal and directed differentiation of human embryonic stem cells in chemically defined conditions.* Proceedings of the National Academy of Sciences of the United States of America, 2006. **103**(18): p. 6907-6912.

6. Thomson, J.A., et al., *Embryonic stem cell lines derived from human blastocysts.* Science, 1998. **282**(5391): p. 1145-7.

7. Amit, M., et al., *Human feeder layers for human embryonic stem cells.* Biol Reprod, 2003. **68**(6): p. 2150-6.

8. Richards, M., et al., *Human feeders support prolonged undifferentiated growth of human inner cell masses and embryonic stem cells.* Nat Biotechnol, 2002. **20**(9): p. 933-6.

9. Amit, M., *Feeder-layer free culture system for human embryonic stem cells.* Methods Mol Biol, 2007. **407**: p. 11-20.

10. Amit, M., et al., *Feeder layer- and serum-free culture of human embryonic stem cells.* Biol Reprod, 2004. **70**(3): p. 837-45.

11. Xu, C., et al., *Feeder-free growth of undifferentiated human embryonic stem cells.* Nat Biotechnol, 2001. **19**(10): p. 971-4.

12. Martin, M.J., et al., *Human embryonic stem cells express an immunogenic nonhuman sialic acid.* Nat Med, 2005. **11**(2): p. 228-232.

13. Hakala, H., et al., *Comparison of biomaterials and extracellular matrices as a culture platform for multiple, independently derived human embryonic stem cell lines.* Tissue Eng Part A, 2009. **15**(7): p. 1775-85.

14. Brafman, D.A., et al., *Defining long-term maintenance conditions of human embryonic stem cells with arrayed cellular microenvironment technology.* Stem Cells Dev, 2009. **18**(8): p. 1141-54.

15. Ludwig, T.E., et al., *Feeder-independent culture of human embryonic stem cells.* Nat Methods, 2006. **3**(8): p. 637-46.

16. Braam, S.R., et al., *Recombinant vitronectin is a functionally defined substrate that supports human embryonic stem cell self-renewal via alphavbeta5 integrin.* Stem Cells, 2008. **26**(9): p. 2257-65.

17. Mei, Y., et al., *Combinatorial development of biomaterials for clonal growth of human pluripotent stem cells.* Nat Mater, 2010. **9**(9): p. 768-78.

18. Melkoumian, Z., et al., *Synthetic peptide-acrylate surfaces for long-term self-renewal and cardiomyocyte differentiation of human embryonic stem cells.* Nat Biotechnol, 2010. **28**(6): p. 606-10.

19. Mei, Y., et al., *Mapping the Interactions among Biomaterials, Adsorbed Proteins, and Human Embryonic Stem Cells.* Advanced Materials, 2009. **21**(27): p. 2781-86.

20. Brafman, D.A., et al., *Long-term human pluripotent stem cell self-renewal on synthetic polymer surfaces.* Biomaterials, 2010. **31**(34): p. 9135-44.

21. Villa-Diaz, L.G., et al., *Synthetic polymer coatings for long-term growth of human embryonic stem cells.* Nat Biotechnol, 2010. **28**(6): p. 581-3.

22. Derda, R., et al., *Defined substrates for human embryonic stem cell growth identified from surface arrays.* ACS Chem Biol, 2007. **2**(5): p. 347-55.

23. Derda, R., et al., *High-throughput discovery of synthetic surfaces that support proliferation of pluripotent cells.* J Am Chem Soc, 2010. **132**(4): p. 1289-95.

24. Nishihara, S., et al., *Heparan sulfate regulates self-renewal and pluripotency of embryonic stem cells.* Journal of Biological Chemistry, 2008. **283**(6): p. 3594-3606.

25. Furue, M.K., et al., *Heparin promotes the growth of human embryonic stem cells in a defined serum-free medium (vol 105, art no 13409, 2008).* Proceedings of the

National Academy of Sciences of the United States of America, 2008. **105**(46): p. 18071-18071.

26. Kim, B.S. and D.J. Mooney, *Development of biocompatible synthetic extracellular matrices for tissue engineering.* Trends Biotechnol, 1998. **16**(5): p. 224-30.

27. Xu, C.H., et al., *Basic fibroblast growth factor supports undifferentiated human embryonic stem cell growth without conditioned medium.* Stem Cells, 2005. **23**(3): p. 315-323.

28. Taipale, J. and J. Keski-Oja, *Growth factors in the extracellular matrix.* FASEB J, 1997. **11**(1): p. 51-9.

29. Galzie, Z., A.R. Kinsella, and J.A. Smith, *Fibroblast growth factors and their receptors.* Biochem Cell Biol, 1997. **75**(6): p. 669-85.

30. Capila, I. and R.J. Linhardt, *Heparin-protein interactions.* Angew Chem Int Ed Engl, 2002. **41**(3): p. 391-412.

31. Liekens, S., et al., *Modulation of fibroblast growth factor-2 receptor binding, signaling, and mitogenic activity by heparin-mimicking polysulfonated compounds.* Mol Pharmacol, 1999. **56**(1): p. 204-13.

32. Liekens, S., et al., *The sulfonic acid polymers PAMPS [poly(2-acrylamido-2-methyl-1-propanesulfonic acid)] and related analogues are highly potent inhibitors of angiogenesis.* Oncol Res, 1997. **9**(4): p. 173-81.

33. Sangaj, N., et al., *Heparin Mimicking Polymer Promotes Myogenic Differentiation of Muscle Progenitor Cells.* Biomacromolecules, 2010. **11**(12): p. 3294-3300.

34. Ayala, R., et al., *Engineering the cell-material interface for controlling stem cell adhesion, migration, and differentiation.* Biomaterials, 2011. **32**(15): p. 3700-3711.

35. Varghese, S., et al., *Role of hydrophobicity on structure of polymer-metal complexes.* Journal of Physical Chemistry B, 2001. **105**(23): p. 5368-5373.

36. Miyoshi, H., et al., *Development of a self-inactivating lentivirus vector.* Journal of Virology, 1998. **72**(10): p. 8150-8157.

37. Zufferey, R., et al., *Self-inactivating lentivirus vector for safe and efficient in vivo gene delivery.* Journal of Virology, 1998. **72**(12): p. 9873-9880.

38. Livak, K.J. and T.D. Schmittgen, *Analysis of relative gene expression data using real-time quantitative PCR and the 2(T)(-Delta Delta C) method.* Methods, 2001. **25**(4): p. 402-408.

39. Willert, K., et al., *Wnt proteins are lipid-modified and can act as stem cell growth factors.* Nature, 2003. **423**(6938): p. 448-52.

40. Yap, L.Y., et al., *Defining a threshold surface density of vitronectin for the stable expansion of human embryonic stem cells.* Tissue Eng Part C Methods, 2010. **17**(2): p. 193-207.

41. Engler, A.J., et al., *Matrix elasticity directs stem cell lineage specification.* Cell, 2006. **126**(4): p. 677-689.

42. Discher, D.E., P. Janmey, and Y.-l. Wang, *Tissue Cells Feel and Respond to the Stiffness of Their Substrate.* Science, 2005. **310**(5751): p. 1139-1143.

43. Shelton, R.M., A.C. Rasmussen, and J.E. Davies, *Protein adsorption at the interface between charged polymer substrata and migrating osteoblasts.* Biomaterials, 1988. **9**(1): p. 24-9.

44. Benoit, D.S.W., et al., *Small functional groups for controlled differentiation of hydrogel-encapsulated human mesenchymal stem cells.* Nat Mater, 2008. **7**(10): p. 816-823.

45. Ayala, R., et al., *Engineering the cell-material interface for controlling stem cell adhesion, migration, and differentiation.* Biomaterials, 2011. **32**(15): p. 3700-11.

46. Roach, P., D. Farrar, and C.C. Perry, *Interpretation of protein adsorption: surface-induced conformational changes.* Journal of the American Chemical Society, 2005. **127**(22): p. 8168-8173.

47. Xu, L.-C. and C.A. Siedlecki, *Effects of surface wettability and contact time on protein adhesion to biomaterial surfaces.* Biomaterials, 2007. **28**(22): p. 3273-3283.

48. Allen, L.T., et al., *Surface-induced changes in protein adsorption and implications for cellular phenotypic responses to surface interaction.* Biomaterials, 2006. **27**(16): p. 3096-3108.

49. Phadke, A., et al., *Templated Mineralization of Synthetic Hydrogels for Bone-Like Composite Materials: Role of Matrix Hydrophobicity.* Biomacromolecules, 2010. **11**(8): p. 2060-2068.

50. Miceli, M.V., D.A. Newsome, and D.J. Tate, *Vitronectin is responsible for serum-stimulated uptake of rod outer segments by cultured retinal pigment epithelial cells.* Investigative Ophthalmology & Visual Science, 1997. **38**(8): p. 1588-1597.

51. Hayman, E.G., et al., *Vitronectin - a Major Cell Attachment-Promoting Protein in Fetal Bovine Serum.* Experimental Cell Research, 1985. **160**(2): p. 245-258.

52. Meng, Y., et al., *Characterization of integrin engagement during defined human embryonic stem cell culture.* The FASEB Journal, 2010. **24**(4): p. 1056.

53. Rodin, S., et al., *Long-term self-renewal of human pluripotent stem cells on human recombinant laminin-511.* Nat Biotechnol, 2009. **28**(6): p. 611-5.

54. Ludwig, T.E., et al., *Derivation of human embryonic stem cells in defined conditions.* Nat Biotechnol, 2006. **24**(2): p. 185-7.

55. Gerecht, S., et al., *Hyaluronic acid hydrogel for controlled self-renewal and differentiation of human embryonic stem cells.* Proc Natl Acad Sci U S A, 2007. **104**(27): p. 11298-303.

56. Janssens, S., et al., *Autologous bone marrow-derived stem-cell transfer in patients with ST-segment elevation myocardial infarction: double-blind, randomised controlled trial.* The Lancet, 2006. **367**(9505): p. 113-121.

CHAPTER 5: Conclusions and Future directions

In this work, by controlling tunable physico-chemical cues presented in the hydrogel-based system as a valid tool to enlighten the roles of cell-matrix interaction, we have possibly decoupled or identified the various properties that contribute to the various cell behaviors.

First, PEG cryogels with similar chemical composition but distinctly different microstructures were synthesized by manipulating the kinetics of polymerization. The effect of freezing temperature and degree of supercooling on cryogel formation and their microstructure was also evaluated. We showed for the first time that monolithic heterogeneous networks containing both cryogel-like and hydrogel-like structures can be synthesized using cryogelation techniques by manipulating the polymerization kinetics. The ability to control the microstructure of cryogels via concentration of the initiator (accelerator) introduces a new "knob" to manipulate the structural properties of such materials. Using the same approach with slight modification, i.e., introduction of preferential nucleation sites, we have successfully controlled the directionality and geometry of internal pore structures without altering precursor concentrations. We also found that the mechanical and swelling properties of the cryogels were strongly dependent upon their network microstructure. These highly elastic interconnected macroporous structures could undergo large deformation without altering their structural properties. The tunable structural and mechanical properties, high elasticity, swelling behavior favoring enhanced mass transport of PEG cryogels along with their ability to support cell growth make them excellent scaffolds for cell and tissue engineering.

Second, this study demonstrates the potential of macroporous PEG cryogels as a cell scaffold for cartilage tissue engineering using primary bovine chondrocytes. We evaluated the highly interconnected and macroporous internal morphology of cryogels by various microscopic analyses. The seeded chondrocytes were found to be successfully distributed within the macroporous network. The seeded chondrocytes proliferated, maintained chondrocyte phenotype and secreted cartilage-specific matrix within the cryogels. Our findings described in this manuscript demonstrate that the PEG cryogels can successfully support cell proliferation and cartilage-specific ECM production, showing their promising application as scaffolds for cartilage tissue engineering.

Lastly, developing cost-effective and scalable synthetic matrices for long-term expansion of human pluripotent stem cells (hPSCs) is an important intermediate step to meet the need for large cells required to realize their applications, ranging from drug screening platforms to regenerative medicine. Here, we report the development of a synthetic hydrogel comprising of heparin mimetic moieties, capable of supporting long-term expansion of hPSCs for over 20 passages in chemically defined Stempro® medium. HPSCs expanded on these hydrogels maintained their characteristic morphology, colony forming ability, karyotypic stability, and differentiation potential. HPSCs expanded on this synthetic matrix exhibited pluripotency markers comparable to those cultured on Matrigel. Additionally, we report the correlation between various material properties, such as functional group, hydrophobicity, charge density, and rigidity, on various cellular responses of hPSCs. The observed cellular responses are explained through matrix mediated binding of ECM proteins and growth factors, along with subsequent upregulation of specific adhesion molecules in adhered hPSCs. Such synthetic matrices

comprising of “off-the shelf” components are easy to synthesize and do not require any sophisticated processing thus making them cost-effective and translational. Beyond this promising translational application, synthetic matrices with defined bulk and interfacial properties are an ideal tool to probe the molecular mechanisms that control fate and commitment of hPSCs.